THE COMPARISON OF MODEL-BASED AND CONVENTIONAL PRESSURE CONTROL FOR A PLASMA REACTOR

by

HOSHANG E. SUBAWALLA, B.E.

A THESIS

IN

CHEMICAL ENGINEERING

Submitted to the Graduate Faculty
of Texas Tech University in
Partial Fulfillment of
the Requirements for
the Degree of

MASTER OF SCIENCE

IN

CHEMICAL ENGINEERING

Approved

Accepted

December, 1993

ACKNOWLEDGEMENTS

I thank the chairman of my committee, Dr. Russell Rhinehart, for his advice and encouragement throughout this work. Appreciation is also extended to the other members of my committee, Dr. J. B. Riggs and Dr. M. E. Parten. My gratitude to Dr. R. S. Narayan and Dr. R. E. Desrosiers for their encouragement, trust and support through the last two years. I would also like to thank my colleagues, Vikram and Soundar, for their constant endeavor to help me "get a life." A special thank you to Tammy Kent for her assistance during word processing.

My gratitude to my family back in India as well as in the USA for their constant encouragement and financial assistance. Last, but not the least, a special thank you to Kermeen, without whose support this work would not have been possible.

TABLE OF CONTENTS

LIST OF TABLES

LIST OF FIGURES

CHAPTER 1
INTRODUCTION

1.1 Overview

Today, state-of-the-art integrated circuit manufacture depends on the mass replication of tightly controlled micron-sized features in a variety of materials (Manos and Flamm, 1989). Fabrication of these components involves a variety of complex physical and chemical processing steps including crystal growth, oxidation, lithography (patterning of the various layers), chemical vapor deposition, etching and alloying operations. Plasma etching has the ability to replicate patterns efficiently and with a high yield. The early 1970's found widespread replacement of the earlier technology (wet solvent resist stripping) with dry plasma assisted etching because the latter had simpler processing sequences, used safer non-toxic gases instead of corrosive liquids, offered the possibility of simpler automation and precise process control and more importantly made possible a vertical etch rate that greatly exceeded the horizontal etch rate (anisotropic etching). As designs advanced dry etching was found to give better control of critical dimensions of the pattern such as higher circuit density.

1.2 Plasmas and Plasma Processing

A plasma is an ionized low pressure gas with equal number of free positive and negative charges. The free charge is produced by the passage of electrical current through the discharge when a voltage is applied between the electrodes on opposite sides of the plasma reactor. The positive charge is mainly in the form of simply ionized neutrals, either atoms, radicals or molecules from which a single electron has been removed. The majority of negatively charged particles are usually free electrons. Their low weight and mobility make them the main current carriers. The large difference in

weight between the electrons and the neutral species causes the electrons to attain a high average energy after collision, leading to extremely high electron temperatures. The elevated electron temperature is responsible for exciting high temperature type reactions forming free radicals in a low temperature neutral gas. Without a plasma the same reactions would require a temperature in the range of 10^3 to 10^4 K, which would cause irreparable damage to the substrate. The reactive neutral and charged species chemically react with the substrate material on the electrode surface to form volatile products, thus etching the substrate. The glow of a plasma is due to the characteristic light emission when electrons in the excited ionized species return to their ground state.

Many phenomena play a role even in the simplest forms of plasma etching. The chemical and electrical properties of the system are highly coupled and the effect of a change in any given parameter is difficult to isolate. This has made plasma modelling and control extremely difficult. Different recipes are often employed for different processes. There are a multitude of reactions taking place in each case with very little information on their rates. In this work a CF_4/O_2 mixture was employed as it is a system which has been investigated to a great extent in the past and is still commercially relevant. The chemistry of this system includes a forty nine reaction set (Plumb and Ryan, 1986) with only about half the rate constants being known. The reactions generally are one of three types: reactions which represent the dissociation of CF_4 and O_2 with electron impact, gas phase recombination reactions between the products of dissociation such as CF_3, CF_2, free fluorine (F) and atomic oxygen (O) and three-body recombination reactions which take place between the products of dissociation with the help of a third surface such as the reactor wall or a neutral molecule. The etchant species is free fluorine, (F). Oxygen is added to scavenge radical species such as CF_2 and CF_3 so as to reduce the

recombination of Fluorine with these species and hence increase the etch rate on account of the larger amount of etchant species.

The complexity of the plasma process makes it extremely difficult to relate manipulated variables power, pressure, flow and oxygen percentage in the feed mixture to etch performance variables such as increased etch rate, etch anisotropy, etch uniformity (the evenness of the etch across the substrate) and etch selectivity (its ability to remove a film while leaving the substrate intact). In addition the performance variables cannot be measured on-line and hence the some other form of continuous measurements, that can be related to the performance variables, need to be employed. These include the spectroscopic measurements of the concentration of species such as atomic fluorine and oxygen. Hence this system represents a highly coupled multivariable problem. Most current control strategies employ an empirical approach based on the specific reactor geometry and the recipe used. These are rarely reproducible from reactor to reactor or for different recipes. In addition the initial condition of the reactor can be influenced by accumulation of etch products, exposure to the ambient atmosphere (with adsorption of air and moisture on reactor surfaces) and surface modification brought about by reaction with chemical plasmas in the equipment. All these factors contribute to the need for a phenomenological feedback control approach.

1.3 Model-Based Control

The increasing availability of cheap computational resources has made the use of model-based control strategies popular in the chemical process industry. Several model-based control algorithms have been developed and many have been industrially implemented. Embedded in each algorithm is a model of the process which helps the controller make "intelligent" control decisions. The various algorithms

differ in their approach used to develop the model. Among the most widely used techniques are the Model Predictive Control (MPC) strategies (Cutler and Ramaker, 1980; Richalet et al., 1980). These employ a set of numerical coefficients obtained from process time series data as the model. Internal Model Control (IMC) (Garcia and Morari, 1983) strategies use Laplace transfer function models obtained from step response data. Reference System Synthesis (RSS) structures which include Generic Model Control (GMC) (Lee and Sullivan, 1988) and internal decoupling (Balchen at al., 1988), use a nonlinear model of the process and a desired process response (the reference trajectory) to determine the appropriate control action. While MPC and IMC are linear model based strategies, GMC is a nonlinear model based strategy. However both MPC and IMC have their nonlinear extensions. Since most chemical processes are nonlinear using nonlinear models has certain advantages. Process models developed from first principles have a phenomenological basis thus allowing their use for process diagnosis.

1.4 Scope of This Work

At present, there is no global control strategy which is effective for any given process as each strategy has its pros and cons. This work addressed this issue by experimentally comparing various model-based and conventional control strategies for pressure control in a plasma reactor. The aim of this work was to experimentally compare a nonlinear model-based controller, a linear model-based controller and a conventonal controller for different cases. For this work, GMC and IMC were selected as representatives of nonlinear and linear control. The plasma reactor system which is extremely complex to model and nonlinear in its behavior served as an ideal vehicle for the comparison in performance between a nonlinear control strategy and a linear control strategy. Process nonlinearity in part is brought about in part by the

valve characteristics. Processes which are nonlinear are often so on account of the nonlinearity inherent in sensors, transmitters and final control elements. Pressure control in a plasma reactor helps to maintain uniform operating conditions and hence ensure an even etch. These model-based control strategies were compared to conventional proportional-integral(PI) control in order to evaluate the advantages of using model-based control. Various issues such as engineering effort required to develop the models and algorithms, the ease of implementation and performance of certain key variables were examined. This work in particular looked at implementation issues such as dynamic compensation using a time constant developed from the ideal gas law, gain-scheduling characteristics and feedforward disturbance rejection.

The initial work involved the development and validation of a simulator to represent the process. The simulator incorporated kinetic rate data obtained from literature as well as experimental data such as the valve characteristics, reactor volume and vacuum pressure. The simulator maintained a balance between a phenomenological basis and an accurate representation of the process. Certain parameters such as electron density were estimated using available correlations. Validation of the simulator was performed using both dynamic open loop response data as well as steady-state spectroscopic concentration data. The controller models developed were tested on the simulator to gain some process insight before their actual implementation on the experimental system. The comparison included evaluating the performance of both the controlled as well as manipulated variables.

Chapter 2 surveys some of the work in plasma modelling, model-based control and control of plasma processes. Chapter 3 is dedicated to describing the experimental system and the theory behind some of the apparatus. Chapters 4 and 5 discuss the development and validation of the simulator. Chapter 6

includes the development of the controller models. Chapter 7 outlines some of the issues involved in controller testing on the simulator while Chapter 8 discusses implementation issues on the actual process. Chapters 9 and 10 summarize some of the results obtained, conclusions drawn and recommendations suggested.

CHAPTER 2
LITERATURE SURVEY

2.1 Introduction

Ever since the semiconductor industry shifted from wet etching to dry etching, using a plasma as a medium, there has been a proliferation of articles on plasma chemistry, modelling and simulation and other aspects of plasma processing. The documentation of this survey is restricted to plasma processes related to etching and more specifically etching of silicon and silicon dioxide films using carbon tetrafluoride or carbon tetrafluoride/oxygen mixtures.

The industrial success of model-based control (MBC) has led to an increase in the work in this area. The literature survey in this area covers some comprehensive reviews on various model based control strategies as well as articles relating to the application of process model based control (PMBC). This is in order with the goal of this work which deals with the application and comparison of PMBC with other model based control strategies as well as conventional control. Other work surveyed in this area includes Internal Model Control (IMC) and its applications and a few specific articles related to process control of plasma processes.

2.2 Review of Plasma Modelling

The most detailed and relevant work in this area from a chemical kinetic standpoint is that of Plumb and Ryan (1986). Their study consists of the development of a kinetic model for both CF_4 and CF_4/O_2 discharges and its experimental validation. The model they proposed contains twenty two species participating in 49 reactions. Rate constants for each of their reactions was obtained using the extensive experimental kinetic information they possessed. However, quite a few of these were either estimated parameters or "best fits" for the reactor geometry they employed. Among the conclusions drawn

was the fact that CF_2 chemistry plays an important role in CF_4/O_2 discharges. They also concluded that free radical gas phase recombination were more important than previously surmised, while wall effects were negligible and that molecular oxygen was not as important as a reactant as atomic oxygen.

Edelson and Flamm (1984) in a simulation study of CF_4 etching silicon concluded that fluorine atoms are the main reactive species in a plasma and that gas phase chemistry is dominated by neutral reactions. Interestingly they have clearly demarcated two distinct regions for simulation; the plasma and afterglow regions. However the transition is not gradual and values of electron dissociation are reset at the boundary.

Schoenborn et al. (1989) performed a numerical simulation of a CF_4/O_2 plasma and correlated their results with spectroscopic and etch rate data. In many ways the first part of this work closely resembles the work done by them. They also employed a chemical kinetic, well mixed reactor model including first order electron impact dissociation and neutral gas phase reaction rate constants from Plumb and Ryan (1986a,b). They employed power density to scale their dissociation constants while the approach in the work carried out in this thesis used a more reliable parameter, electron density. They used actinometry to measure the concentration of the selected species. They concluded that an insensitivity to power variation indicated that uncertainties in the electron dissociation rate constants do not contribute greatly to uncertainties in model prediction.

Smolinsky and Flamm (1979), in one of the earliest known experimental studies of CF_4 and CF_4/O_2 plasmas, concluded that in pure CF_4 plasmas, C_2F_6 was an important recombination product while it was almost non existent in CF_4/O_2 plasmas. They reported a sharp increase in the concentration of O atoms as the oxygen level in the feed was increased beyond the point

at which a maximum F atom level was observed. They concluded that carbonyl fluoride predominates at lower oxygen levels in the feed. This conclusion was later on drawn by Plumb and Ryan (1986) who used their work to validate some of their simulation studies.

Dalvie and Jensen (1990), in their combined experimental and modelling study of uniformity in the etching of silicon using CF_4/O_2 plasmas used some of the same assumptions that we employed in our work. They concluded that the larger residence times in commercial systems makes diffusion the major transport mechanism in most of the reactor. They stressed the importance of surface recombination reactions of atomic fluorine and oxygen. They concluded that the concentration of atomic fluorine at lower flow rates which were corroborated by the findings of this work. They assumed a spatially uniform electron distribution in the plasma region which rapidly falls to zero outside the plasma.

A work which best sums up the effect of oxygen addition to CF_4 plasmas is that of Mogab et al. (1978). They were the first to observe that etch rate as well as atomic fluorine concentration increased, with increasing oxygen concentration in the feed, up to a certain maximum and then declined. They also observed that the maxima in etch rate occurred at a lower oxygen concentration than that for the atomic fluorine concentration. They concluded that oxygen reacts with fluorine containing species to liberate fluorine atoms and that conversion of CF_4 diminishes with oxygen addition because the electron energy distribution is shifted to lower energies. Their explanation for the variation of atomic fluorine with respect to oxygen concentration in the feed was based on the dual role of oxygen which enhanced production of the etchant [F] while depleting the active sites on the surface thus retarding etching.

2.3 Review Of Model-Based Control

Among the most important articles in this section is the review by Bequette(1991) which surveys the field of nonlinear control system techniques ranging from process specific strategies to predictive control approaches. His suggestions included carrying out more experimental comparisons between linear and nonlinear strategies. He also suggested that the variation in manipulated variable be considered an integral part of control performance evaluation.

Lee and Sullivan (1988) first introduced the GMC algorithm. This technique imbeds a nonlinear description of the process derived from first principles in the control algorithm. The authors state that the algorithm retains a time horizon approach while solving a single step optimization problem and is robust in the face of large process-model mismatch.

Henson and Seborg (1990) tried to unify the various approaches based on the concepts from differential geometry. They suggest that RSS methods such as GMC are only applicable to models in which the rate of change of each output is directly coupled to at least one input, or in mathematical terms which has a relative degree of one. They suggested that the structure of the GMC controller is such that it always results in overshoot for setpoint changes for controller tuning parameters normally employed and that the structure also requires that the decoupling matrix be non-singular.

There have been numerous articles on the implementation of the GMC algorithm. Cott et al. (1989) used GMC in a simulation study of temperature control of an exothermic batch reactor. They tested their controller for the initial start-up and subsequent temperature maintenance. They used an online estimator to determine the amount and rate of heat released by reaction and used it as model feedback. They compared their controller to a dual mode controller and found the GMC-based controller to be more robust with respect to

changes in process parameters and model mismatch. Lee and Sullivan (1988) have implemented a GMC algorithm on a depropanizer distillation column. The regulatory performance of the GMC-based controller was as good as that of the previous material balance strategy. However, its advantage lay in its servo performance because of reduced response time and tighter control. Pandit et al. (1989) have demonstrated both servo and regulatory model-based control on a non-ideal binary distillation column by using the GMC framework. However, they employed steady state tray to tray models instead of short-cut steady state mechanistic models. The adjustable model parameters they employed were a tray efficiency parameter and a vapor boil-up bias.

Riggs et al. (1990) have used the GMC law in combination with a variety of models on industrial distillation columns. Applications include the simulation of a binary side-stream draw column using the Smith-Brinkley algebraic model and the use of ideal tray-to-tray models to control low relative volatility columns. Adjustable parameter used include the theoretical number of trays and the Murphree stage efficiency. They report a lower variation in product impurity and energy savings of 60% over the existing material balance strategy.

Lee and Sullivan (1989) have simulated a GMC-based controller on a forced circulation single stage evaporator. They compared their results with a single loop conventional and predictive control strategies and found that the nonlinear model based controller's performance was significantly better.

Mahuli, Rhinehart and Riggs (1992, 1993) have developed a nonlinear model-based controller using the GMC technique in conjunction with an approximate steady state, three parameter phenomenological model. Their results show good control performance for both ramp and step changes as well as flow rate upsets. The controller was tested using industrial waste-water as well as mixtures prepared with acetic, phosphoric and sulphuric acids.

Among the earliest developed model-based control structures is the technique termed Internal Model Control (IMC). The name was coined by Garcia and Morari (1983) who extensively studied the theory and gave it the necessary mathematical rigor. IMC uses a linear process model in parallel with the actual process. Modifications to the original linear structure include the development of a nonlinear approach for IMC called NLIMC by Economou et al. (1986). They use the nonlinear inverse of the process as the controller model and iteratively integrate to find the manipulated variable action for the next time step. To ensure robust control a filter was employed to reduce the effects of large fluctuations in the desired trajectory. IMC has been tested on an experimental heat exchanger system by Arkun et al. (1986). They deliberately used wrong model parameters in order to study how process-model mismatch affected the performance of the controller for setpoint changes. Their results indicated that if a model was good, then a rapid and stable response could generally be obtained by using the exact inverse. Using a poor model they found that the IMC filter could be easily tuned to provide a satisfactory response.

An interesting comparison between two nonlinear model based controllers was carried out by Rhinehart and Riggs (1988). A nonlinear process model-based controller and a nonlinear internal model controller were compared on single input single output (SISO) CSTR and heat exchanger systems. The idealized CSTR was a open-loop unstable lumped parameter process without dead-time while the heat exchanger was an open loop stable distributed parameter process with transport delay. Both controllers gave essentially the same performance with robust control over a wide band of process gains. They also found that these methods were relatively insensitive to process/model mismatch as long as the approximate model expressed the major nonlinear character of the process. They also noted that though the GMC formulation in the strictest

sense could only be applied to systems with a relative order of one, there was no practical limitation to GMC since the manipulated variable could be related to variables which do appear in the dynamic models for the output variables.

Recent papers on GMC have tried to address some of the problems faced by this formulation. Signal and Lee (1990) tried to compensate for process-model mismatch, and subsequent deterioration in control performance, by regularly updating model parameters. They state that the maximum number of model parameters that can be updated is equal to the number of controlled variables. A simpler and as effective model parameterization method is suggested by Rhinehart and Riggs (1991). The online incremental model parameterization method (IMPOL) uses a one-step-ahead filtered process-model mismatch and the modelled output-parameter sensitivity to calculate an incremental adjustment to the model parameter at each sampling interval. Either a dynamic or steady state model may be employed.

A separate literature survey could be done on model predictive control (MPC) methods by itself. However, this study is restricted to a limited number of articles. Cutler and Ramaker (1980) were among the first to introduce a technique of representing process dynamics with a set of numerical coefficients. They termed the algorithm developed as Dynamic Matrix Control (DMC). This uses plant dynamic data for the process to calculate manipulated variable actions for the present time and a number of future time periods by minimizing the integral of the error. They suggest that this feature enables this technique to handle systems with large deadtime as well as systems with unusual dynamic behavior. Simultaneously and independently Richalet et al. (1980) developed a similar strategy and showed how constraints could be handled online. Patwardhan et al. (1990) have developed a nonlinear model predictive control (NLMPC) strategy by incorporating nonlinear models to predict future control

actions. These methods involve solving a nonlinear programming problem by using methods such as successive quadratic programming (SQP).

2.4 Review of Process Control of Plasma Etch Processes

The need for feedback control is unanimously considered an impediment in reliable operation of low pressure reactive plasma systems (Elta et al., 1993). However this is one of the few areas of agreement. Process control strategies for plasma systems are largely recipe driven and what may work for one system rarely works for another. There are a few articles, however which deal with the systematic modelling and control analysis of the etching of silicon and silicon dioxide using a gas mixture (CF_4/O_2) or pure CF_4.

Among the most important articles in this area are those of Butler et al. (1989) and McLaughlin et al. (1989). They developed dynamic models from step tests on an actual Reactive Ion Etching (RIE) system. These yielded relationships between the process variables and the manipulated variables as well as between performance variables and manipulated variables. Four manipulated variables (pressure, flow, incident power and percentage of oxygen in feed), four measured variables and seven performance variables were chosen. Measurements of the concentrations of F, CF_2 and CO & CO_2 and dc bias were chosen as process variables. Performance variables included etch rates, etch uniformity, anisotropy and selectivity. The transfer function models were used to determine suitable variable pairings for feedback control. Though their conclusions arose from a steady-state analysis and were restricted to the region near the operating point they were for the most part phenomenologically sound.

Using this central idea, Elta et al. (1993) have developed a framework for real time feedback control for a RIE process. They conceptually decomposed the RIE system into two

functional blocks, the plasma factory (PF) and the wafer etch factory (EF). These separate the generation of the important chemical and physical species from the action of etching the surface of the wafer. The key to this idea was to regulate the inputs to the EF by precisely controlling the outputs of the PF. The desired etch characteristics were used to obtain set points for the PF control system. Process recipes were now specified in terms of the dc bias and fluorine concentration rather than power, flow, pressure, etc. This led to tighter control. A part of the work presented here may be considered to be a subset of their work as the aim of this work is to maintain pressure at its setpoint regardless of external disturbances. Thus one set of controlled-manipulated variable pairings have been handled in this work. The authors have chosen bias voltage and concentration of fluorine as the key plasma parameters to be controlled thus effectively reducing the set chosen by Butler et al. (1989) by half. In addition they have employed laser reflectometry to monitor etch rate on line, a technique employed by Buschmann (1992) in his work.

CHAPTER 3
EXPERIMENTAL SET-UP AND THEORY OF OPERATION

3.1 The Plasma Reactor System

3.1.1 Introduction

The equipment primarily consists of a single slice plasma reactor with a modified parallel plate plasma chamber with software controlled parameters. The reactor assembly consists of three main units (Figure 3.1): the reactor, the RF generator cabinet and the remote vacuum pump. The process chamber encloses one wafer at a time in a controlled process environment. The plumbing system supplies the process gases, effluent exhaust and chamber vacuum. The effluent exhaust vacuum is furnished by a remote vacuum pump unit. The electrical system consists of the computer system, RF generator, sensor system and power supply. The RF generator power supply is also remotely located from the reactor. Capability for two process gases (CF_4 and O_2) is supplied in the standard configuration with expansion to four process gases, if necessary. This extension is useful when a gas used for actinometry (e.g., argon), or a gas used to purge the reactor (e.g., nitrogen) needs to be pumped into the chamber.

3.1.2 Design and Operation Features

The process chamber system primarily consists of an enclosure, electrode plate and substrate plate. The plumbing system supplies the various gases to the machine. The process gas flows to the chamber are controlled and monitored by solenoid valves and mass flow controllers. The removal rate of the effluent gases from the chamber is controlled by a software actuated throttle valve. The chamber pressure is also maintained by this valve. Nitrogen is used to purge the chamber.

The electrical system controls and monitors the operation of the machine. The control system is primarily comprised of

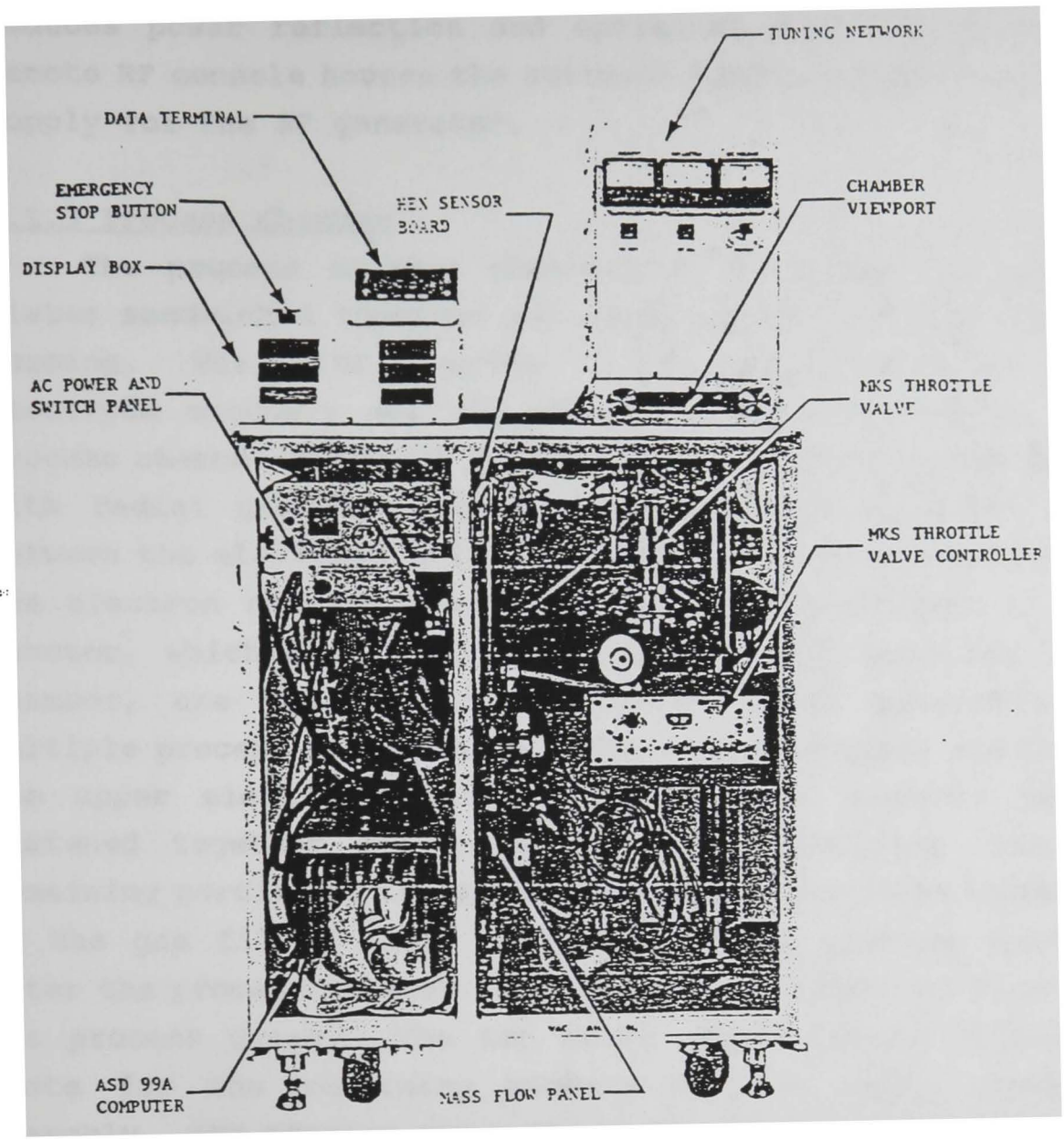

Figure 3.1: Plasma reactor assembly (reference Texas Instuments ASPR manual)

the computer system, an operator display RF tuning assembly, remote RF console and power supply. The RF tuning assembly reduces power reflection and optimizes power output. The remote RF console houses the automatic power control and power supply for the RF generator.

3.1.3 Process Chamber

The process chamber consists of a number of machined plates sandwiched together and attached to a central chamber housing. The major elements of the chamber are the upper electrode assembly and the chamber housing assembly. The process chamber incorporates a parallel plate electrode design with radial gas flow, with an oscillating electric field between the electrode and the substrate plate, which produces the electron and ion concentrations. The features in this reactor, which depart from the conventional parallel plate chamber, are the use of a non-flat upper electrode and multiple process gas entrance orifices in the upper electrode. The upper electrode assembly consists of numerous plates fastened together and is electrically insulated from the remaining portion of the process chamber. The first component is the gas filter block which allows the process gases to enter the process chamber. The block also houses a filter for the process gases. The top cover serves as an attachment plate for the remaining members of the upper electrode assembly. The process gases flow through a central passage in the top cover to the electrode. To insulate the electrode assembly from the process chamber, an insulating ring surrounds the edges of the spacers and electrode.

The electrode plate is the final component of the upper electrode assembly. The upper side of the electrode plate has a gas plenum chamber to equalize the flow from the multiple orifices. The gas orifices (24 total) are radially distributed with greater density toward the center. The lower surface of the electrode plate is in the shape of a shallow

inverted cone, thinning toward the edge. The upper electrode is connected to the RF generator through the tuning network to ensure maximum power transfer.

The primary components of the chamber housing assembly are the bottom plate and the view port. The bottom plate is the lower enclosing surface of the process chamber. The substrate plate assembly is fastened to the bottom plate with interposing spacers to provide an exhaust passage for the effluent gases. The bottom plate has numerous ports for various accesses to the chamber. The effluent gases are extracted from the chamber through the exhaust flange. The pressure in the chamber is monitored by the chamber pressure sensor assembly which is fitted to a port in the bottom plate. There is a port in the right side wall of the process chamber housing for the optical emission detector signal.

3.1.4 Process Gas Facilities

Up to four process gases can be supplied at any time. This work mainly employed CF_4 and O_2 with argon as the actinometric gas. A port for hydrogen was also provided. Each process gas is passed through the following components in sequence: an electronically operated solenoid valve, a mass flow controller, a normally closed air operated bellows valve, a process gas plenum chamber and a normally closed air operated valve on top of the chamber. The solenoid valves are software controlled and the normally closed air operated valves are safety features in case of machine failure. The normally closed valves are opened by air from electronically actuated solenoid valves. The normally closed valve, above the chamber, is the valve which allows the process gases to be admitted to the process chamber. Process gas is piped in through the floor of the machine directly to the mass flow panel. A hardware interlock is incorporated to keep the solenoid valve closed unless the chamber is at vacuum. Chamber gases are exhausted through the high vacuum pump.

3.1.5 High Vacuum System

The high vacuum system is supported by a direct drive rotary vane pump and is used to pump down the process chamber and exhaust the process gases. Connection is made between the pump and the reactor via 2 inch (5 cm) inside diameter tubing. The MKS Instrument Incorporated manufactured throttle valve controls chamber pressure by metering the flow to the pump in response to signals received by the software controlled stepping motor.

The chamber pressure monitor sub-system communicates the chamber pressure to the computer. The three primary components of the monitor are the vacuum switch, isolation valve and manometer. The combined function of these components is to allow the pressure monitor (MKS Instruments Incorporated manufactured manometer) to be exposed to the chamber vacuum when the chamber pressure is below a specified limit. The vacuum switch serves the function of switching 24V dc through a relay to the gas flow solenoids and the R.F. generator. In this way these systems are interlocked OFF unless the chamber is at vacuum.

3.1.6 RF Power Generation System

The purpose of this system is to supply the Radio Frequency (RF) electrical power which causes a discharge of electrons resulting in the formation of a plasma. The principal unit of the system is a 500 watt radio frequency generator operating at 13.56 MHz. It consists of a crystal controlled oscillator driving a single-ended RF power amplifier through a buffer stage. The output of the power amplifier is connected to the tuning network. The generator is normally switched ON and OFF by the computer through the signal provided to a D/A output board. It can also be switched ON and OFF by using the switches on the tuning network. An automatic power control unit is used with the RF generator. The automatic and regulated modes are used during

normal operation. Either of these modes can be selected by using the appropriate position of the PROCESSOR/OPERATOR switch. The automatic mode of operation is selected by placing the switch in the "processor" position. The computer receives a sample of both forward and reflected power and controls the "set RF" signal. The purpose of the matching or tuning network is to maximize the power dissipation in the discharge and to protect the generator. Power dissipation in the discharge is maximized when the impedance of the power supply along with its associate cabling and the conjugate impedance of the discharge chamber and the tuning network combined are equal. The matching network is placed close to the discharge chamber so as to avoid power losses due to the large reactive currents flowing between the matching network and reaction chamber.

3.2 Pressure Controller System

The control system shown in Figure 3.2 consists of two basic parts: (1) the pressure sensor and (2) the controller and control valve. The pressure sensor is a MKS Baratron^{R} Capacitance manometer whose output is 0 to 5 V (volt) dc. Since the input flow rate is controlled by the mass flow controllers, the system pressure is maintained by controlling the flow out of the reactor. The dc pressure transducer signal is scaled to obtain a pressure reading, compared to the setpoint and the valve positioned, so that it will drive the actual pressure to the set pressure.

The front panel controls shown in Figure 3.3 are used to control the exhaust valve controller. The Int/Ext switch (2) is used to select whether the valve is to be driven by an external signal from the computer or by the existing Type 252 exhaust valve controller. Other important settings are the valve mode switch (9) which is maintained in the EXT position as external open and close commands will only be accepted in this mode. The OPEN/CLOSE switch (8) allows the operator to

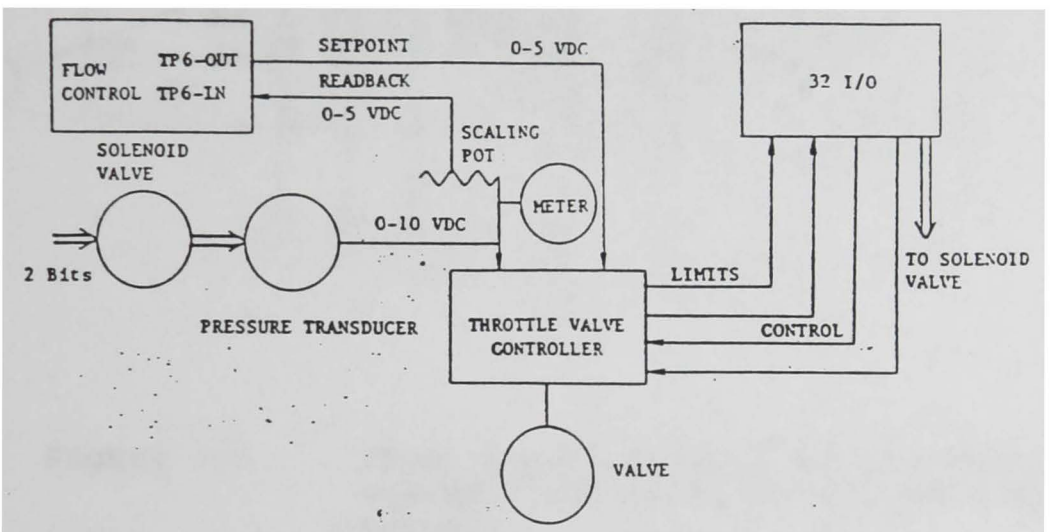

Figure 3.2: Pressure controller system (reference Texas Instuments ASPR manual)

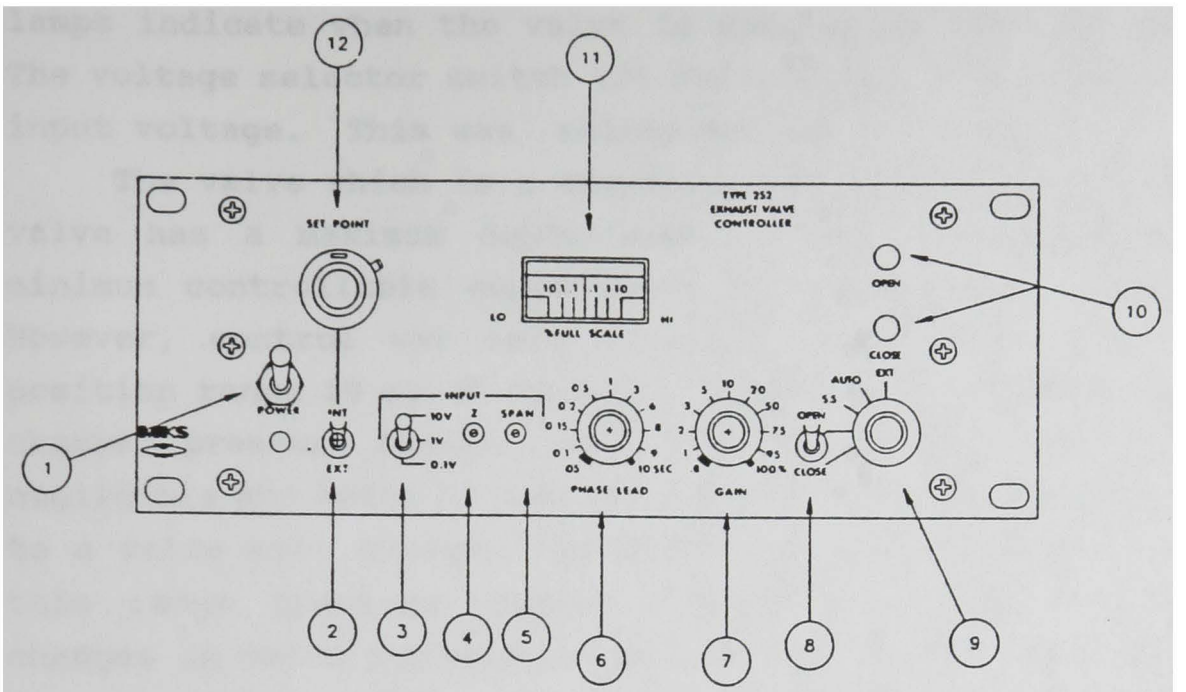

Figure 3.3 Front panel controls for pressure control system (reference Texas Instruments ASPR manual).

manually control the valve. This feature, along with the open and close lamps (10), was extensively employed during valve calibration to ensure the actual position of the valve. The lamps indicate when the valve is completely open or closed. The voltage selector switch (3) selects the full range of the input voltage. This was maintained at 10 V (volt).

The valve which is a standard 1 inch (2.5 cm) butterfly valve has a maximum conductance of 150 liters/sec and a minimum controllable conductance of about 0.15 liters/sec. However, control was only possible within the valve stem position range 20 to 65 degrees. Above 65 degrees the plasma chamber pressure change, with change in valve position was negligible and below 20 degrees the chamber pressure increased to a value well outside the plasma operating range. Within this range pressure changed appreciably with even small changes in valve percentage opening thus making it difficult for accurate control. The valve is controlled by a stepper motor which receives digital pulses from the A/D board. The analog signal may be a 0 to 10 V (Volt) or a 0 to 1000 mV (millivolt) signal depending on the accuracy or the resolution required. The actual number of degrees which the valve was supposed to turn was divided into increments of 0.2 degrees. The computer then sent a signal to the board for that period of time it took for a valve to turn 0.2 degree. This was determined from the time it took the valve to move from a full open to full close position or vice-versa. The frequency at which this signal was sent was adjusted to make the response of the valve either slower or faster. The frequency was adjusted to 100 Hz such that the valve took approximately 6 seconds to move from the fully open to the fully close positions. The program written to drive the valve was set up such that a dummy DO-loop ran for that period of time it took the valve to move 0.2 degree. The signal was then "immediately" stopped so that the valve did not move any more than required. This operation was repeated until the

necessary valve position was attained. Sample calculations for a 1 degree change in valve position are outlined.

Step 1: Determine the number of times the valve is required to move;

$$N = \frac{1^{\circ}}{0.2^{\circ}/move} = 5\ moves. \qquad (3.1)$$

Step 2: Time required by the valve to move 0.2 degrees

$$\frac{6.25\ (sec/90^{\circ})\ x\ 0.2^{\circ}}{90^{\circ}} = .013888\ sec/.2^{\circ}. \qquad (3.2)$$

This time is allowed to elapse on the computer by running a dummy DO loop.

Step 3: Determine an approximate value for this counter.

An approximate value for the counter for this loop was obtained by running a test loop for a large number of iterations and determining the time it took to achieve the required count. For example to run a loop of 100000 counts took 22.35 seconds on the Packard Bell PB286 12 MHz personal computer used for interfacing. Hence an approximate value for our dummy DO-loop counter was

$$\frac{.013888(s/.2^{\circ})\ x\ 100000}{22.35\ s} = 62.14\ counts/.2^{\circ}. \qquad (3.3)$$

This dummy DO-loop was then executed for the number of times the valve was required to move.

Plumbing and tubing between the pressure transducer and the chamber is maintained less than six inches long and no less than .25 inch in diameter. The exhaust control system can be externally controlled with two inputs on the interface connector.

3.2.1 Development of Valve Characteristics

The final control element often determines the effectiveness of control. To accurately determine the valve characteristics is important. Changes in the leak rate and

the vacuum suction pressure affect the determination of parameters such as the valve coefficient. However, the general shape of the valve characteristic curve remains the same.

For gas and vapor service at subcritical flow (Masoneilan, 1993) the flow through a valve is given by,

$$Q = a \cdot f(s) \cdot \sqrt{\Delta P \cdot (P_1 + P_2)} \tag{3.4}$$

or,

$$Q = a \cdot f(s) \cdot \sqrt{P_1^2 - P_2^2}, \tag{3.5}$$

where, Q = Volumetric flow rate at standard conditions,
P_1 = Pressure upstream of the valve,
P_2 = Pressure downstream of the valve,
f(s) = Inherent valve characteristic,

and,

$$a = K \cdot C_v, \tag{3.6}$$

where, K = a constant for a given gas at a constant temperature,
C_v = valve flow coefficient.

The upstream pressure is the measured reactor chamber pressure, P, and the downstream pressure is the vacuum pressure, P_v. Substituting these in Equation (3.6) the final form of the equation employed is,

$$Q = a \cdot f(s) \cdot \sqrt{P^2 - P_v^2}. \tag{3.7}$$

The vacuum suction pressure, P_v and the constant "a" were first determined before determining the valve characteristics. The constant "a" includes the valve flow coefficient C_v. C_v can only be determined at conditions when the valve is completely open as the valve flow coefficient is defined as the flow through the valve at standard conditions when the

valve is at its fully open position. For this case the inherent valve characteristic, f(s) is unity. Squaring Equation (3.7) and substituting f(s)=1, gives,

$$Q^2 = a^2 \cdot (P^2 - P_v^2) . \qquad (3.8)$$

Taking logarithms on both sides gives,

$$\log(Q^2) = \log(a^2) + \log(P^2 - P_v^2) . \qquad (3.9)$$

This equation has the form of a straight line given by,

$$y = mx + c, \qquad (3.10)$$

where, $y = \log(Q^2)$,
$x = \log(P^2 - P^v_2)$,
$m = 1$,
$c = \log(a^2)$.

The experimental data was obtained by measuring the pressure in the outlet line upstream of the completely open valve for different gas flow rates and was regressed using Equation (3.9). The regression involved experimenting with various values of P_v till the slope of the regressed line reduced to unity. This value was used to calculate the constant "a" from the intercept of the regressed straight line. It was observed that vacuum suction pressure increased with increasing flow and hence a wide range of flow conditions were employed. Flow rate was varied from 25 sccm to 200 sccm at intervals of 25 sccm to ensure accuracy.

The valve characteristics were determined using Equation (3.7) in its rearranged form given by,

$$f(s) = \frac{Q}{a \cdot (P^2 - P_v^2)} . \qquad (3.11)$$

For a given flow rate, which was maintained constant for a single set of readings, the valve position was varied in small increments and the pressure for each valve position noted. To

ensure accuracy increments of 1 degree in valve travel were made in the region where the maximum pressure change was observed. The valve had significant hysterisis and hence the pressure was noted for both cases, that is, with the valve changing its position from open to close and vice-versa. These values were averaged and employed in Equation (3.11). Since all the quantities except f(s) were known a relationship between the inherent valve characteristic and the percentage valve opening are obtained. Hence, one set of f(s) values was obtained for valve positions ranging from completely open to completely close for a single flow rate. This set of experiments was repeated for 8 different flow rates ranging from 25 to 200 sccm at intervals of 25 sccm. Each set gave a distinct 'S' shaped curve. These values were then averaged to obtain a relationship between the inherent valve characteristic and the valve stem position. The details of these calculations are included in Appendix A. Figure 3.4 shows the valve characteristics.

3.2.2 Controller Hardware

The controller consists of two main sections the analog and digital sections. The analog section contains the input amplifier where the front panel zero is added to the pressure feedback signal. The full scale output of this amplifier is 5 volts. There is also a buffer amplifier for the external setpoint signal. It also has an output of 5 volts. The difference between the conditioned feedback signal and the setpoint signal is determined by a third amplifier which multiplies it by 0.5. The two digital signals used to drive the stepping motor are produced by two different amplifiers, which determine the direction in which the valve turns and which produce the pulses to advance the motor in the direction decided.

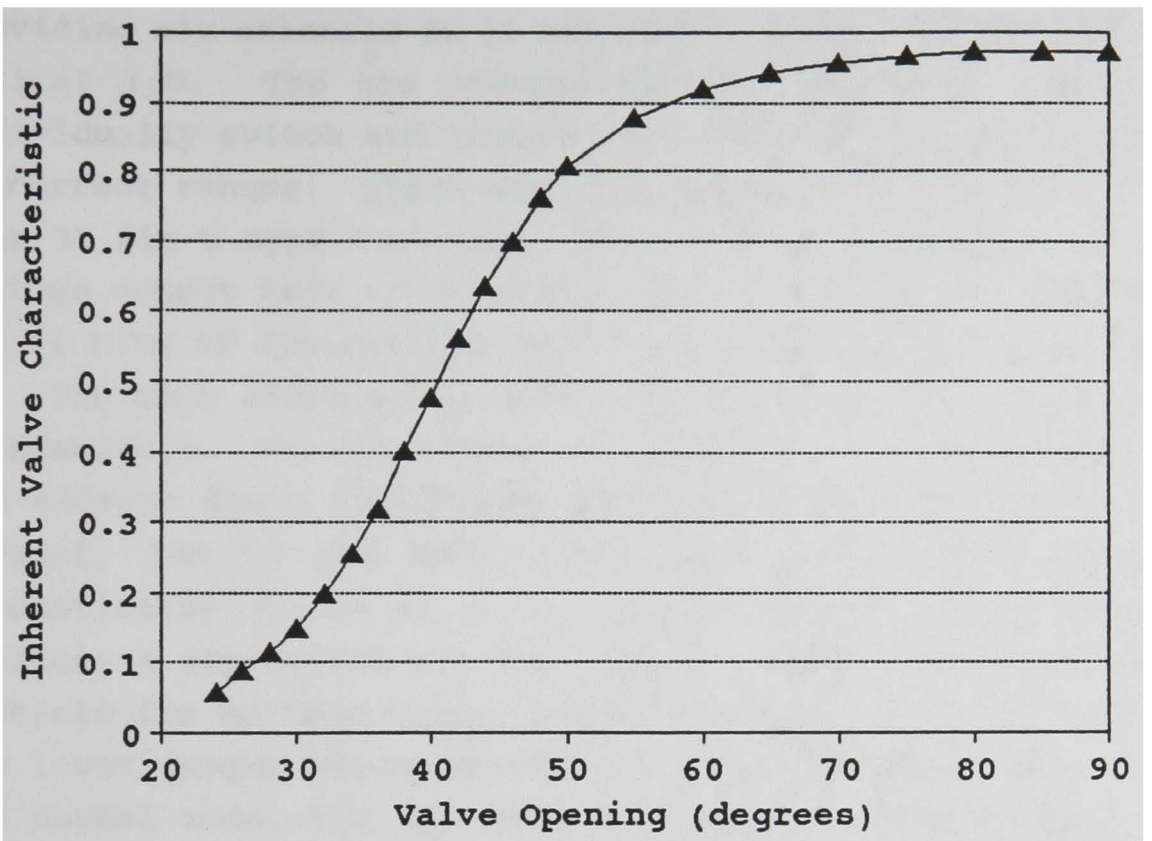

Figure 3.4 Inherent valve characteristics.

3.2.3 Interfacing

A DDA-06 Analog/Digital Expansion Board (Keithley Metrabyte Corporation, 1985) is used to exchange information between the computer and the system. DDA-06 is an D/A and A/D Input/Output expansion board for the IBM personal computer providing six channels of 12 bit analog output and 24 lines of digital I/O. The six independent D/A converters are each individually switch and jumper selectable to any of 6 voltage or current ranges. Since each D/A output uses one pin of the rear 37 pin D type connector, they may be operated in either voltage output mode or current output mode, but not together. The 24 bits of digital I/O consist of 3 ports of 8 bits each.

The base address dip-switch has been set for &H300 (300 Hexadecimal). The DDA-06 uses 16 consecutive addresses in the I/O address space (available addresses run from 256 to 1008 decimal, 100 to 3FO Hex). The base or starting address automatically falls on a 16 bit boundary. Each channel includes a dip-switch and two jumper blocks. The dip-switch controls the voltage output range of the D/A of that channel. The lower jumper block controls the data transfer mode. In the normal mode, the D/A mode will update after writing the high byte. The upper jumper block controls whether the channel output is voltage or current. There are three types of operations that can be performed by each I/O device. These are (1) Read only (R), (2) Write Only (W), and (3) Read/Write (R/W). A read of any address in range Base + 0 through B performs a simultaneous update of those D/A's jumpered for this task.

The twelve bits are divided into four most significant bits and eight least significant bits. Data is written to the D/A's in true binary right justified form. When writing to any D/A port the data is first split into high and low bytes. Once the division of the bytes is achieved it is written to the selected D/A ports. This type of execution occurs when simultaneous updating is not selected.

3.3 Optical Emission Spectroscopy

3.3.1 Measurement Principles

Optical emission spectroscopy is among the more popular plasma diagnostic techniques used to determine concentrations of species. It is relatively simple, non intrusive and is based on the fact that the intensity of emissions from electronically excited species is proportional to the density of that species in the plasma. The intensity is both a function of the density of the species as well as the electron energy distribution function, and changes in plasma parameters affect both these plasma characteristics. As a result monitoring the number density of reactive species becomes infeasible. To overcome this problem Coburn and Chen (1980) suggested adding a small amount of noble gas to a reactive plasma and monitoring the emissions of that gas concurrently with those of the reactive particles. Since the noble gas (normally Argon) density is known, the excitation efficiency of any of its levels is determined simply by dividing the emission intensity of that level by the noble gas density. If the excited state which causes the light emission from the reference gas has approximately the same energy level as that responsible for an emission from a reactive species, then the same group of electrons will be responsible for the excitation of both levels. In the case of a hypothetical species "x,"

$$I_x = k_x \cdot n_x \cdot \eta_x, \tag{3.12}$$

where, I_x is the optical emission intensity from species x, n_x is the density of species x in the ground state, η_x is the excitation efficiency of the discharge to promote species x from the ground state to the electronically excited state responsible for the optical emission and k_x is a proportionality constant. Their approach assumes that,

$$n_F = k \cdot \eta_{Ar}. \tag{3.13}$$

This assumption is reasonable if the energies of the excited

states responsible for the optical emission are similar in energy for both species of interest. Thus Equations (3.12) and (3.13) when combined give,

$$\frac{n_F}{n_{Ar}} = K \cdot \frac{I_F}{I_{Ar}}. \qquad (3.14)$$

Since I_F and I_{Ar} are measured, n_{Ar} is known and K is a constant independent of the discharge parameters, changes in n_F can be easily determined.

Donnely et al. (1981) checked the validity of this method for a CF_4/O_2 plasma by simultaneously checking the fluorine concentration with a titration method and found both to be in agreement within experimental error.

3.3.2 Optical Emission Detection System

The major components of the light detection system, shown in Figure 3.5, are a light collector, spectrograph, light detector, detector interface and a host computer. The light is collected and sent to a spectrograph which separates the different wavelengths of light. The detector determines the intensity of the different wavelengths of light which are sent to the computer, via the detector interface, where they are displayed. The light emissions are collected through a small window on the side of the reactor chamber approximately between the lower and upper electrodes. A flexible cable consisting of optical fibers is used to collect plasma light emissions.

The spectrograph is an EG&G PARC Model 1229 spectrograph. Light enters the instrument through the entrance slit and strikes the collimating mirror, from where it is reflected to the grating. The grating defracts the light into its component wavelengths and directs them to the focussing mirror which reflects the light out of the exit assembly.

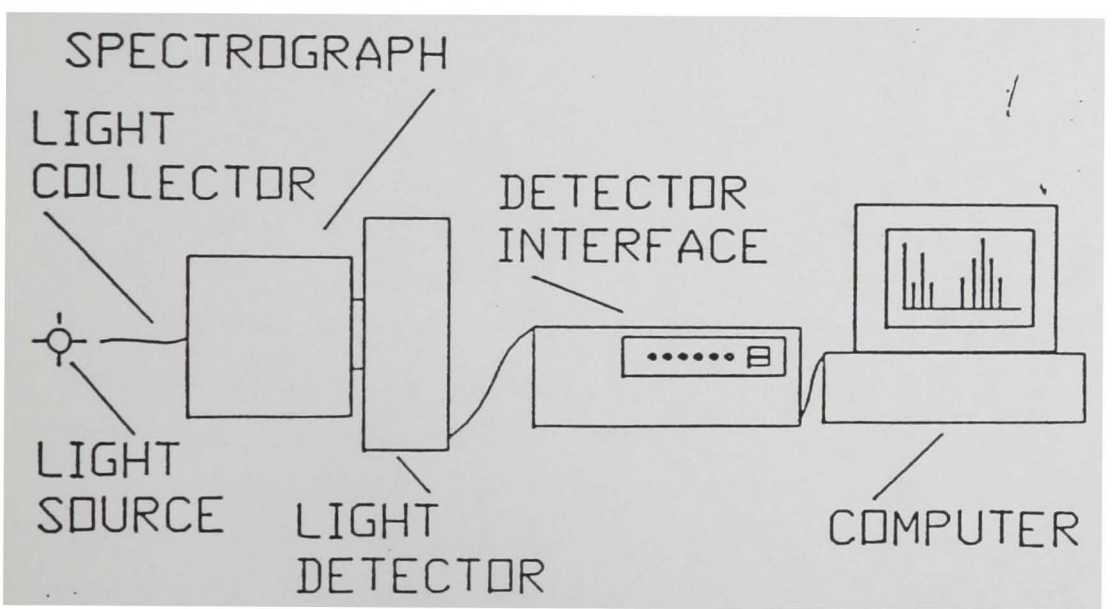

Figure 3.5 Optical emission detection system.

The light detector is a EG&G PARC Model 1452A detector. The detector has an array of 512 silicon photodiodes spaced along the diffracted light path, which senses the 512 wavelengths coming from the spectrograph. The detector senses the intensity of light and sends an analog signal to its controller which is mounted on the detector interface. The detector interface is an EG&G PARC Model 1461 interface. The detector interface along with its controller and detector are referred to as an Optical Multichannel Analyzer (OMA). The OMA system is run through software present in the host computer. The computer has an IEEE-488 General Purpose Instruction Bus (GPIB) board that it uses to communicate with the detector interface.

CHAPTER 4

DEVELOPMENT OF THE DYNAMIC SIMULATOR

4.1 Introduction

As a first step to designing and testing the pressure controller, a simulator, which qualitatively described the features of the process, was developed. The aim while developing the simulator was to try and make it as phenomenologically sound and yet try to reproduce the characteristics of the process. Various approaches which were attempted are documented.

4.2 Approach Based on First Principles

Initially an extremely simple approach based on an input-output mole balance type of relationship was developed. This accounted for a single gas entering the reactor (CF_4), its dissociation into new species as a result of the voltage supplied and subsequent removal of both the new species formed as well as the unreacted species. From previous measurements on similar systems (Singh, 1990) it was noted that dissociation of CF_4 varied from 10 to 15%. Since dissociation is a function of electron density which in turn is a measure of the transmitted power, dissociation was modelled as a function of power. As described in the previous chapter, the entire amount of power supplied by the source is rarely utilized by the plasma. A part of it is reflected, some losses take place due to heating etc. The reflected power is maximum when the supply is turned on. The matching network minimizes reflected power such that it decreases with time. The relationship between reflected power and time is empirical and differs from matching network to matching network.

This relationship was modelled as an exponential decay of the form,

$$R = R_0 \cdot \exp\left(-\frac{t}{\tau}\right), \qquad (4.1)$$

where, R = reflected power at any time t,
R_0 = reflected power at time t = 0, effectively some fraction of the incident power,
τ = time constant for decay, approximately 1/3 the time taken for the reflected power to reach its minimum value.

The dissociation was then expressed as a function of transmitted power using a power law relationship of the form,

$$\alpha = a \cdot (W-R)^{b}, \qquad (4.2)$$

where, α = dissociation,
W = incident power,
R = reflected power,
a,b = constants in the power law relationship.

This form was chosen based on observed process behavior at the initiation of the discharge. There was a sudden creation of new species followed by a gradual increase to its final steady state value. A power law type of relationship satisfied these observed charateristics and was hence employed. The power law constants were calculated using previous experimental data which related dissociation to incident power. This type of modelling led to a dissociation versus time relationship having a characteristic first order type of the response. The final equation was of the form,

$$V_R \cdot \frac{dC_{tot}}{dt} = (Q_i + Leak\ Rate) \cdot C_{tot} \cdot \alpha - Q_o \cdot C_{tot}, \qquad (4.3)$$

where, V_R = volume of the reactor,
Q_i & Q_o = volumetric flow in and out,
C_{tot} = total concentration of all species,

α = dissociation.

This same relationship in terms of pressure can be expressed as,

$$\frac{dP}{dt} = \frac{[(Q_i + Leak\ Rate)\cdot P\cdot\alpha]}{V_R} - \frac{[Q_o\cdot P]}{V_R}. \qquad (4.4)$$

The underlying assumption in this type of modelling was that the net dissociation at any point in time was independent of all other quantities except power. This simplistic model failed to account for the fact that the dissociation reactions were faster than the slower recombination reactions. Dissociation actually increased sharply when the power was turned on due to the rapid creation of new species. With the resultant recombination of CF_4, the net dissociation gradually approached its steady-state value. This model failed to reproduce the same characteristics as that of the process and was not employed for future work. It however helped to indicate the importance of the kinetic scheme.

4.3 Development of a Simulator Involving Kinetics

Numerous researchers (Plumb and Ryan, 1986; Dalvie and Jensen, 1990; Kiss and Sawin, 1992) have reported a host of reactions taking place in CF_4 and CF_4/O_2 plasmas. Depending on the equipment used each study stresses the importance of certain reactions. However most studies, such as those of Dalvie and Jensen(1990) and Kiss and Sawin (1992) employ the reduced reaction set of Plumb and Ryan (1986) with the addition or modification of a few rate constants or reactions. The five reaction reduced set and the thirteen reaction reduced set proposed by Plumb and Ryan (1986), were employed in this work, for the case of CF_4 and CF_4/O_2 systems respectively. These are included in Tables 4.1 and 4.2, respectively.

Table 4.1 Reduced Reaction Set for CF_4 With Rate Constants (Plumb and Ryan, 1986)

Reaction	Rate Constant
CF_4 ----> CF_3 + F	$k_1 = 6\ s^{-1}$
CF_4 ----> CF_2 + 2F	$k_2 = 14\ s^{-1}$
CF_3 + F ----> CF_4	$k_3 = 1.3*10^{-11}$ cc/molecule-s
CF_2 + F ----> CF_3	$k_4 = 4.2*10^{-13}$ cc/molecule-s
CF_3 + CF_3 ----> C_2F_6	$k_5 = 8.0*10^{-12}$ cc/molecule-s

Table 4.2 Reduced Reaction Set for CF_4/O_2 With Rate Constants (Plumb and Ryan, 1986)

Reaction	Rate Constant
CF_4 ----> CF_3 + F	$k_1 = 6\ s^{-1}$
CF_4 ----> CF_2 + F	$k_2 = 14\ s^{-1}$
CF_3 + F ----> CF_4	$k_3 = 1.3*10^{-11}$ cc/molecule-s
CF_2 + F ----> CF_3	$k_4 = 4.2*10^{-13}$ cc/molecule-s
O_2 ----> O + O	$k_5 = 6.5 + 7.5 + 6 = 20\ s^{-1}$
CF_3 + O ----> COF_2 + F	$k_6 = 3.1*10^{-11}$ cc/molecule-s
CF_2 + O ----> COF + F	$k_7 = 1.4*10^{-11}$ cc/molecule-s
CF_2 + O ----> CO + 2F	$k_8 = 4.0*10^{-11}$ cc/molecule-s
COF + O ----> CO_2 + F	$k_9 = 9.3*10^{-11}$ cc/molecule-s
COF + F ----> COF_2	$k_{10} = 8.0*10^{-13}$ cc/molecule-s
COF_2 ----> COF + F	$k_{11} = 20\ s^{-1}$
CO_2 ----> CO + O	$k_{12} = 40\ s^{-1}$
CO + F ----> COF	$k_{13} = 1.3*10^{-15}$ cc/molecule-s

Initially the simulator used only those reactions which dealt with the dissociation and subsequent recombination of CF_4. The reactions dealing with CF_4/O_2 mixtures were incorporated later. The simulator consisted of a set differential equations with each equation representing a dynamic mole balance for each species in the reactor. A Runge-Kutta-Gill fourth-order method, with a variable step size was used to integrate these equations. The concentration of each species was thus obtained at each time step. Since the total transient time was only 4 to 5 seconds, to accurately represent the process required an extremely small step size in certain regions where the change in dependent variable with time was appreciable. The sum of the concentration of each species was then used to determine the pressure as a function of time using the ideal gas law as shown;

$$P = C_{tot} \cdot R \cdot T, \tag{4.5}$$

where, P = pressure at any time t,
R = ideal gas constant,
T = temperature in the reactor,
C_{tot} = total concentration at any time t.

The reduced reaction set consists of two main groups of reactions, the dissociation reactions and the recombination reactions. The latter are further sub-divided into two categories, three-body reactions and free radical gas phase reactions. The dissociation and recombination reactions have markedly different mechanisms and influence conditions in the reactor accordingly. This initially developed simulator assumed that all the reactions had the same influence over the entire volume of the reactor and did not account for these different reactor conditions. To remedy this flaw the concept of two regions was developed.

4.3.1 The Concept of Two Regions

The geometry of the reactor is such that it can be distinctly divided into two regions, the dissociation zone between the two electrodes and the non-dissociation zone which includes the rest of the reactor including the space under the bottom electrode as well as the outlet line up to the exhaust valve. The region between the two electrodes is where the highly energized electrons collide with the CF_4 molecules and cause its dissociation. On the other hand the walls of the reactor and the outlet line serve as the third body for the recombination reactions and hence these reactions along with neutral gas phase free radical recombination reactions dominate in the region termed as the "afterglow." This understanding of the relative importance of the reactions led to the incorporation of two regions in the simulator. In the region between the electrodes both electron-aided dissociation reactions as well as recombination reactions take place. Hence, terms pertaining to both these types of reactions were included in the mole balance for each species. The rest of the reactor, which effectively constitutes the non-dissociation zone, incorporates only the recombination reaction rate terms in the individual mole balances.

Inherent in this two region concept was the underlying assumption that many other studies (Schoenborn et al., 1989; Dalvie and Jensen, 1990) have also made, that of the total concentration being uniform throughout the reactor, that is it was modelled as a Continuous Flow Stirred Tank Reactor (CSTR). This enabled the explicit determination of the total molar flow from region 1, the dissociation region, to region 2, the non-dissociation or fall-off region. Thus, while there may be a spatial distribution in the individual species concentrations, the total concentration and hence the total pressure in each region remain the same.

The fraction of the total volume occupied by each region was determined first before employing the concept of the two regions. The volume was measured using a standard experimental procedure which gave a reasonably accurate result. A small known volume of gas at atmospheric pressure is passed in to the evacuated chamber and the resulting increase in pressure noted with time. The total volume of the reactor was then determined using the ideal gas law as the low pressure conditions cause the gas to be near ideal conditions. The detailed calculations are included in Appendix B. The final equation is of the form,

$$V_r = \frac{p.\frac{dQ}{dt}}{\frac{dp}{dt}}, \qquad (4.6)$$

where, P = pressure at which the gas enters the reactor (standard pressure),

V_R = volume of the reactor,

Q = volumetric flow at standard conditions,

R = gas constant,

T = temperature of the gas in the reactor,

p = pressure in the reactor.

The exhaust valve was closed and the increase in pressure noted for three different flow rates. The change in pressure with time was the effective rise in pressure, that is, the observed increase in pressure less the pressure rise due to leaks into the reactor.

Pressure increased almost linearly with time and hence the slope of the line was used to account for the derivative term in Equation (4.6). Each set of readings was used to obtain the reactor volume and the average of these values employed in all subsequent calculations. The average volume was 2750 cubic centimeters (cc).

The leak rate was determined by first closing the valve and noting the rise in pressure with no gas flowing into the

reactor. Equation (4.6) when rearranged gives the leak rate;

$$\frac{dQ}{dt} = \frac{V_R \cdot \frac{dp}{dt}}{P \cdot R \cdot T}. \qquad (4.7)$$

The leak rate changed every time the reactor was opened and hence only an approximate value of the leak rate could be obtained which was 10 mtorr/sec. The fraction of the total reactor volume occupied by each region was obtained from the physical dimensions of the reactor. The reaction zone consists of the region between the bottom electrode plate and the top electrode mesh and the surrounding region within the square boundaries of the reactor chamber. The reaction chamber was approximately 1780 cc which implied that the dissociation region occupied approximately 65% of the total reactor volume.

4.3.2 Importance and Effect of Each Group of Reactions

To actually obtain a "feel" of the process, a thorough study of the kinetics and their effect on the simulator was carried out. As mentioned previously there are two main sets of reactions: dissociation and recombination reactions, with the latter being further sub-divided into two types. CF_4 system kinetics involve two dissociation reactions and three recombination reactions. Plumb and Ryan (1986) concluded that the dissociation of CF_4 into CF_2 was almost twice that of CF_4 to CF_3. This work employed the same ratio. The three recombination reactions are all three body reactions. In these type of reactions a third body takes part in the collision process and this third body allows the recombination process to simultaneously satisfy the conservation requirements of energy and momentum. The third body is often a wall, ubiquitous in any plasma reactor, or it may be another gas atom. The probability of the gas atom taking part in the process will increase with increasing pressure and hence total

concentration. The most significant reaction from among these three body recombination reactions is reaction 3 of Table 4.1. The dissociation reaction rate constants are based on measured values of conversion of CF_4 as well as electron density. As Plumb and Ryan (1986) suggest they may be wrong by more than an order of magnitude. However, these were the best estimates available and hence they were employed in the simulator.

For the case of CF_4/O_2 mixtures the kinetics are even more complicated. The reduced sub-set of 13 reactions includes gas phase recombination reactions between neutral species. Oxygen is added to enhance etching as it prevents the recombination of free fluorine atoms with neutral CF_x radicals, by reacting with the radicals to form a wide range of oxidized products and additional free fluorine. The general reaction is,

$$CF_x + O \dashrightarrow COF_{x-1} + F. \qquad (4.8)$$

This reaction also serves as a source of free fluorine . It was suspected that these reactions take place in both the dissociation as well as the fall-off regions and hence, all the kinetic terms pertaining to these reactions were included in the dynamic mole balance for both regions. These reactions are not directly dependent on parameters such as electron density or total concentration. There are four reactions of this type in the reduced set.

The three body recombination reactions are normally restricted to the fall-off region, and their importance is accentuated for reactors where the residence time is large and where the fall-off region occupies a sufficiently large volume of the reactor. These reaction rate terms have been included in the equations pertaining to both regions because there is always a probability of these reactions taking place in the dissociation region as well. This probability arises due to the increased concentration in the dissociation zone owing to the rapid formation of new species. The rate constants

supplied are valid for a pressure of 500 mtorr. These can be adapted for any pressure based on literature values of "sticking coefficients" and collision diameters. Four such reactions are incorporated in the simulator.

The possibility of including three body reactions as part of the "fall-off" region, only, was also explored. This possibility was based on the observation that the residence time in the dissociation region was extremely small and hence these reactions being kinetically "slower" would not have a very large effect on the dynamics of the process. However, including three body reactions as part of the "afterglow" only failed to reproduce the process characteristics obtained from spectroscopic measurements and were hence not employed. The detailed differential equations representing the mole balance for each species in the simulator are developed in Appendix C.

4.3.3 Incorporating Fluid Dynamics

As mentioned previously the inherent valve characteristics were nonlinear. Hence, a nonlinear function of the form shown in Equation (4.9) was used to model these characteristics.

$$f(s) = \frac{A \cdot e^{-\frac{b}{s}}}{1 + A \cdot e^{-\frac{b}{s}}}, \qquad (4.9)$$

where, f(s) = inherent valve characteristic,
s = percentage valve opening,
A,B = regressed constants.

The constants A and B were obtained by performing a linear regression. The data was first put in the form of an equation representing a straight line by rearranging and taking the logarithms on both sides of Equation (4.9) to give,

$$\ln\left[\frac{F(s)}{1 - F(s)}\right] = \ln(A) - \frac{B}{s}. \qquad (4.10)$$

This is of the form,

$$y = mx + c, \tag{4.11}$$

where, $y = \ln(Y)$ and $Y = F(s)/(1 - F(s))$,

$m = -B$,

$x = 1/X$,

$c = \ln(A)$.

Data used for the regression corresponded to pressure readings for valve stem position ranging from 25% open to 70% open. The rationale being, that at the lowest flow rate employed (25 sccm) the lower operating pressure limit (200 mtorr) was attained with the valve 25% open, and at the highest flow rate the upper operating pressure limit (900 mtorr) was attained with the valve 70% open. This data set gave sufficiently accurate regressed parameters. The advantage of using a continuous explicit function is that it can be easily solved, by rearranging its form, so that the dependent variable becomes the independent variable and vice-versa.

Other relationships to represent the inherent valve characteristic were also experimented with including a power law type of relationship and a nonlinear regressed relationship. A single power law relationship was not sufficient to describe the entire curve and the region of operation had to be divided into three sub-regions and a power law fitted to each region. The nonlinear equation represented the characteristic curve adequately, but involved solving a cubic equation at each control interval in order to determine the appropriate valve stem position from the inherent valve characteristic. This would involve considerably greater computation than solving an explicit relationship. Based on the above arguments the relationship given in Equation (4.9) in the simulator was employed. The comparison between the experimentally obtained valve characteristics and the regressed curve fit is shown in Figure 4.1.

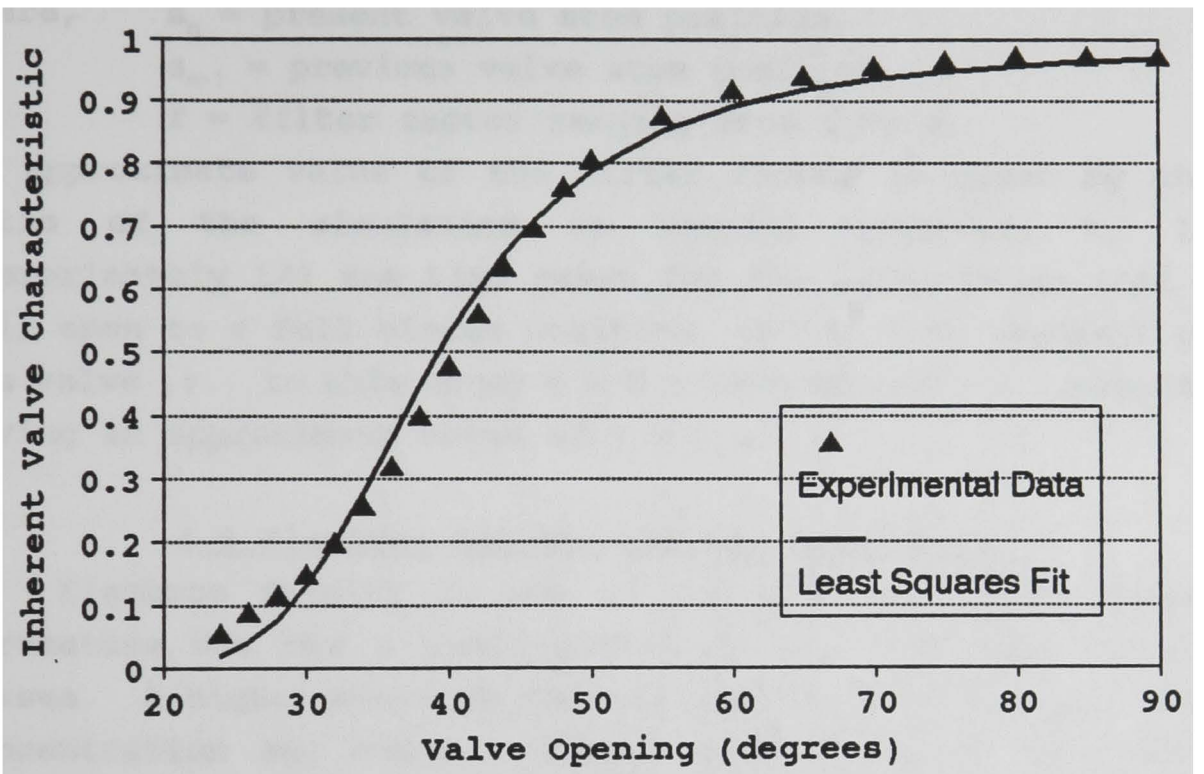

Figure 4.1 Comparison between experimental and modelled Inherent valve characteristics.

Valve dynamics were also incorporated in the simulator. A simple first-order filter of the form given in Equation (4.12) was used to represent the time lag in the operation of the valve. The filter is given by,

$$s_n = s_{n-1}\cdot(1 - f) + s_n\cdot f, \qquad (4.12)$$

where, s_n = present valve stem position,
s_{n-1} = previous valve stem position,
f = filter factor ranging from 0 to 1.

An approximate value of the filter factor is given by the ratio of the simulation or control interval, t, to approximately 1/3 the time taken for the valve to go from a full open to a full closed position, or the time constant of the valve ,τ. In this study $t \approx 0.2$ seconds and $\tau \approx 2$ seconds giving an approximate value of $f \approx 0.1$.

4.4 Electron Density and its Importance

Electron density is one of the most important plasma parameters and has a great effect on the character of the plasma. A higher electron density implies a higher electron concentration and hence a larger probability of collision between an energetic electron and a ground state species. Higher electron densities lead to higher dissociation rates. Electron density is a function of the power density with the number of electrons generated being higher when a larger amount of power is supplied. Hence, a direct correlation exists between power density and dissociation.

Plumb and Ryan (1986) have reported their first-order dissociation rate constants as a function of their electron and power densities. Since the reactor geometry and the conditions employed differ substantially in this study from those they have employed the electron and power density will also differ. Hence, the rate constants employed in the simulator in this work have been scaled based on the electron density ratio. Schoenborn et al. (1989) have used power

density to scale their dissociation rate constants. This work employs electron density as a scaling factor rather than power density, as electron density is a more direct measure of the dissociation taking place. This is based on the fact that each first order dissociation reaction can be expressed in terms of electron density as follows:

$$CF_4 + e^- \longrightarrow CF_3 + F + e^-. \qquad (4.13)$$

The reaction rate is therefore given by,

$$r_{CF_4} = -k\cdot[CF_4]\cdot[e^-]. \qquad (4.14)$$

Thus each dissociation kinetic rate term is actually proportional to the electron density.

Generalized correlations were used to estimate electron density as the use of an electrostatic probe proved to be unsuccessful. These correlations are functions of an important plasma parameter, Λ, the electron diffusion length which has units of length. For a self-sustained plasma a specific area per volume ratio must be maintained. This constraint is obtained from an electron diffusion-production balance. The electron diffusion length is dependent on the reactor geometry and the diffusivity of electrons in the medium. The average electron density is calculated from a knowledge of the gas pressure and the electron diffusion length. Detailed calculations based on the reactor geometry and plasma conditions employed in this work are included in Appendix D. The approximate electron density obtained was then used to scale the dissociation rate constants as follows;

$$k_{scaled} = k_0\cdot\frac{n_e}{n_{e0}}, \qquad (4.15)$$

where, k_{scaled}= scaled constant employed in the simulator,

k_0 = rate constant used by Plumb and Ryan (1986),

n_e = estimated electron density,

n_{e0} = base case electron density that is electron density used in the work of Plumb and Ryan (1986).

The scaled reaction rate constants were not able to produce the same amount of dissociation as that experimentally observed and hence the scaled electron density was multiplied by a factor of 5. This scaling factor was chosen solely on the basis of the observed open-loop responses and kept constant for all subsequent validation studies.

CHAPTER 5
VALIDATION OF THE SIMULATOR

5.1 Introduction

Before the simulator developed could be used for control studies it had to be ascertained that the simulator was an adequate representation of the process. This involved validating the simulator with experimental data. Both dynamic as well as steady-state data were employed. Dynamic data employed included responses in time to both setpoint changes as well as disturbances. Steady-state bench-marking was done using the data obtained from optical spectroscopic measurements. The process of bench-marking and validation involved the definition of a nominal operating point and the state space around it. This procedure helped reduce the number of experiments to a minimum.

5.2 Development of the Experimental State Space

Three parameters were varied in order to ascertain the characteristics of the process. These were pressure, total flow rate and the composition, that is the oxygen content of the feed. For any single experiment two of these parameter were kept constant and one was varied. The range of conditions were selected such that the region of operation remained true to the conditions generally found in Reactive Ion Etching (RIE) processes. Pressure was varied from 300 to 900 mtorr, total flow from 80 to 160 standard cubic centimeter per minute (sccm) and oxygen content from 0 to 50%. Power was kept constant at 100 W as changes in power caused the electron energy distribution to change, thus altering the electron density. The simulator, on the other hand, employed a constant electron density as a relationship could not be established between incident power and electron density. Pressure was varied in steps of 150 mtorr, total flow in steps

of 20 sccm and oxygen content in the feed, in steps of 5%. For the dynamic tests the nominal operating point was chosen to be at 500 mtorr with flow being varied between 80 and 100 sccm and oxygen content from 0 to 25%. The experimental steady-state tests are detailed in Table 5.1.

In order to carry out the dynamic open-loop tests the reactor chamber was pumped down to the nominal operating pressure. The power was then turned on and the process allowed to reach steady state after absorbing the effect of the power disturbance. A second disturbance was then created by either changing the total flow or both the total flow and oxygen content. Step tests performed included changing the valve position and observing the pressure response.

Steady-state bench-marking involved measuring the intensity of emission of atomic fluorine (F), atomic oxygen (O) and argon. These were obtained using the optical spectroscopic method presented in Chapter 3. The ratio of the concentrations of fluorine to argon and oxygen to argon were calculated and scaled by a proportionality constant which effectively represented a host of parameters which were independent of the discharge including emission probabilities, excitation efficiencies, etc. The intensity ratio was then compared with the scaled concentration ratio of the same two species obtained from the simulator. All simulator measurements were obtained from the dissociation region (region 1) as they corresponded to those obtained experimentally from the region between the top and bottom electrodes in the reactor. The emission intensities obtained represent an averaged intensity of light emission by a particular species during the period of the scan. These experimental measurements correspond to the concentration measurements obtained from the simulator after the initial transient is over and the concentration of the species concerned has reached a steady value. In order to obtain accurate results the reactor needed to be conditioned for at

Table 5.1: Design of Experiments For Steady-State Tests.

Pressure (mtorr)	Flow rate (sccm)	O_2 Content (Percent)
300	120	25
450	120	25
600	120	25
750	120	25
900	120	25
600	80	25
600	100	25
600	140	25
600	160	25
600	120	25
600	120	0
600	120	5
600	120	10
600	120	20
600	120	30
600	120	35
600	120	40
600	120	45
600	120	50

least twenty minutes or more, especially when using oxygen. To eliminate the effect of any random disturbances each experiment was carried out for a time period of at least eight minutes. During this period three measurements were normally taken at times of three, five and seven minutes. It was observed that the intensity ratios calculated from the measurements obtained at five and seven minutes were significantly closer in value than those obtained at three and five minutes. This meant that the reactor conditions had not stabilized even though five minutes had elapsed since the power disturbance was created. Hence only those measurements made after five minutes had elapsed, were employed to determine emission intensity.

5.3 Results and Discussion

5.3.1 Steady-State Validation

Figures 5.1 and 5.2 show the comparison between the experimental and simulated intensity ratios as a function of percentage of oxygen in the feed. The experimental [F]/[Ar] intensity ratio increased with increasing concentration up to a composition of approximately 22% and then rapidly declined. The simulated [F]/[Ar] intensity ratio increased more gradually and reached a maximum at a feed composition of approximately 38% oxygen before showing a gradual decline. The experimental [O]/[Ar] ratio increased slowly up to a concentration of 20% and then displayed a marked upswing. The simulated ratio, on the other hand, increased sharply at the beginning and then "tailed" off after the oxygen content had reached 20%.

From the experimental trends observed it was postulated that the increasing oxygen concentration favored the neutral gas phase recombination reactions of the type given by,

$$CF_x + [O] \longrightarrow COF_{x-1} + F, \qquad (5.1)$$

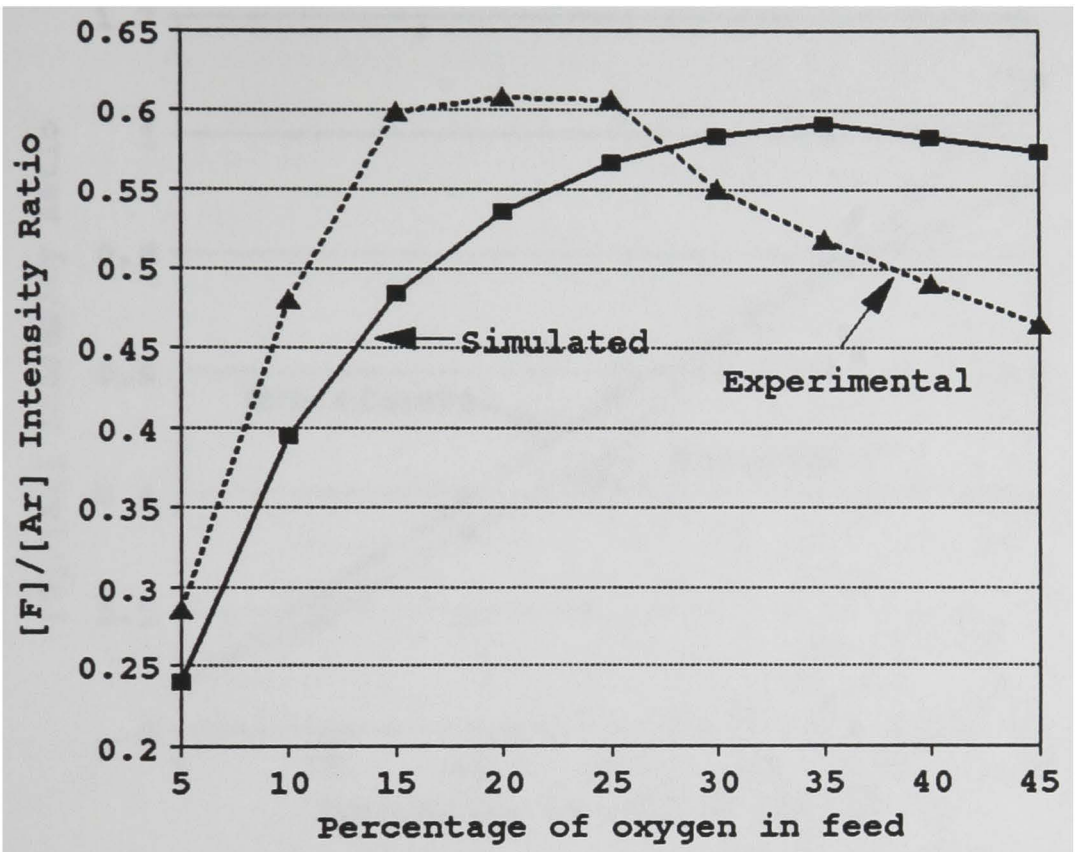

Figure 5.1 Comparison between experimental and simulated [F/Ar] intensity ratios as a function of the percentage of oxygen in the feed.

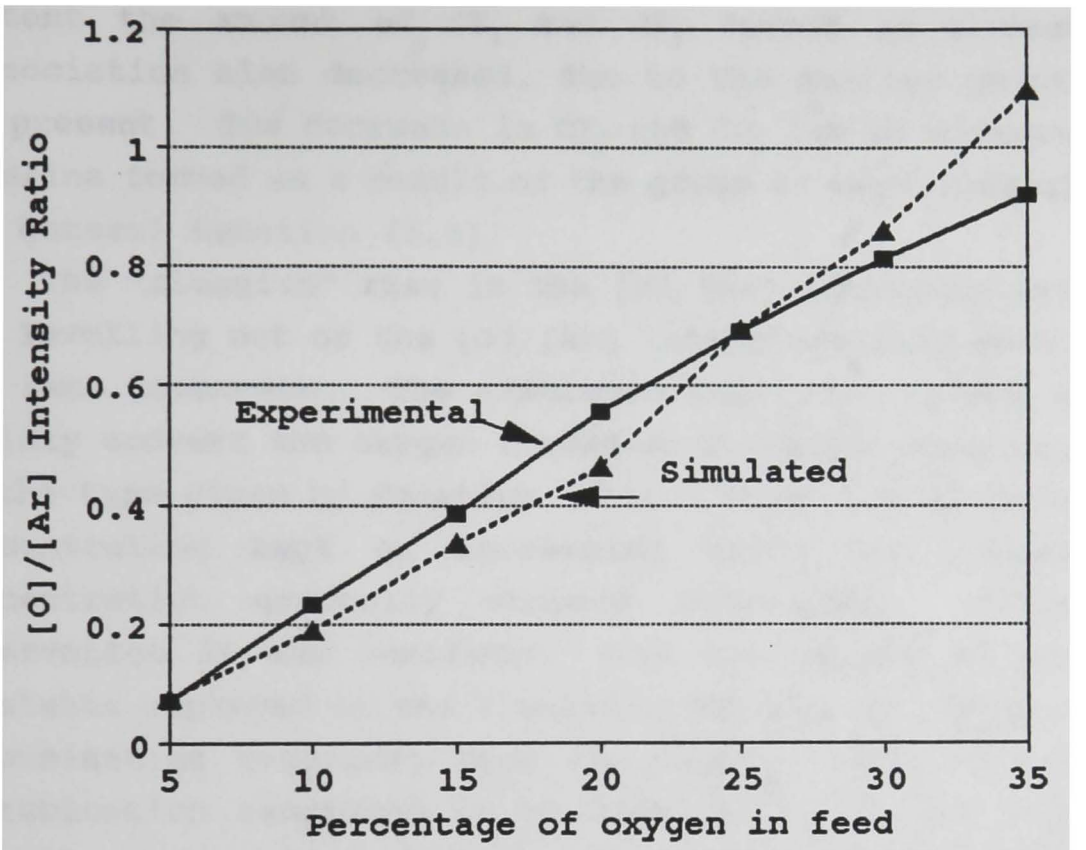

Figure 5.2 Comparison between experimental and simulated [O/Ar] intensity ratios as a function of the percentage of oxygen in the feed.

up to an oxygen content of approximately 20-22%. As oxygen content was increased beyond this point the recombination reactions were no longer able to "keep up" with the oxygen atom produced due to dissociation and hence, the oxygen atom concentration increased rapidly. With increasing oxygen content the amount of CF_2 and CF_3 formed as a result of dissociation also decreased, due to the smaller quantity of CF_4 present. The decrease in CF_2 and CF_3 led to a decrease in fluorine formed as a result of the group of reactions given by the general Equation (5.1)

The "sluggish" rise in the [F]/[Ar] intensity ratio and the levelling out of the [O]/[Ar] intensity ratio were due to the same phenomena. The simulated reaction set was able to rapidly convert the oxygen formed to fluorine using reactions of the type given by Equation (5.1). Thus, the fluorine atom concentration kept on increasing while the oxygen atom concentration gradually stopped increasing. From this observation it was concluded, that the values of the rate constants employed by the simulator for the gas phase neutral recombination reactions were too large. This caused the recombination reactions to be kinetically faster than they actually were when compared to the experimental conditions.

The experimental and simulated intensity trends as a function of flow shown in Figures 5.3 and 5.4 indicate that the [F] to [Ar] ratio decreased with increasing flow rate while the [O] to [Ar] ratio increased linearly with increasing flow rate. The simulated trends show the same result in the case of the [F]/[Ar] ratio but indicate that the [O]/[Ar] ratio remained almost constant over the range of flow rates employed. With increasing flow there is a decrease in the residence time. This does not favor the slower recombination reactions as the oxygen atoms and the CF_x radicals have less time to react. The production of oxygen atoms remained unchanged as the dissociation reactions were relatively unaffected by the residence time. The depletion however

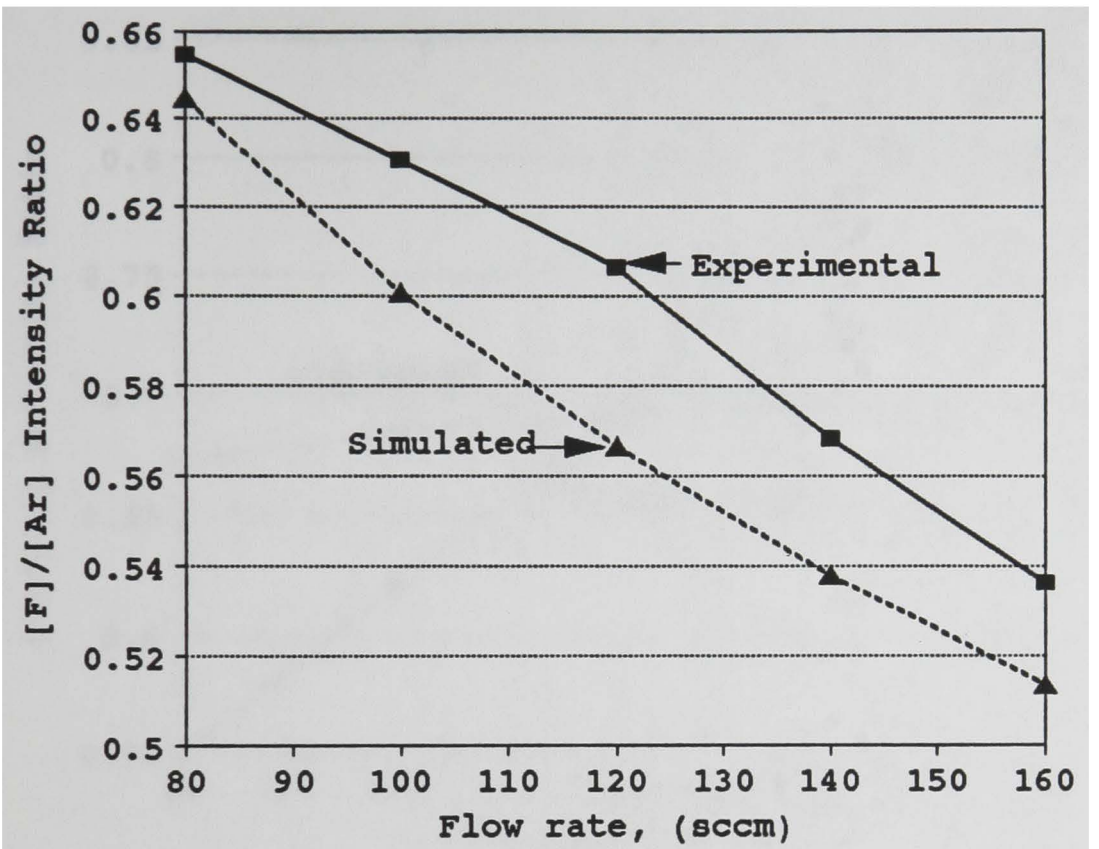

Figure 5.3 Comparison between experimental and simulated [F/Ar] intensity ratios as a function of the total flow rate.

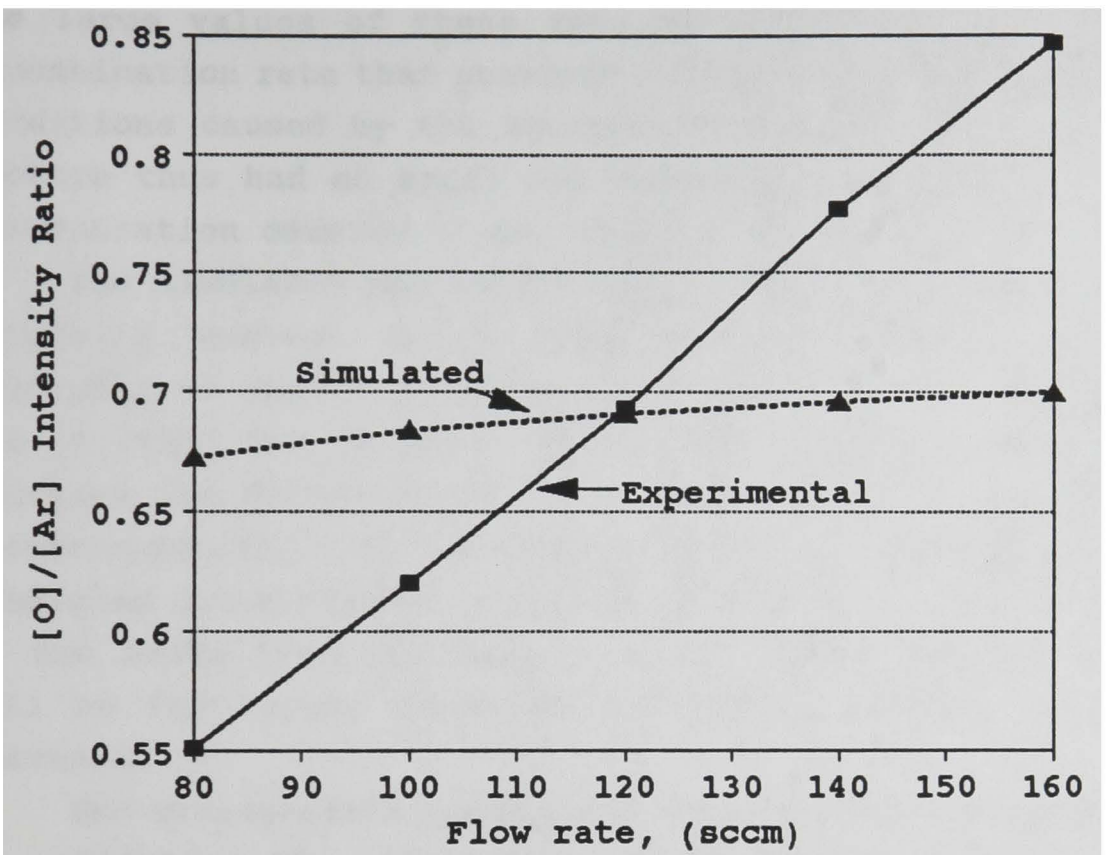

Figure 5.4 Comparison between experimental and simulated [O/Ar] intensity ratios as a function of the total flow rate.

increased thus causing an increase in the oxygen atom concentration. The shorter residence time also caused the production of fluorine atoms, by the gas phase recombination reactions, to decrease. The values of the rate constants employed in the simulator were the cause for this discrepancy. The large values of these rate constants led to a greater recombination rate than observed, which offset the unfavorable conditions caused by the shorter residence time. These two factors thus had an equal and opposite effect on the oxygen concentration causing it to remain unchanged.

The simulated and experimental trends obtained for both intensity ratios, as a function of pressure, compared favorably as seen from Figures 5.5 and 5.6. The decrease in the [F]/[Ar] and [O]/[Ar] ratios occurred on account of the decrease in dissociation as a result of the decrease in electron density with increasing pressure. The experimentally predicted concentration ratios were slightly higher on account of the leaks into the reactor which caused the fluorine as well as the oxygen concentration ratios in the reactor to increase.

The steady-state comparison served as an excellent means of validating the simulator especially with respect to the kinetics of the reactions employed. The discrepancies observed were used to make appropriate changes in the simulator. Rate constants were altered within the limits of experimental error prescribed by the authors (Plumb and Ryan, 1986). The predictions obtained from the simulator improved marginally after these changes were incorporated. The simulator predictions generally reproduced the experimental trends observed. The aim of the simulator was to make it as phenomenologically sound as possible and at the same time use it as an effective vehicle for control studies. This purpose was served and hence no further modifications were made while comparing the dynamic open-loop responses.

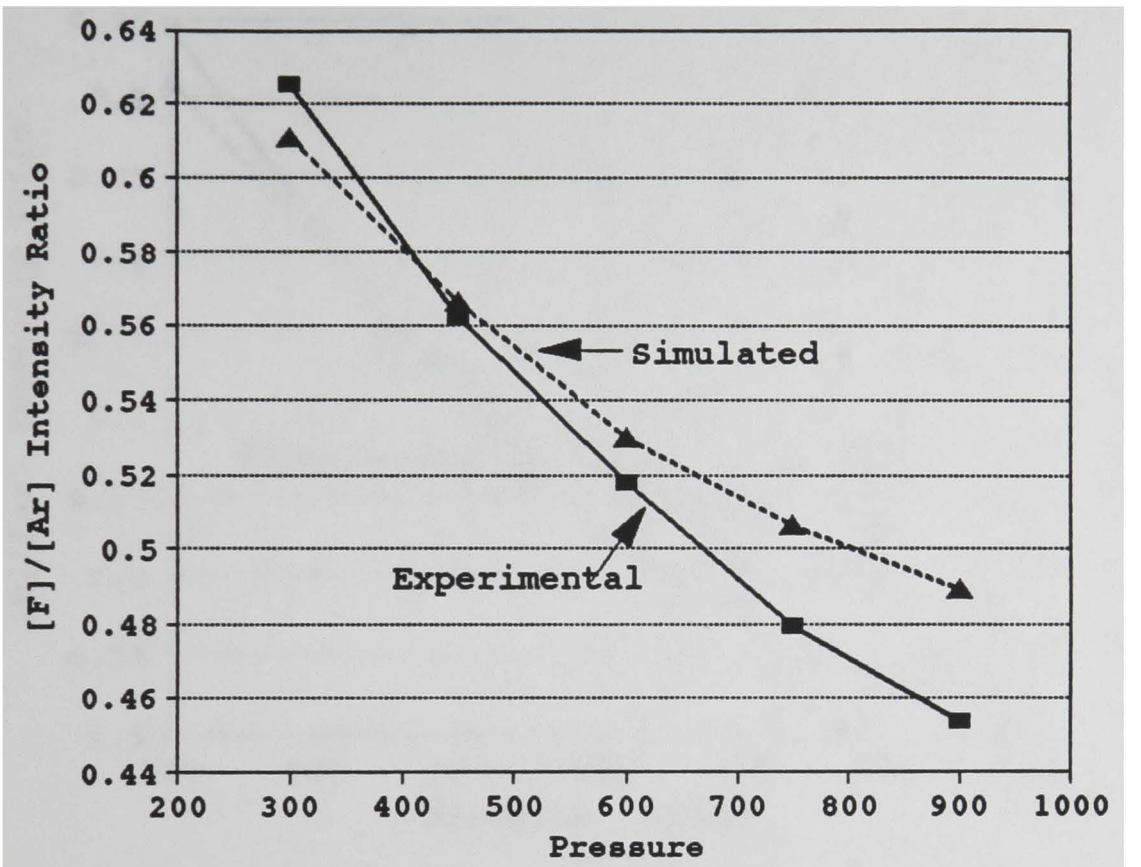

Figure 5.5 Comparison between experimental and simulated [F/Ar] intensity ratios as a function of pressure.

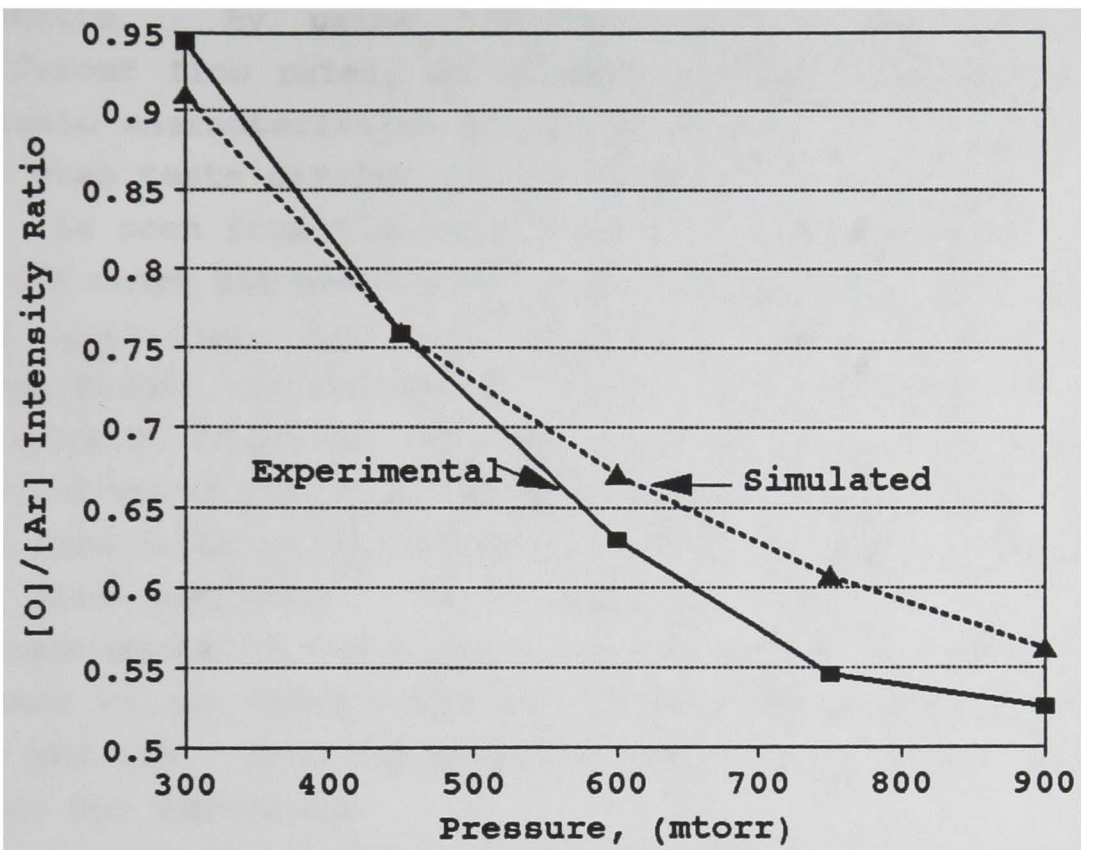

Figure 5.6 Comparison between experimental and simulated [O/Ar] intensity ratios as a function of pressure.

5.3.2 Dynamic Validation

The response of the process to disturbances was used to verify the dynamics of the process. These tests helped validate the accuracy of the valve characteristics employed or more generally the fluid dynamics as well as the reaction dynamics. By using different oxygen compositions and different flow rates, an attempt was made to determine the dynamic characteristics of the process. The description of the step tests carried out is as shown in Table 5.2

As seen from Figures 5.7 to 5.11 the pressure was close to 500 mtorr but never exactly at 500 mtorr. This was because the controller, that was originally present, was a simple proportional controller and hence, could not remove offset. In order to reproduce the same effect using the simulator, the initial valve position was adjusted till the pressure reached the same value as that of the process. It was then maintained at this position. Valve position was critical in the determination of the dynamics of the process, as even a small change in the valve position caused a considerable effect on the process. Once the pressure had reached steady-state the power was turned on.

One of the criteria used initially to gauge the dynamics was the peak that occurred in pressure as a result of the sudden creation of new species caused by the power discharge. The simulator which employed the scaled rate constants was unable to reproduce the initial dissociation that actually occurred in the process. The rate of dissociation was proportional to the dissociation rate constants and the electron density. Since the rate constants were fixed, based on the values of Plumb and Ryan (1986), the only parameter that could be changed was the electron density ratio. This was initially scaled by a factor of seven. However, a scaling factor of this magnitude caused the net dissociation to increase considerably. On account of the greater net dissociation the steady state pressure that the simulator

Table 5.2 Open-Loop Response Tests

Test Case Number	Initial Conditions	Final Conditions
1	80 sccm (10% O_2)	100 sccm (25% O_2)
2	100 sccm (25% O_2)	80 sccm (10% O_2)
3	80 sccm (20% O_2)	100 sccm (25% O_2)
4	100 sccm (10% O_2)	120 sccm (25% O_2)
5	120 sccm (25% O_2)	100 sccm (10% O_2)

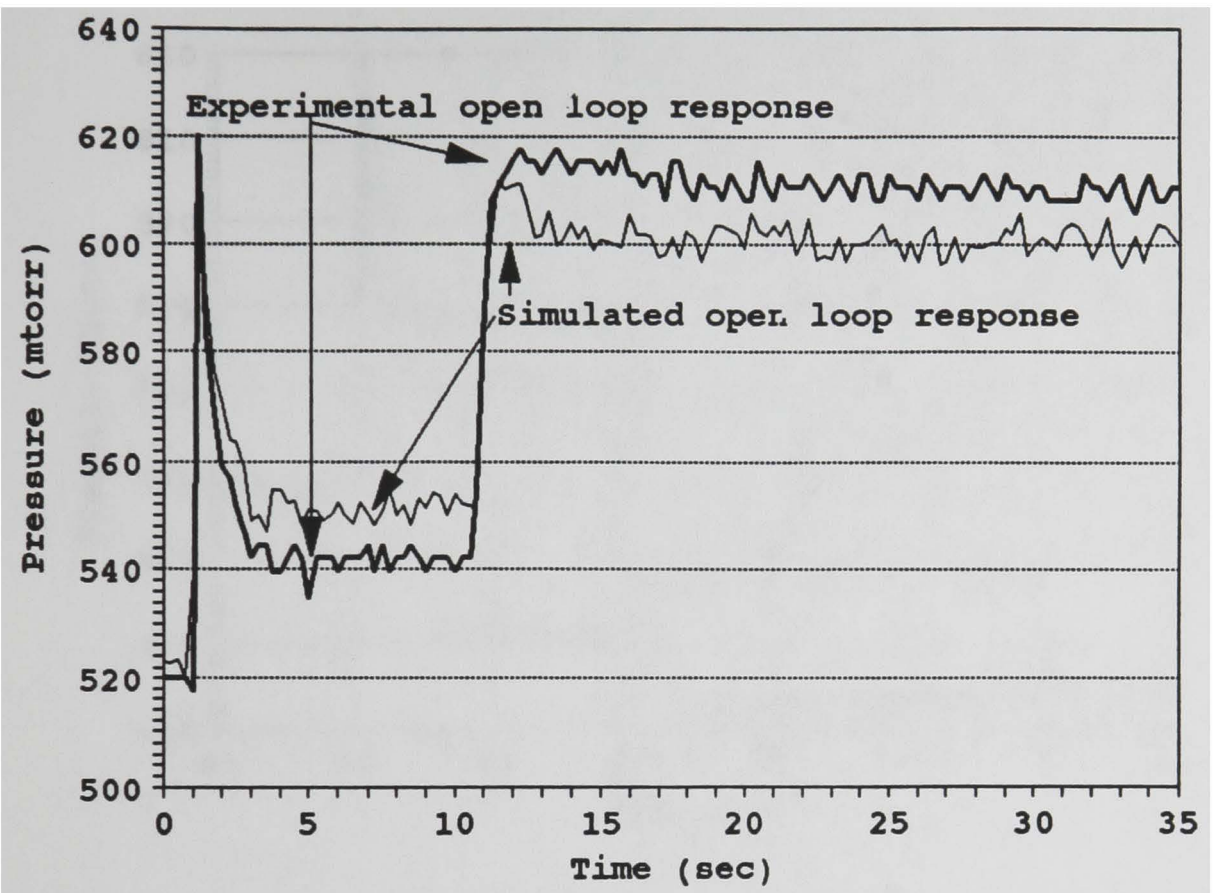

Figure 5.7 Dynamic Open-Loop Response Comparison (Case 1)

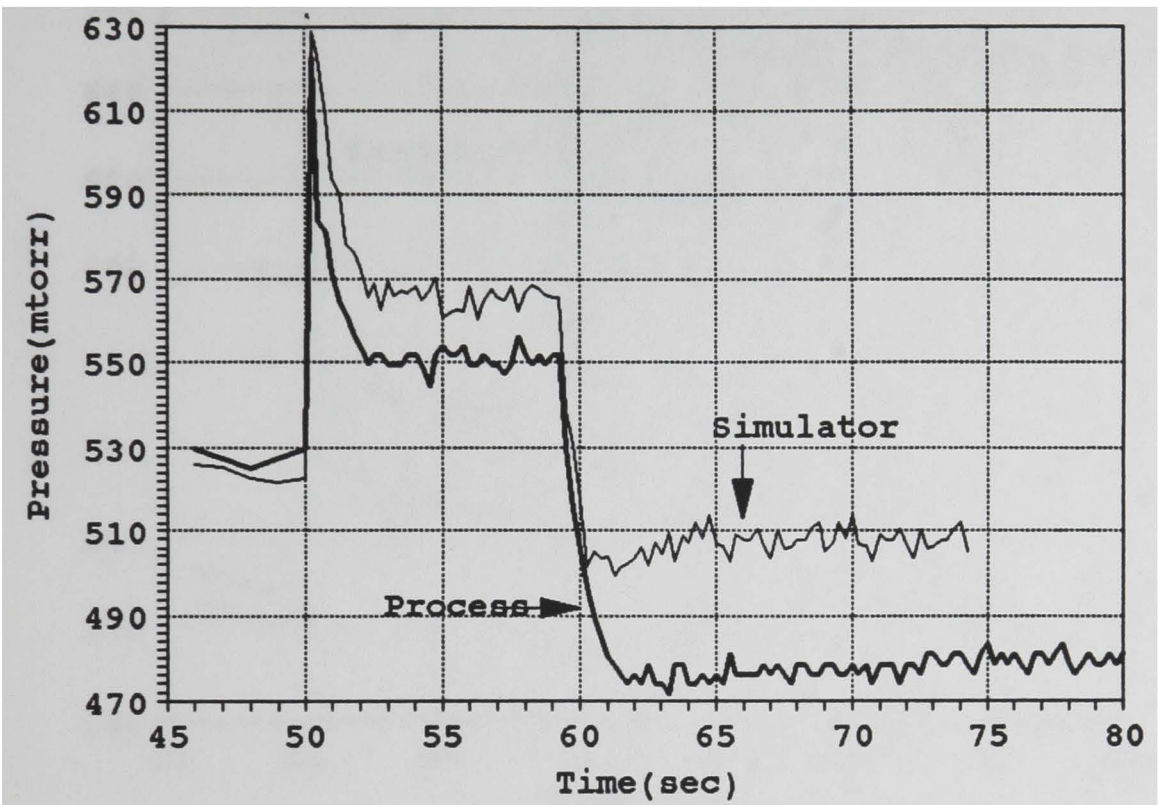

Figure 5.8 Dynamic Open-Loop Response Comparison (Case 2)

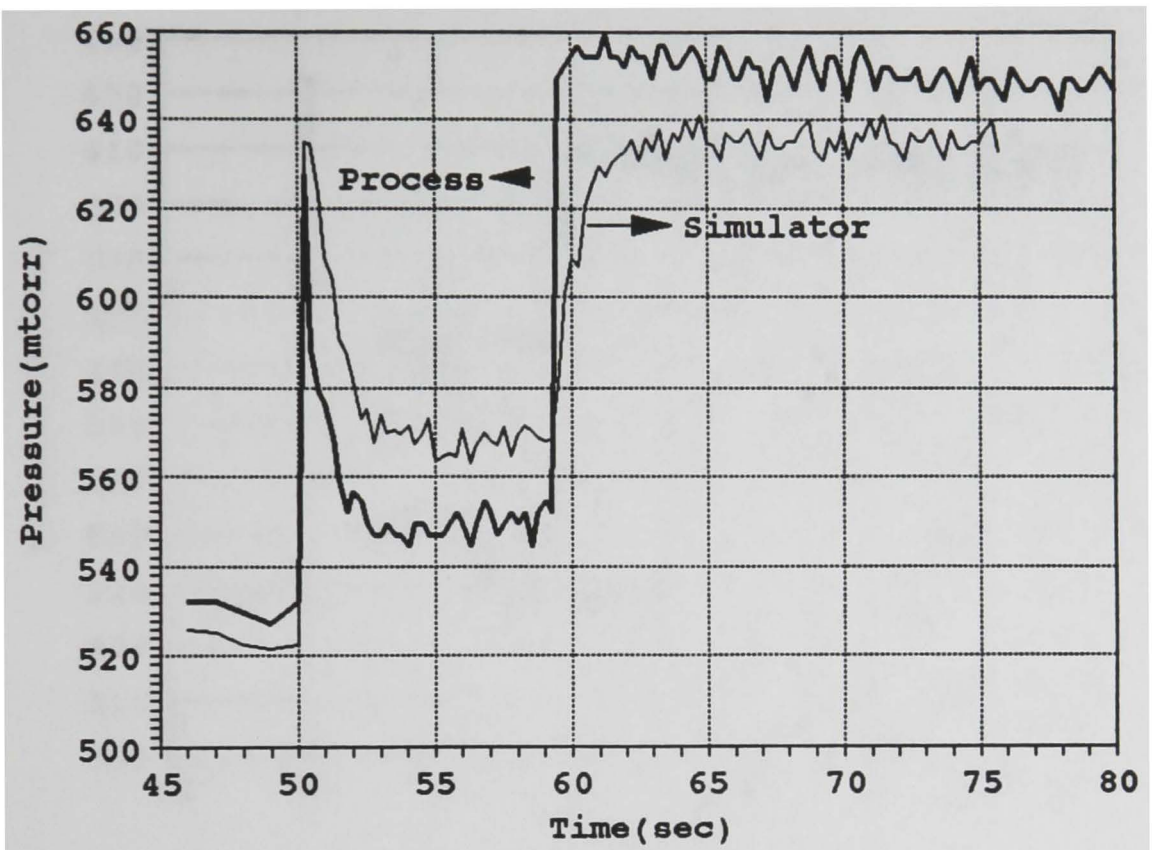

Figure 5.9 Dynamic Open-Loop Response Comparison (Case 3)

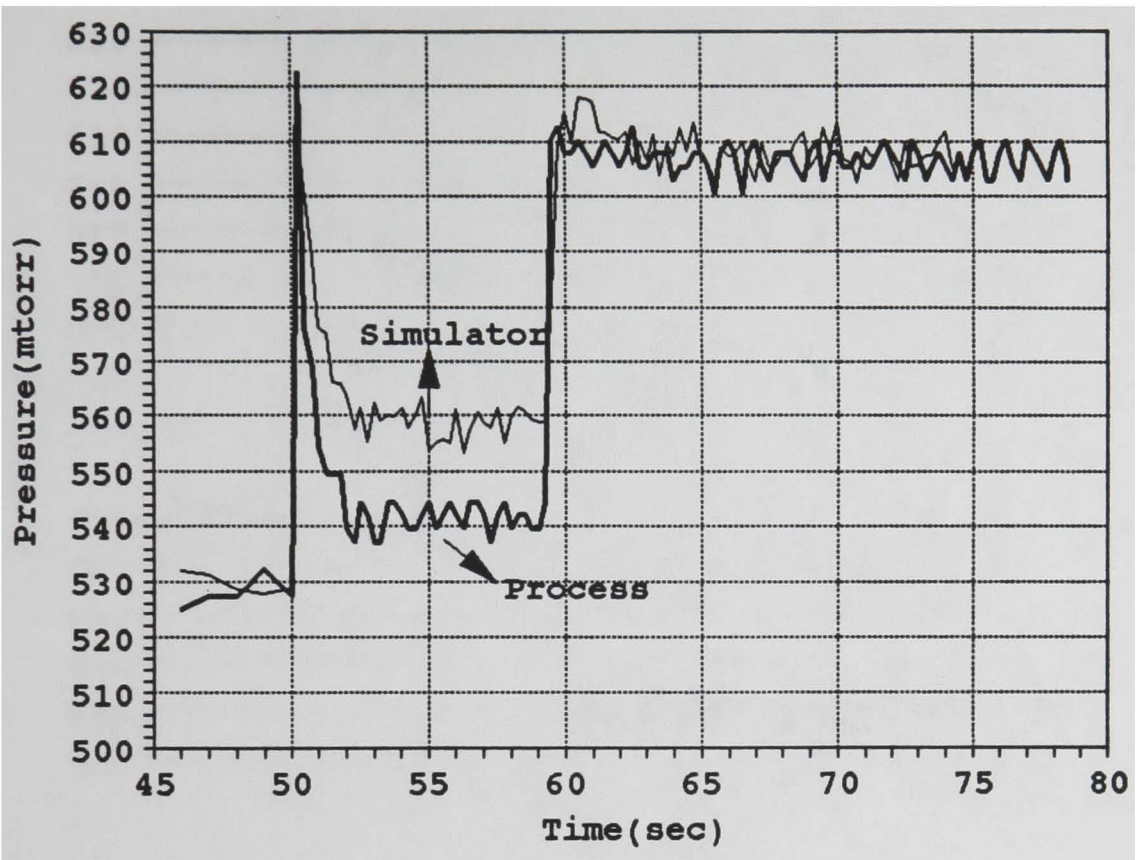

Figure 5.10 Dynamic Open-Loop Response Comparison (Case 4)

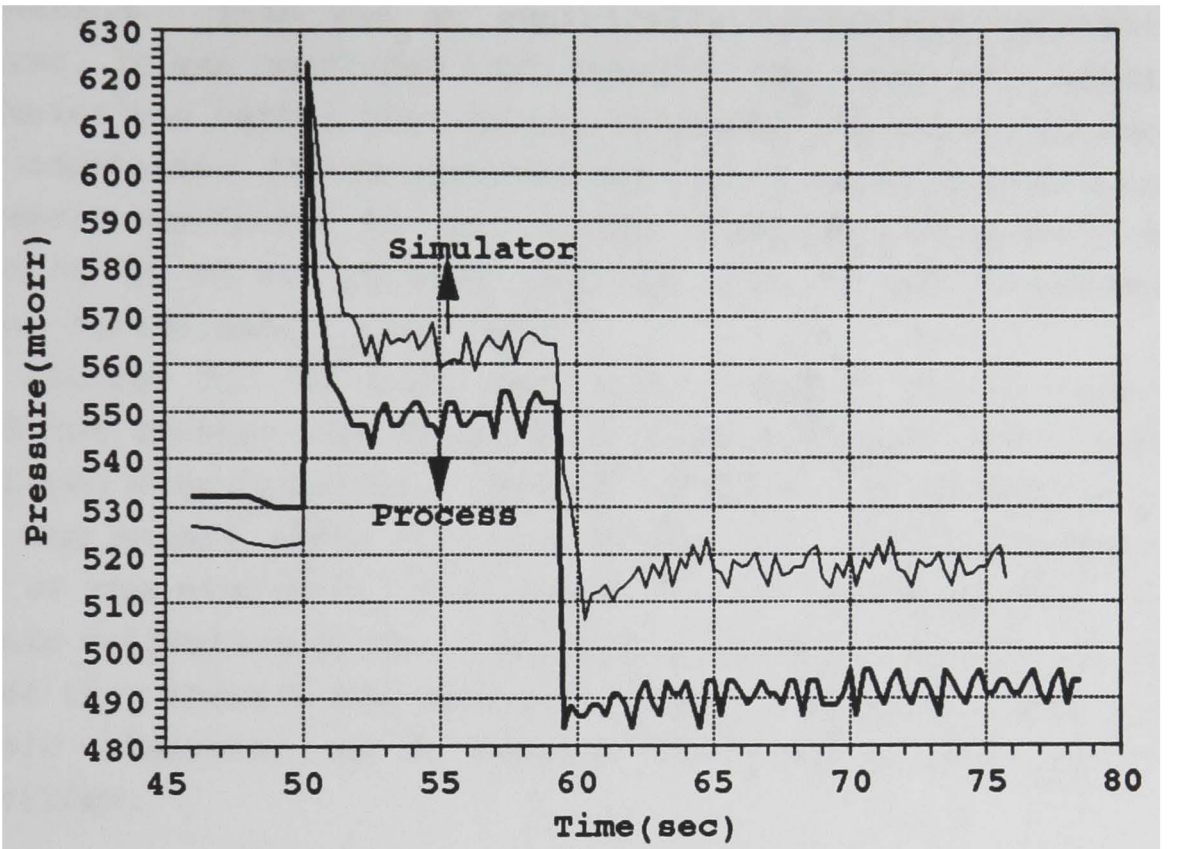

Figure 5.11 Dynamic Open-Loop Response Comparison (Case 5)

attained, after the initial dissociation, was considerably higher than that attained by the process. A trade-off between these two factors was made and the electron density ratio was scaled by a factor of five. This was kept constant for all other open-loop tests as well as the steady state simulator validation. This was an empirically determined constant. However, it was concluded that changing the value of a single parameter was better than trying to change the values of many rate constants. It was observed that the process dynamics wee extremely sensitive to the oxygen dissociation reactions, given by 8a to 8c in Table 4.2, as well as the three-body oxygen recombination reactions.

Figures 5.7 to 5.11 show that although the simulator could not exactly reproduce the process dynamics, the trends displayed were identical. The time taken by the process to go from one steady state to another was also quite similar to that of the simulator, thus lending more credibility to the dynamic validation of the simulator. In conclusion, it can be stated that these tests were sufficient to justify using this dynamic simulator as a vehicle for testing the control algorithms.

CHAPTER 6
CONTROL ISSUES AND MODEL DEVELOPMENT

6.1 Model-Based Control (MBC)

Model-based controllers, as the name suggests, use a model of the process to make control decisions. When compared to conventional controllers like the proportional-integral-derivative (PID) type of controller, these controllers are more "intelligent" (Rhinehart, 1993) owing to their intuitive understanding of the process. A model-based controller calculates the desired manipulated variable action based on its knowledge of a specified response that the controlled variable should follow. Hence, if the model mimicked the process exactly, the inverse of the model, which represents the controller, when coupled with the process, would give perfect control. However, models being imperfect is more the rule than the exception and hence some form of compensation for the process-model mismatch is required. A representation of a typical MBC strategy is shown in Figure 6.1, where the difference, d, between the model, M, and the process output is monitored and used to adjust, A, a controller feature, c. The controller is all three I, M and A functions and not simply the inverse I.

The major difference between various MBC approaches is their manner of representation of the process, with the three dominant approaches being transfer function (either Z or Laplace transforms), time series models or approaches derived from fundamental mass and energy balances. Secondary differences include the formulation of the control law from the desired objective, the process-model mismatch adjusting mechanism and other features such as constraint handling and optimization. Bequette (1991) suggests that the majority of nonlinear control techniques have a goal of obtaining a linear system by some of linearization, because it is easy to design stable linear controllers and understand linear closed-loop

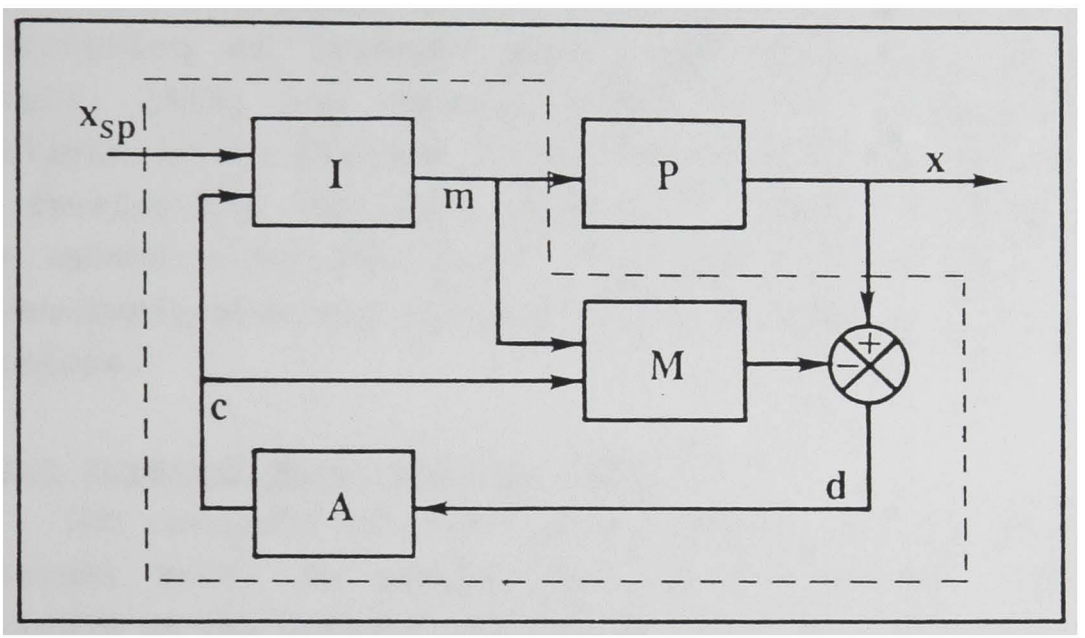

Figure 6.1 The model-based control (MBC) concept; Inverse, Model and Adjustment (Rhinehart, 1992)

responses. Nonlinear methods such as process model based control (PMBC) (Rhinehart,1992), however, use phenomenological models directly to obtain the control law.

In addition to better control performance both in the servo and regulatory modes, there is in general only one tuning parameter, which determines the speed of response. In contrast conventional control strategies require at least two if not three parameters to be specified. With the cheap availability of high speed computing, MBC algorithms are becoming increasingly easy to implement industrially. A brief description of Internal Model Control (IMC) (Garcia and Morari, 1983) and Generic Model Control (GMC) (Lee and Sullivan, 1988) follows, as we have used these two strategies to develop and implement controller models for our system. The actual controller model development and issues such as parameterization and noisy data are handled in the following sections.

6.1.1 Internal Model Control (IMC)

IMC consists of four parts (Garcia et al., 1983): (1) Internal model to predict the effect of the manipulated variable on the output; (2) filter to achieve a desired degree of robustness; (3) control algorithm to compute future values of the manipulated variable; and (4) feedback to bias the setpoint. IMC uses open-loop step or impulse response Laplace transfer function models. Very often the digital equivalent of the Laplace transform, the Z transform is employed.

A hypothetical first-order-plus-deadtime (FOPDT) model is employed to illustrate the concept of IMC. Consider a process which can be described by a FOPDT transfer function, given by,

$$G_p = \frac{K_p}{\tau_p s+1} e^{-\theta_p s}, \qquad (6.1)$$

where, G_p = process transfer function,

K_p = process gain,

τ_p = process time constant,

θ_p = process dead time.

From the block diagram (Figure 6.2), it is seen that ideally the controller should be the inverse of the process such that the controlled variable remains at its set point. Thus the controller transfer function, G_c, is represented by,

$$G_c = 1/G_p = \frac{\tau_p s+1}{K_p} e^{+\theta_p \cdot s}, \qquad (6.2)$$

and, in the Laplace domain, the required control action as represented by the change in manipulated variable given by,

$$\hat{m} = \frac{e^{\theta_p s}}{K_p}(\tau_p s + 1) \overset{\wedge}{X_{sp}}, \qquad (6.3)$$

or in the real time domain,

$$m = \frac{1}{K_p}\left[x_{sp}(t+\theta_p) + \tau_p \frac{dX_{sp}(t + \theta_p)}{dt}\right]. \qquad (6.4)$$

This control action is unrealizable because it implies that the controller must make the change before the setpoint changes. In addition, for a step setpoint change, the derivative term becomes infinite. Various other problems exist if the controller function is used in this form, such as changes in K_p and τ_p with time, spikes due to derivative action and the presence of inverse action. The latter involves a process transfer function of the form,

$$\frac{K_p(1-\tau_3 s)}{(\tau_1 s+1)\cdot(\tau_2 s+1)}, \qquad (6.5)$$

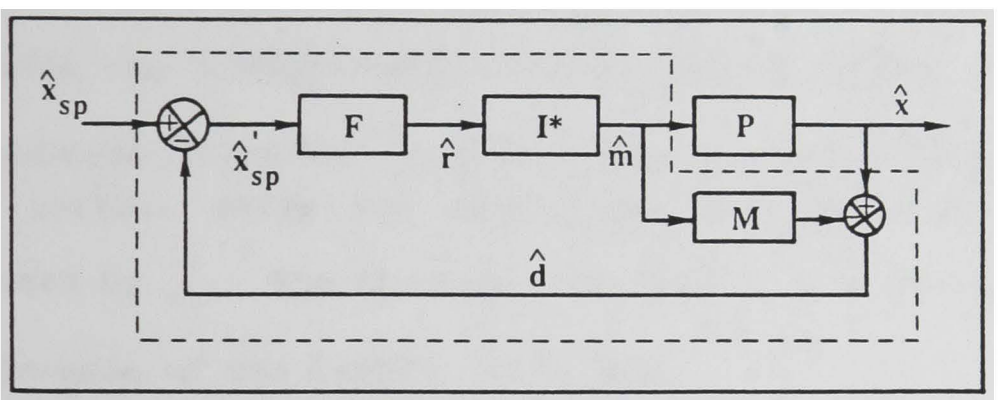

Figure 6.2 The Basic Internal Model Control Structure

which when inverted gives,

$$G_c = \frac{1}{G_p} = \frac{1}{K_p} \frac{(\tau_1 s+1)\cdot(\tau_2 s+1)}{(1-\tau_3 s)}, \qquad (6.6)$$

again a form which is not realizable because there is a time for which the corresponding value of "s" makes the denominator zero. To eliminate these deadtime and inverse action problems in the controller, the process is approximated by a model with a transfer function,

$$\tilde{G}_p = \tilde{G}_+ \tilde{G}_-. \qquad (6.7)$$

$\tilde{G}_+$ contains the unrealizable (when inverted) parts of the actual process transfer function such as the deadtime and inverse action, while the realizable and stable part is represented by $\tilde{G}_-$. The transfer function of the control law is the inverse of the latter, such that

$$G_c^* = \frac{1}{\tilde{G}_-}. \qquad (6.8)$$

As shown in Figure 6.2, the error between process and model is used to bias the setpoint. Since the errors are subject to random noise, the setpoint will change considerably. This is not conducive to good control and hence filtering is carried out. A filter basically adjusts the extent to which the new value of a particular variable is allowed to influence the process. For example, a first-order filter is of the form,

$$PV_{f_{new}} = \lambda PV_{new} + (1 - \lambda)\ PV_{f_{old}}, \qquad (6.9)$$

where, λ = weighing factor = $(1 - e^{-T/\tau_f})$, $0 \leq \lambda \leq 1$,

T = control interval,

τ_f = filter time constant.

The smaller the value of λ, the smaller the influence of the new value of the process variable. In the Laplace domain the first-order filter is a first-order lag given by,

$$F = \frac{1}{\tau_f s + 1}. \tag{6.10}$$

Either the error (the process-model mismatch) or the corrected setpoint may be filtered. The latter is preferable as it reduces the effect of noise as well as prevents the derivative spikes (the derivative term becoming infinite) for a setpoint step change.

With a FOPDT model, the IMC structure simplifies to that shown in Figure 6.3. The controller is a combination of the transfer functions $\tilde{G}_p$, F and G_c^* analogous to Figure 6.1, where the controller is represented by the dotted line enclosing M, A and I.

The single tuning parameter in IMC is the filter time-constant and it determines the time taken by the process to return to its setpoint. Lower values of this parameter leads to a more aggressive action while higher values cause smaller changes in the process variable, as is evident from Equation (6.8). The controller transfer function is then given by,

$$G_c = \frac{FG_c^*}{1 - FG_c^*G_p}. \tag{6.11}$$

When processes cannot be reasonably represented by first-order models then higher order models may be used. The filter used should at all times have the same order as the process model denominator. Hence,

$$F = \frac{1}{(\tau_f s + 1)^n}, \tag{6.12}$$

where n is the order of the model.

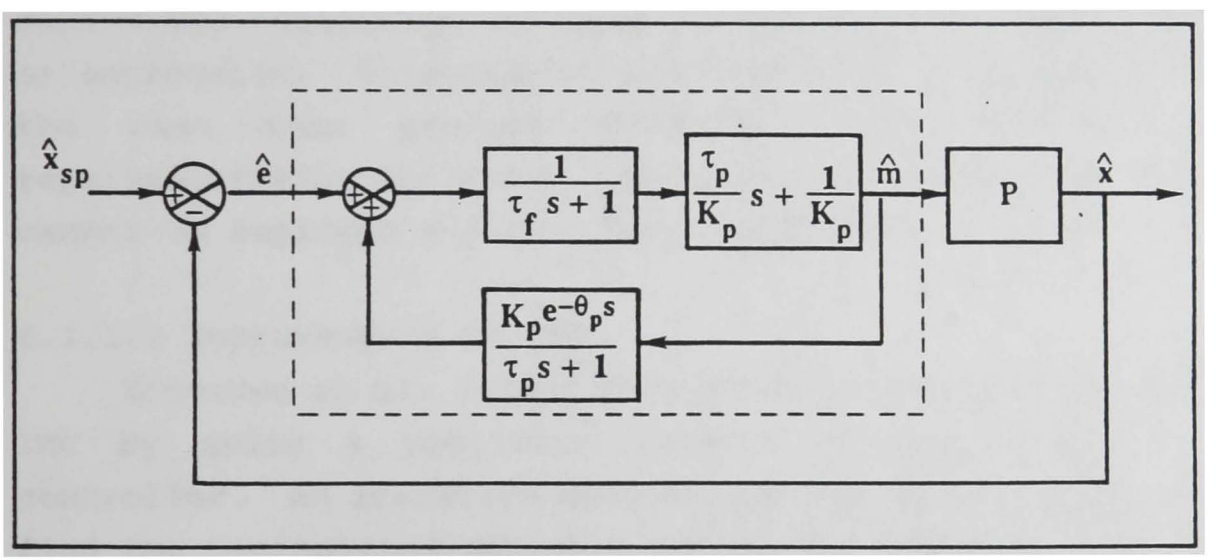

Figure 6.3 Internal Model Control structure for a FOPDT modelled process with the blocks rearranged to show implementation.

IMC has several advantages. The closed-loop response is always stable for a linear process, for a sufficiently large τ_f, and the quality of the response and the robustness are virtually independent of each other. Constraints on the manipulated variable can be anticipated and corrective action can be taken. It also allows for deadtime compensation. A single tuning parameter, which has a physical significance in that it requires the output to follow a desired reference trajectory makes on-line tuning quite easy.

The models used by IMC are linear and stationary and this is one of its chief drawbacks. Nonlinear processes have significant differences in process gain from region to region. Time constants may change in non-stationary processes. This causes the controller response to become either too sluggish or aggressive. This requires retuning the controller, or in the case when process dynamics change substantially, reparameterizing the model. Another disadvantage is that IMC cannot be employed for open-loop unstable processes.

6.1.1.1 Improvements to IMC

Economou et al. (1986) developed a nonlinear approach to IMC by using a nonlinear inverse of the model in the controller. An iterative Newton type search was performed to find the manipulated variable action for the next time step. The rest of the IMC structure remained unchanged. Their approach is computationally intensive as it calls for repeated integration of the differential equations representing the process for each iterative value of the manipulated variable. Gain scheduling is employed in this work to account for nonlinearity. By varying the model gain either as a function of the manipulated variable, controlled variable or the controlled variable setpoint, an attempt is made to keep the controller model true to the process. In the process considered in this work, the settling time and the time constant in different regions of operation were different.

However, no attempt was made to vary the time constant based on the region of operation. Instead a time constant for the process model was determined from an averaged open-loop response of open-loop responses representing different regions of operation and hence different process dynamics.

6.1.2 Generic Model Control (GMC)

GMC (Lee and Sullivan, 1988) like any other Reference System Synthesis (RSS) technique uses a model of the process to force the controlled system to follow a desired trajectory. This is accomplished by specifying a desired control system response and calculating the control action using the deviation of the process from the desired response as the driving force. Where GMC differs from other RSS techniques is that it directly imbeds a nonlinear model of the process derived from fundamental mass and energy balance considerations. The control law is obtained by combining the desired control objective with the model of the process.

Consider a process described by

$$\frac{dx}{dt} = f(x,u,d,t), \tag{6.13a}$$

and,

$$y = g(x), \tag{6.13b}$$

where, x = vector of all possible states,
u = vector of manipulated variables,
d = vector of disturbance variables,
y = vector of output.

Normally f and g are some nonlinear functions such that,

$$\frac{dy}{dt} = G_x \cdot f(x,u,d,t), \tag{6.14}$$

where,

$$G_x = \frac{\partial g}{\partial x}. \tag{6.15}$$

The trajectory of y is compared against some nominal trajectory, $y^*(t)$ and the control objective formulated. If the reference trajectory is chosen to be some arbitrary function such that,

$$\left(\frac{dy}{dt}\right)^*(t) = r^*(y), \tag{6.16}$$

where, r = some user specified reference trajectory.

The control objective is two-fold: (1) The rate of change of the process or controlled variable should be such that the process is returning to its desired steady state, that is,

$$\frac{dy}{dt} = K_1 \cdot (y^* - y), \tag{6.17}$$

where y^* = vector of output variable setpoints.

(2) The process should have zero offset such that

$$\frac{dy}{dt} = K_2 \cdot \int (y^* - y) \cdot dt. \tag{6.18}$$

These two objectives combined give the desired controlled objective or reference trajectory such that,

$$\left(\frac{dy}{dt}\right)^* = K_1 \cdot (y^* - y) + K_2 \cdot \int (y^* - y) \cdot dt. \tag{6.19}$$

The control objective when combined with the controller model gives the control law in its simplified form;

$$G_x \cdot f(x, u, d, t) - K_1 \cdot (Y^* - y) - K_2 \cdot \int (y^* - y) \cdot dt = 0. \tag{6.20}$$

This is equivalent to a static state feedback control law of the form (Henson and Seborg, 1989),

$$u = \frac{v - L_f \cdot h(x)}{L_g \cdot h(x)}, \qquad (6.21)$$

where, u = manipulated variable vector,
v = input representing the control objective.

The model is of relative degree 1 (r=1) such that,

$$\frac{dy}{dt} = L_f \cdot h(x) + L_g \cdot h(x) \cdot u, \qquad (6.22)$$

where L_f and L_g are the Lie derivatives of the scalar functions representing the process and the desired reference trajectory. For more details the reader should consult the articles by Lee and Sullivan (1988) and Henson and Seborg (1989).

A very simple process model-based control law is given by (Rhinehart and Riggs, 1990)

$$\frac{y_{sp} - y}{\tau} = \frac{dy}{dt}\Big|_y = f(y, u, d, p), \qquad (6.23)$$

where, y_{sp} = process variable setpoint,
u = vector of manipulated variables,
p = vector of adjustable parameters,
τ = time taken by the process to move to its new setpoint,
d = vector of both measured and unmeasured disturbances.

This assumes an elementary first-order process response such that the controlled variable moves to its steady state during the time period τ. When this is combined with the control objective a form similar to the GMC law without the offset correction is obtained. Rearranging Equation (6.23) and setting $K_1 = 1/\tau$ gives,

$$f(y, u, d, p) + K_1 \cdot (y - y_{sp}) = 0. \qquad (6.24)$$

This was the form employed in the controller model. The task of offset removal is handled by the parameterization of the model rather than by a tack-on mechanism. The above form is valid when dynamic models are employed. However, the extension to steady state models is straightforward. The process is represented as,

$$\frac{dy}{dt}\Big|_{y_{ss}} = f(y_{ss}, u_{ss}, d, p) = 0. \qquad (6.25)$$

A first-order elementary response of the form,

$$\frac{dy}{dt} = \frac{1}{\tau_p}\cdot(y_{ss} - y), \qquad (6.26)$$

is assumed. Combining Equations (6.25) and (6.26) and rearranging gives,

$$\frac{1}{\tau_p}\cdot(y_{ss} - y) = f(y_{ss}, u_{ss}, d, p) = 0. \qquad (6.27)$$

When the control objective is combined with Equation (6.27) and rearranged, the final form of the steady state control law without the integral offset correction term is obtained. This is given by,

$$y_{ss} = y + K_1\tau_p\cdot(y - y_{sp}), \qquad (6.28)$$

where, y_{ss} = steady state target for the output variable,
τ_p = time taken by the process to reach steady state target.

GMC has many advantages. It incorporates the nonlinearity inherent in the process within the controller model thus incorporating a more accurate representation of the process. The model has inherent feedforward action, nonlinear decoupling and gain-scheduling. In addition a well chosen model adjustment parameter ensures robust control despite modelling errors. Like any other model-based controller it has a single tuning parameter which determines how fast a process is required to reach its setpoint. The disadvantages

lie in its single time step ahead approach. As a result GMC is unable to handle processes that have ill-behaved dynamics such as inverse response or large dead-times. It also cannot handle constraints on-line.

6.2 Development of the Specific Models

6.2.1 Internal Model Control

The controller model was developed using step response data. The operating pressure range of interest was approximately 200 to 800 mtorr. Within this range the valve stem position varied from approximately 65 degrees to 25 degrees for a flow rate of 100 sccm. Changes in flow rate did not have a very significant effect on the range of valve positions. Two sets of step tests were performed to obtain as accurate a model as possible. One set of tests consisted of 4 steps performed in the following sequence. The valve was first opened by a particular amount (step up) closed by an equal amount (two steps down) and again opened by the same amount (step up). This kind of test procedure helped to capture the major nonlinearity present in the process. The step test was performed by first choosing a nominal operating point. Two operating points were selected with the initial valve positions being 40 and 30 degrees respectively. Valve position was varied in steps of 5 degrees and 3 degrees respectively from the two nominal operating points selected. The latter change was sufficiently large to obtain the desired characteristics of the response. These responses (2 sets of 4 responses each) were superimposed on each other and the average open-loop response obtained. Figures 6.4 to 6.6 show the results of this operation along with the averaged open-loop response for each test.

The averaged open-loop response was used to obtain the linear laplace first-order-plus-dead-time model by using the 1/3 - 2/3 method. This method uses the values of the process responses corresponding to 33.33% and 66.67% of the total

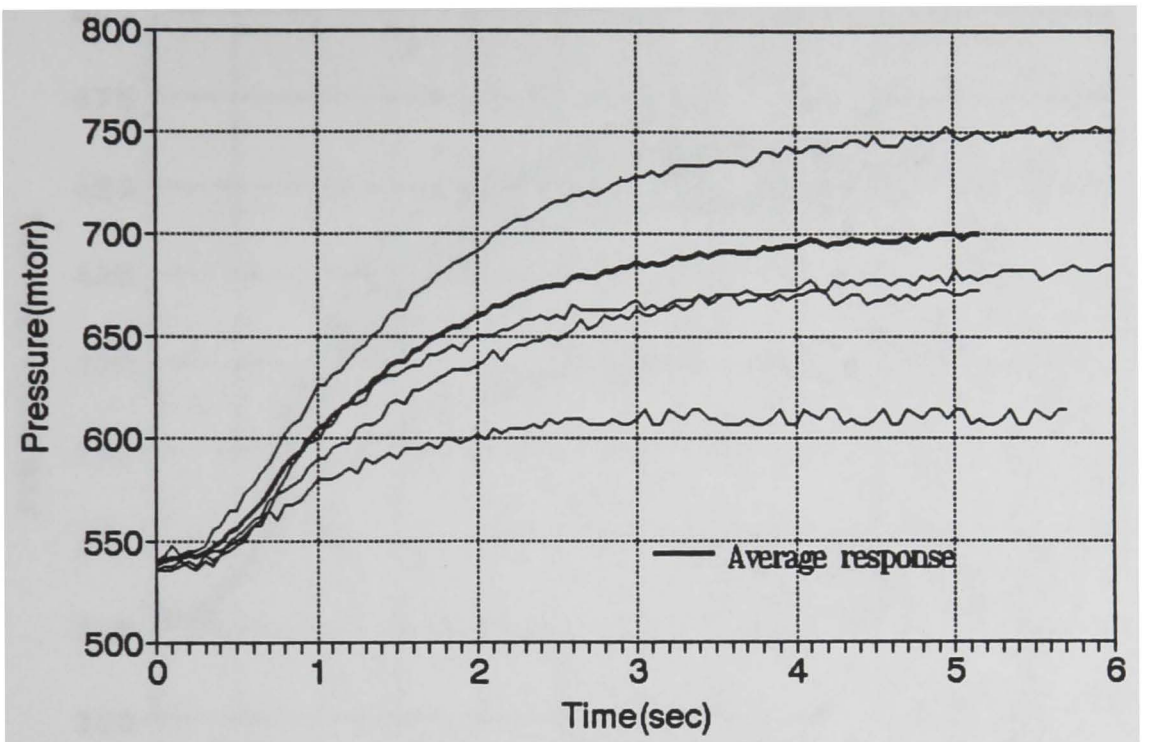

Figure 6.4 Open-loop responses used to determine transfer model for IMC. (Initial valve position = 28 degrees)

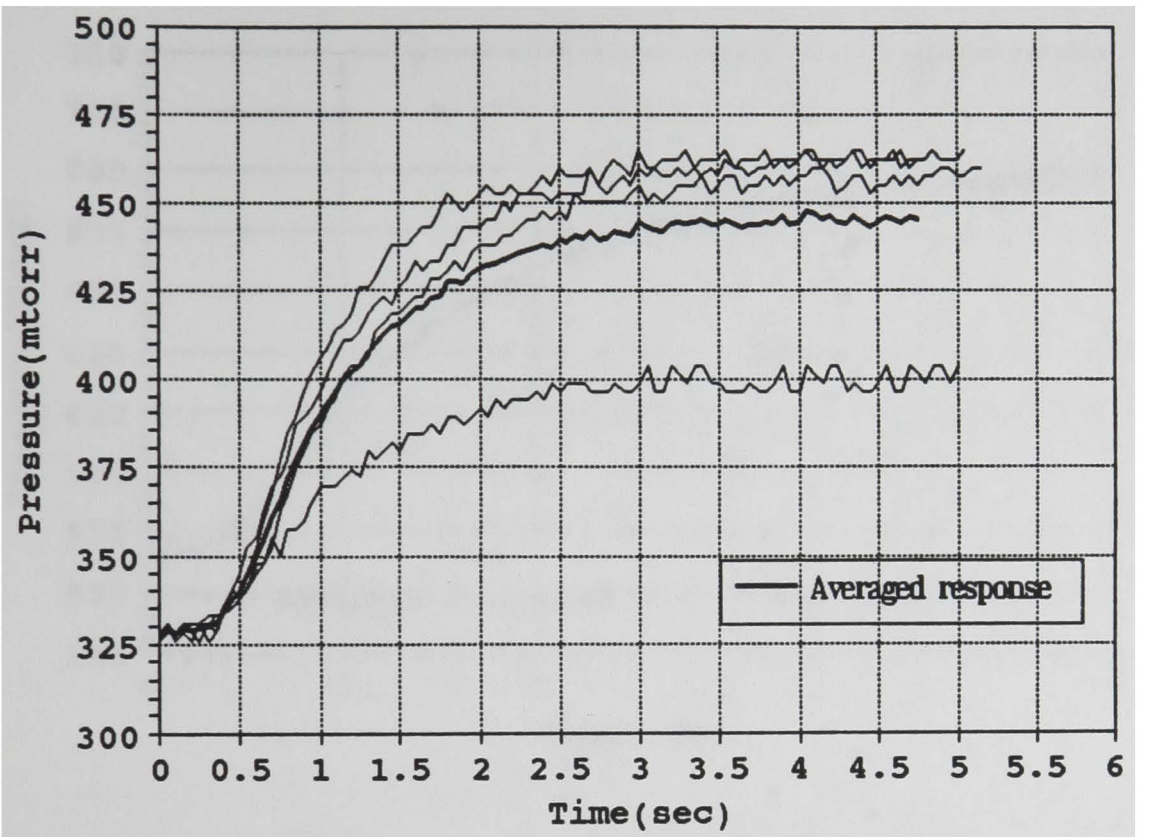

Figure 6.5 Open-loop responses used to determine transfer model for IMC. (Initial valve position = 35 degrees)

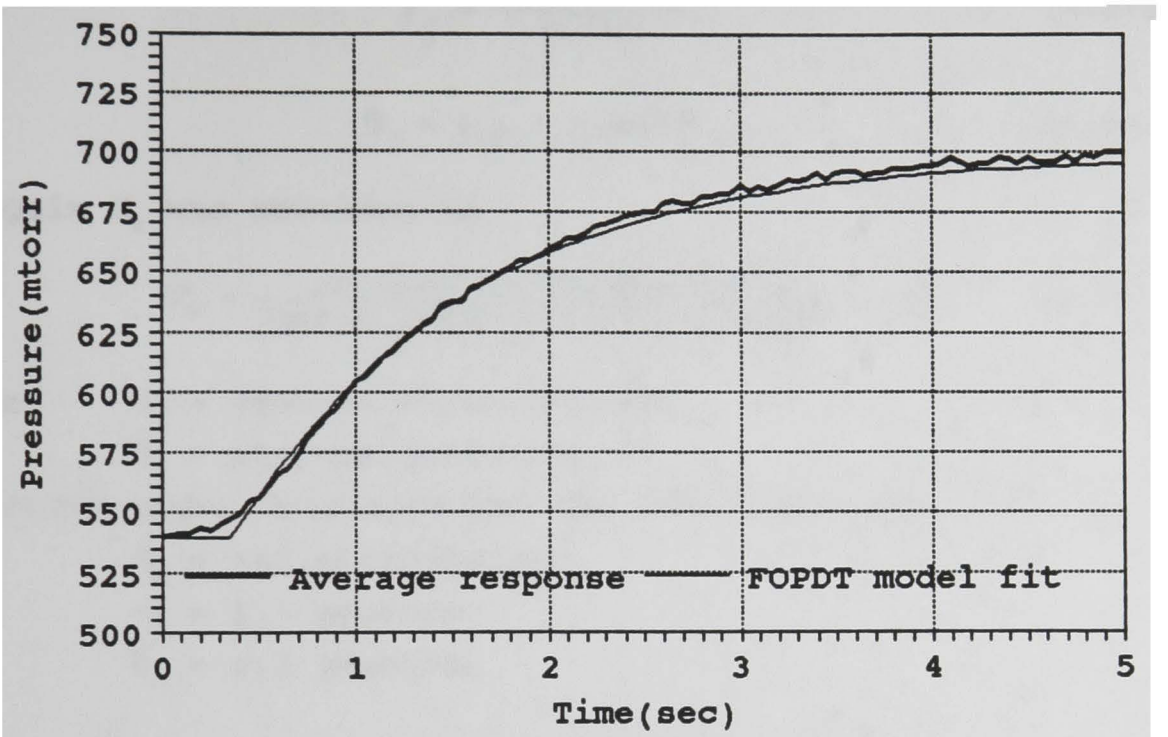

Figure 6.6 Comparison of average process response with transfer function model response.

change in value of the process variable, to determine the time taken to reach 1/3 and 2/3 of its eventual steady-state value. The latter values are used to determine the FOPDT model parameters as given by Equations (6.29) and (6.30).

$$\tau_u = \frac{t_{2/3} - t_{1/3}}{0.693}. \qquad (6.29)$$

$$\theta_u = t_{1/3} - 0.405\tau_u. \qquad (6.30)$$

The gain K_u was obtained as,

$$K_u = \frac{\textit{process variable change}}{\textit{manipulated variable change}} = \frac{\Delta Y}{\Delta u} \qquad (6.31)$$

where, τ_u = process time constant,

θ_u = process dead-time.

The FOPDT model developed had the following parameters.

K_u = -43 mtorr/degree,

τ_u = 1.5 seconds,

θ_u = 0.2 seconds.

6.2.1.1 Gain Scheduling and Disturbance Modelling

IMC uses a linear representation of the process to determine control action. In the process considered in this work the gain varies from -0.1 mtorr/degree when the valve is fully open to -70. mtorr/degree when the valve is open at 20 degrees. The change in gain with valve position is shown in Figure 6.7. If the IMC model were to employ a single gain for the entire region of operation, then the control action taken would be to sluggish in regions where the gain was too low and too aggressive where the gain was too high. To compensate for this inherent deficiency of a linear model the process gain employed by the model was varied as a function of the controlled variable setpoint. The gain can be varied as a function of the manipulated variable, the controlled variable or the controlled variable setpoint. Gain scheduling

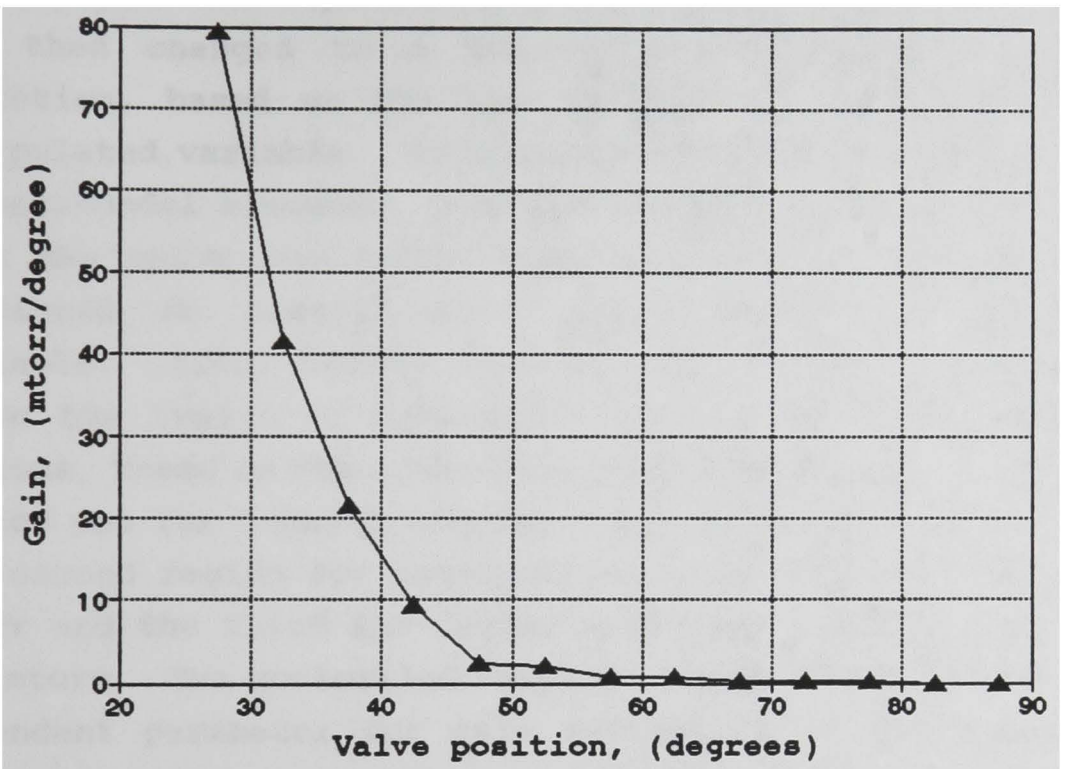

Figure 6.7 Change in gain with valve position

can either be a discrete or continuous function of any of these variables. Relationships between the gain and manipulated and controlled variable were established using experimental data. Continuous relationships, when employed, made the process response very sensitive to slight changes in the manipulated variable as well as process-model mismatch. To remedy this effect, the gain was changed discretely, that is, the gain was kept constant for a given range of operation and then changed to a new value for another region of operation, based on the new position of the controlled or manipulated variable. This change reduced the sensitivity to process-model mismatch. However the gain at start-up, that is when the valve was fully open, was so high that the model predicted an exceptionally large change in manipulated variable. After taking into account the factors described above the region of operation was divided into three main regions, based on the controlled variable setpoint. The first region was for lower pressures ranging from 200 to 350 mtorr, the second region for intermediate pressures from 350 to 650 mtorr and the third for higher pressures ranging from 650 to 900 mtorr. The controlled variable setpoint was chosen as the dependent parameter for gain evaluation as the process was extremely quick to respond to setpoint changes. Hence gain scheduling based on the new setpoint would cause the model to have a gain corresponding to actual process conditions. Since the setpoint remains constant, gain takes discrete values based on the value of the setpoint, thus eliminating sensitivity to process-model mismatch.

Disturbances on account of changes in flow rate are accounted for by the GMC formulation. However the IMC algorithm relies on a purely feedback approach to reject the disturbances. IMC with a feedforward algorithm incorporated as a part of the formulation was employed to reject flow rate disturbances more efficiently. The IMC structure with feedforward control is shown in Figure 6.8. It incorporates

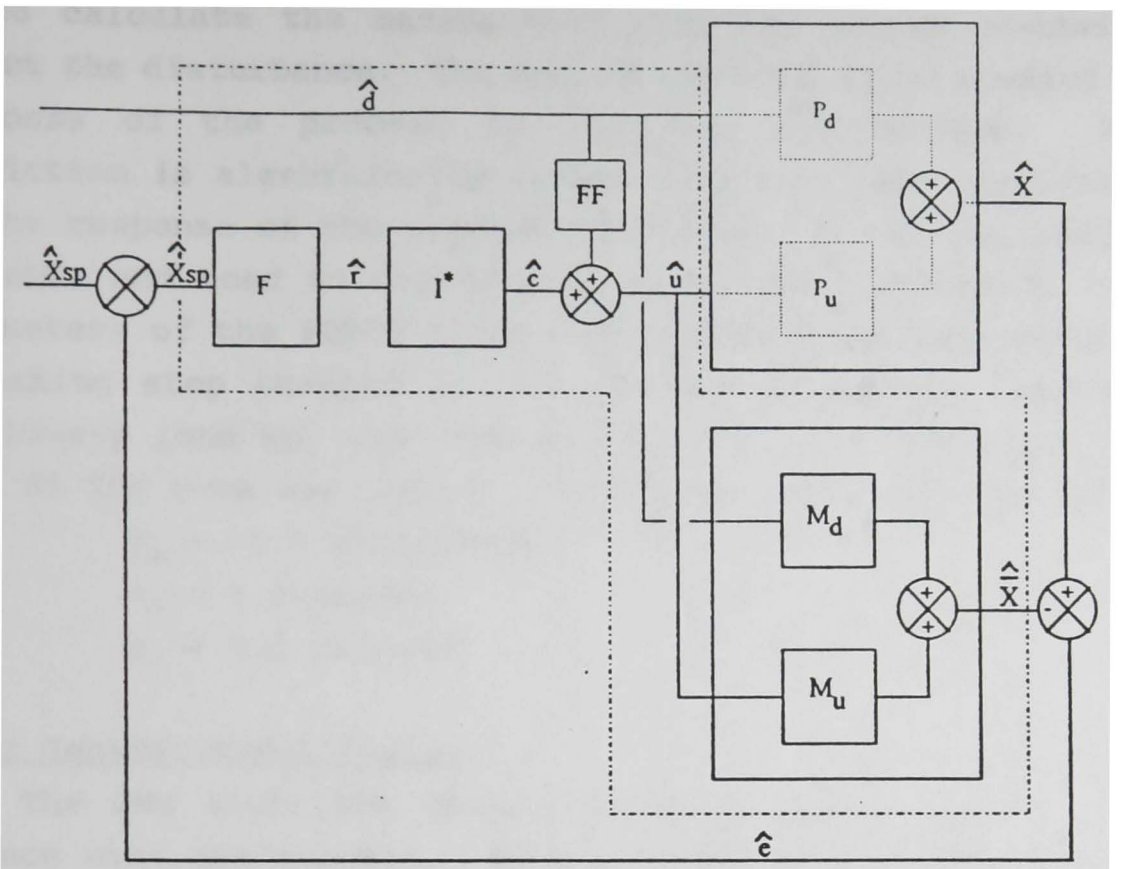

Legend

F - IMC filter
I* - Realizable inverse
FF - Feedforward controller
M_d - Model relating output to disturbance
M_u - Model relating output to manipulated variable
P_d - True unknown process transfer function relating output to disturbance
P_u - True unknown process transfer function relating output to manipulated variable

Deviation Variables

$\hat{X}_{sp}$ - Set-point
$\hat{X}_{sp}$ - Biased set-point
$\hat{d}$ - Disturbance variable
$\hat{c}$ - Controlled variable
$\hat{e}$ - Error or difference between process output and model predicted output
$\hat{X}$ - Process output
$\hat{\hat{X}}$ - Model output

Figure 6.8 IMC structure incorporating feedforward action

an FOPDT model of the process variable response to changes in inlet flow rate. The model has two main functions. The first is to calculate the manipulated variable action needed to reject the disturbance. The second function is to predict the response of the process to the flow disturbance. This prediction is algebraically summed with the model prediction of the response of the process to changes in the manipulated variable and used to calculate process-model mismatch. The parameters of the FOPDT model for disturbances were obtained by making step changes of 25 sccm in the manner described previously (one up, two down and one up). A base case flow rate of 100 sccm was chosen. The parameters obtained were

K_d = +4.1 mtorr/sccm,

τ_d = 4 seconds,

κ_d = 0.6 seconds.

6.2.2 Generic Model Control

The GMC algorithm uses a model developed from a mole balance over the reactor. Both a steady-state and a dynamic mole balance were employed.

6.2.2.1 Dynamic Model

The general form of the dynamic mole balance is

$$\frac{dN}{dt} = F_i \cdot \beta - F_o, \qquad (6.32)$$

where, N = number of moles present in the reactor,

F_i = molar flow rate at the inlet of the reactor,

F_o = molar flow rate at the outlet of the reactor,

β = Model parameter representing the increase in species due to dissociation,

t = time.

Simplifying Equation (6.32) and using the ideal gas law to convert moles to pressure gives,

$$\frac{dP}{dt} = \frac{Q_i \cdot P \cdot \beta}{V} - \frac{Q_o \cdot P}{V}, \qquad (6.33)$$

where, P = pressure in the reactor,

Q_i = volumetric flow rate at reactor conditions at the inlet of the reactor,

Q_o = volumetric flow rate at reactor conditions at the outlet of the reactor,

V = volume of the reactor.

Equation (6.33) was integrated at each control interval to obtain the model predicted pressure. This was compared with the process pressure and the difference used to adjust a model parameter to keep the model true to the process.

Control action was calculated by substituting the simplified GMC control law into Equation (6.33) to give,

$$\frac{dP}{dt} = \frac{Q_i \cdot P \cdot \beta}{V} - \frac{Q_o \cdot P}{V} = K_1 \cdot (P_{sp} - P), \qquad (6.34)$$

where, K_1 = GMC control law constant,

P_{sp} = Pressure setpoint.

Equation (6.34) when rearranged gives,

$$Q_o = Q_i \cdot \beta + \frac{K_1 \cdot (P - P_{sp}) \cdot V}{P}. \qquad (6.35)$$

In Equation (6.35) the only unknown quantity is Q_o, the flow rate out of the reactor, as all the other quantities are either measured or calculated. The flow rate at standard conditions corresponding to the flow rate obtained from Equation (6.35) was then employed to calculate the required manipulated variable action using Equation (3.11) as given by,

$$f(s) = \frac{Q_o}{a\sqrt{(P^2 - P_v^2)}}. \qquad (6.36)$$

The valve stem position, s, was calculated using Equation (4.18). This equation when rearranged gives

$$s = \frac{1}{\log(A) - \log(\frac{Y}{1 - Y})}, \qquad (6.37)$$

where,

$$Y = f(s) = \frac{A \cdot e^{-\frac{B}{s}}}{1 + A \cdot e^{-\frac{B}{s}}}. \qquad (6.38)$$

Hence the controller model can be used with the GMC law to determine the required control action though the controller model does not explicitly relate the manipulated variable to the process variable.

6.2.2.2 Steady-State Model

The steady-state model equation is obtained quite simply from Equation (6.32) by setting the derivative term to zero as the pressure does not change with time at steady state. The simplified equation is,

$$F_i \cdot \beta - F_o = 0. \qquad (6.39)$$

Using the ideal gas law to convert moles to pressure gives,

$$\frac{Q_i \cdot P \cdot \beta}{R \cdot T} - \frac{Q_o \cdot P}{R \cdot T} = 0, \qquad (6.40)$$

or,

$$Q_i \cdot \beta - Q_o = 0 \qquad (6.41)$$

The steady-state formulation of the GMC law as given by Equation (6.28) was employed to determine the steady-state

target pressure,

$$P_{ss} = P + K_1^* \cdot (P - P_{sp}), \tag{6.42}$$

where, P_{ss} = Steady-state target pressure,
K_1^* = Modified GMC law constant.

The steps taken to decide the control action were simple and straightforward. Though the flow rates Q_o and Q_i in Equation (6.41) are at reactor conditions they can be converted to flow rates at standard conditions. The same conversion factor is applied to both sides of Equation (6.41) and hence it retains its original form. The model was first parameterized assuming a pseudo steady-state by using the current measured values of Q_i and P. This step is given by,

$$\beta = \frac{a \cdot f(s) \cdot \sqrt{P^2 - P_v^2}}{Q_i}. \tag{6.43}$$

The steady-state target pressure was then calculated using Equation (6.42). The reparameterized model and the new steady-state target pressure calculated were used to calculate control action using the modified form of Equation (6.41) such that,

$$f(s) = \frac{Q_i \cdot \beta}{a \cdot \sqrt{P^2 - P_v^2}}. \tag{6.44}$$

The valve position required was obtained using Equations (6.38) and (6.39).

6.3 Parameterization

Among the secondary differences in various MBC strategies is the method of handling process-model mismatch. The IMC strategy is to bias the setpoint. Model predictive control (MPC) methods normally assign any process-model mismatch to an unmeasured disturbance and use this to bias all predictions at that time step. The GMC formulation normally handles process-

model mismatch by using an integral term. Signal and Lee (1989) suggest using an adaptive control method of updating model parameters online by employing the error between the predicted and actual outputs to drive the mismatch to zero. Incremental Parameterization Online (IMPOL) (Rhinehart and Riggs, 1991) is a method used to parameterize the model at every control interval regardless of whether steady state is achieved or not. It is simple, extremely easy to apply, computationally efficient and yet has a phenomenological significance. This method and its applications to PMBC using both dynamic and steady-state models was demonstrated in this work and is discussed subsequently. However, the importance of selecting a "good" model parameter is discussed first.

The selection of a model adjustment parameter is one of the critical decisions involved in the selection of a good model. The model parameter selected should be such that it has an influential effect on the process and the model. It normally represents a combination of various other constants or parameters in the model, equations whose effect on the model and hence the process, cannot be determined with a great degree of certainty. The model parameter must be robust enough to handle large mismatches in process and model and yet maintain the model on the correct trajectory. NPMBC offers a significant advantage as regards model parameterization because the model parameter has a phenomenological significance and can be used for process diagnostics.

The model adjustment parameter, β, selected for the controller models used in this work, has embedded within it, the factors in the model that cannot exactly account for the process. These factors include the creation of new species when the discharge is turned on and their subsequent recombination, errors in representing the inherent valve characteristic, errors in flow and pressure measurement and errors in the determination of downstream vacuum pressure and the valve flow coefficient used in the model. The model

parameter is an approximate measure of the dissociation when the plasma is turned on. Its phenomenological basis is demonstrated by considering the model in its simple input-output form,

$$\frac{dN}{dt} = F_i \cdot (1 + X) - F_o, \qquad (6.45)$$

where, N = number of moles in the reactor,
F_i = Flow of moles into the reactor,
F_o = Flow of moles out of the reactor,
X = dissociation at any time t.

Thus β, which represents the term 1 + X, includes changes due to dissociation as well as changes due to input flow disturbances.

6.3.1 Dynamic IMPOL Calculations

The IMPOL method (Rhinehart and Riggs, 1991) aims to find a value of the model parameter, ϕ, such that the differences between the actual output variable and the predicted output variable becomes zero. The predicted value of the output variable is obtained by integrating the differential equation which relates pressure to time. Thus a single step adjustment to ϕ is obtained by applying a Newton's method as given by ,

$$\phi_{new} \sim \phi_{old} - \frac{\epsilon_t}{\frac{\partial \epsilon}{\partial \phi}\Big|_t}, \qquad (6.46)$$

where, ϵ_t = difference between model predicted output and process output at any time t,
ϕ = model parameter.

The form of the parameterization relationship using a dynamic model to determine the sensitivity is,

$$\phi_t = \phi_{t-\Delta t} + \frac{e_t}{\Delta t \cdot \frac{\partial f}{\partial \phi}\Big|_{t-\Delta t}}, \qquad (6.47)$$

where, Δt = parametrization interval,

$\phi_{t-\Delta t}$ = value of the model parameter at the previous sampled instant,

f = functional relationship representing the model.

Since Newton's method is a linearization, Equation (6.47) occasionally over estimates or under estimates the changes in the parameter ϕ. A relaxation coefficient was hence incorporated in Equation (6.47) such that,

$$\phi_t = \phi_{t-\Delta t} + \frac{\alpha \cdot e_t}{\Delta t \cdot \frac{\partial f}{\partial \phi}\Big|_{t-\Delta t}}. \qquad (6.48)$$

This relaxation coefficient adjusts the correction such that tracking is accurate. Larger values of α make parameter tracking more aggressive while smaller values make it sluggish.

The controller model represented by Equation (6.33) when differentiated with respect to the model parameter gives,

$$\frac{\partial f}{\partial \beta} = \frac{Q_i \cdot P}{V}. \qquad (6.49)$$

Using the parameterization relationship given by Equation (6.46) and substituting the result of Equation (6.49) gives

$$\beta = \beta_{old} + \frac{V \cdot (P - P_m)}{\Delta t \cdot Q_i \cdot P}, \qquad (6.50)$$

where, P_m = Pressure predicted by the model,

β_{old} = Value of the parameter at the sampled instant.

Equation (6.50) represents the dynamic form of the parameterization relationship employed in this work. β, in

this case, is a dimensionless parameter just as dissociation is. However, model parameters need not always be dimensionless. α was maintained at the ideal value of unity, though values ranging from 0.5 to 2.0 were experimented with.

CHAPTER 7
CONTROLLER IMPLEMENTATION ON THE SIMULATOR

7.1 Introduction

The controller models developed in Chapter 6 were tested on the simulator. Initial testing on the simulator helped evaluate the performance of the various models before their actual implementation on the process. The models developed were parameterized at an initial steady state, run in parallel with the process and their predictions compared with simulated process output. The variation in the adjustable model parameter, present in the process model-based controller models, was studied in an attempt to determine the effect of the process as well as the process-model mismatch on control performance. Since the model parameter has a phenomenological significance, the trends displayed by the model parameter were used to verify certain phenomena later observed in the actual process. In addition an approximate set of tuning coefficients to be employed was also determined from preliminary controller tuning on the simulator. "Fine tuning" the controller models on the simulator helped to determine and correct any deficiencies in that particular model and hence simplified implementation on the experimental system.

7.2 Simulator Modifications For Testing

Pressure in the experimental system was measured using a pressure sensor and the total concentration of species computed from this measurement using the ideal gas law. The simulator employed the reverse procedure. The equations representing the mole balance of each species over the reactor were integrated to obtain the species concentration at each time step. These concentration measurements were then summed to obtain the total concentration and the pressure calculated from the total concentration.

Every process measurement is corrupted by "noise" on account of the measuring instrument. To reproduce this same effect on the simulator a randomly generated noise was added to the pressure determined by the simulator. Instrument calibrations tend to change with time thus leading to a deterioration in the accuracy of the measurements and hence control performance. This "drift" effect was incorporated in the simulator as well.

Artificial process-model mismatch was created by altering various parameters such as the valve coefficient, the vacuum pressure and the constants employed in the relationship used to describe the inherent valve characteristic. The values used by the process model-based control algorithms were different from those employed in the simulator. Noise and drift were also added to other process measurements such as the reactor chamber temperature and the flow rate measured at the entrance of the reactor. The simulator employs a twenty equation set to represent the process while the controller models employ a single equation. This in itself creates a mismatch between the controller and the simulated process.

The simulation interval used for certain regions of operation was extremely small (10^{-5} seconds). This small interval ensured that even small changes in species concentration during the power and flow disturbances as well as setpoint changes were accurately tracked. However, when there was no dissociation and the conditions in the reactor were near steady state, the simulation interval was increased to 0.1 seconds.

7.3 Controller Model Adaptation

Though the pressure was determined at every simulation step, pressure was sampled every 0.25 seconds irrespective of the simulation interval. Parameterization was carried out at the same frequency as the sampling for both the steady-state model as well as the dynamic model. This constant control and

parameterization interval was maintained by a counter whose value changed depending on the simulation interval. An initial value of unity for the model parameter was supplied to the controller model.

IMC was implemented using the position mode of the algorithm. This involved initializing the variables at some initial reference steady state on account of the negative process gain, that is, the pressure increased with the closure of the valve and vice-versa. All calculations for the IMC algorithm were done in deviation variables with the final manipulated variable action being calculated as a difference from the initial reference point. The PI controller algorithm employed a similar mode with the final manipulated variable action calculated being added to the initial reference value.

The controllers were tested for a large number of cases with different tuning coefficients being employed. The general test case consisted of the initial start-up, power disturbance and a setpoint change or a flow disturbance in that order. The artificial mismatch created was varied based to study the effect on controller performance. Controller constraints such as the limitation in the movement of the valve were also incorporated. Performance of the various controllers was compared using both integral of absolute error (IAE) and Integral of Time Absolute Error (ITAE). The latter test levied a penalty on the control test cases which took a longer time to return to setpoint.

7.4 Overview of Simulated Control Results

Detailed control results are not presented in this section as the simulator was merely a tool employed to determine the effectiveness of the various control algorithms. Figures 7.1 to 7.10 show the results obtained using nonlinear process model-based control (PMBC) and internal model control (IMC). It was observed that the performance of both model-based controllers was equivalent with respect to performance

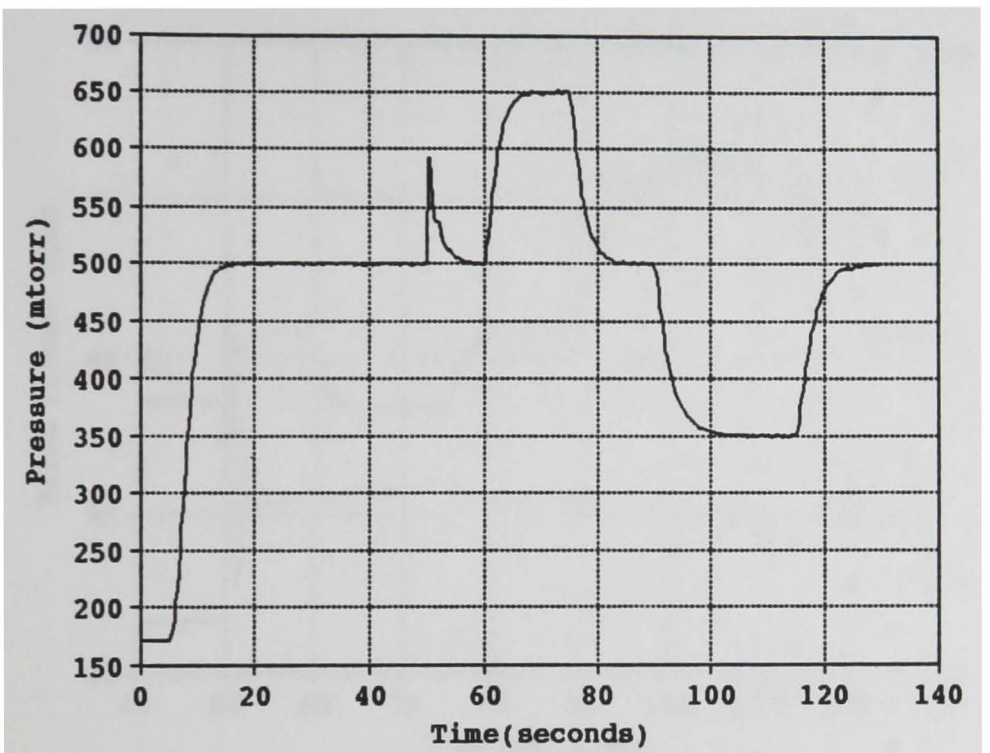

Figure 7.1 Pressure response for setpoint change using PMBC

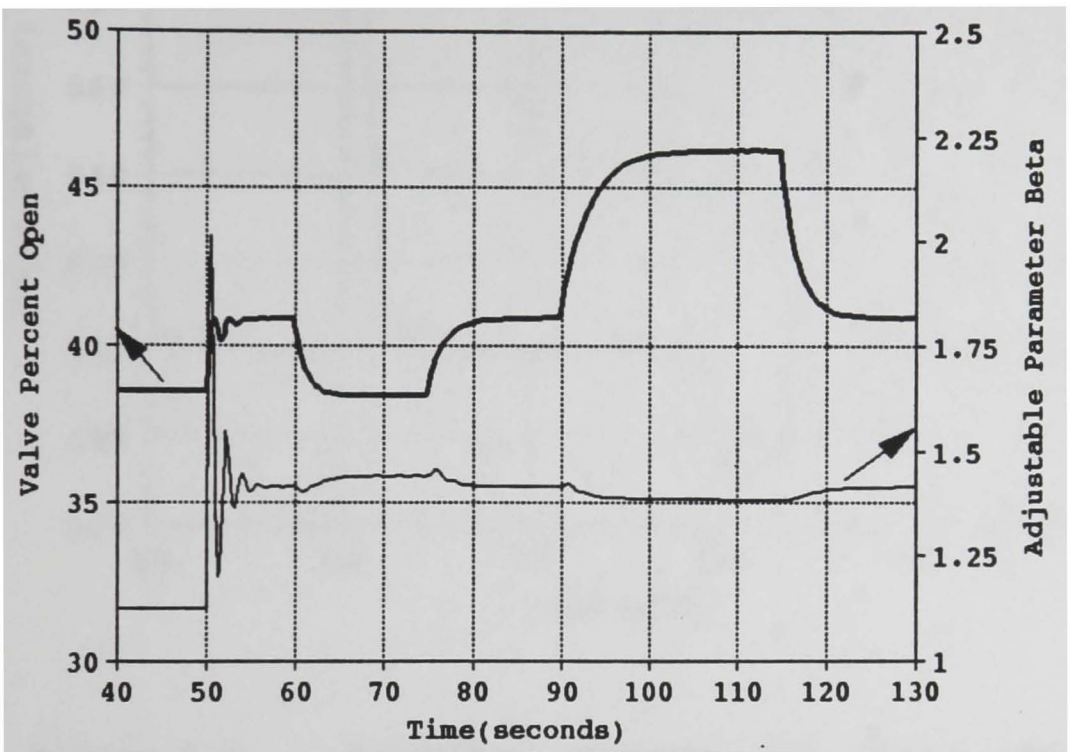

Figure 7.2 Change in valve position and adjustable parameter for setpoint change using PMBC.

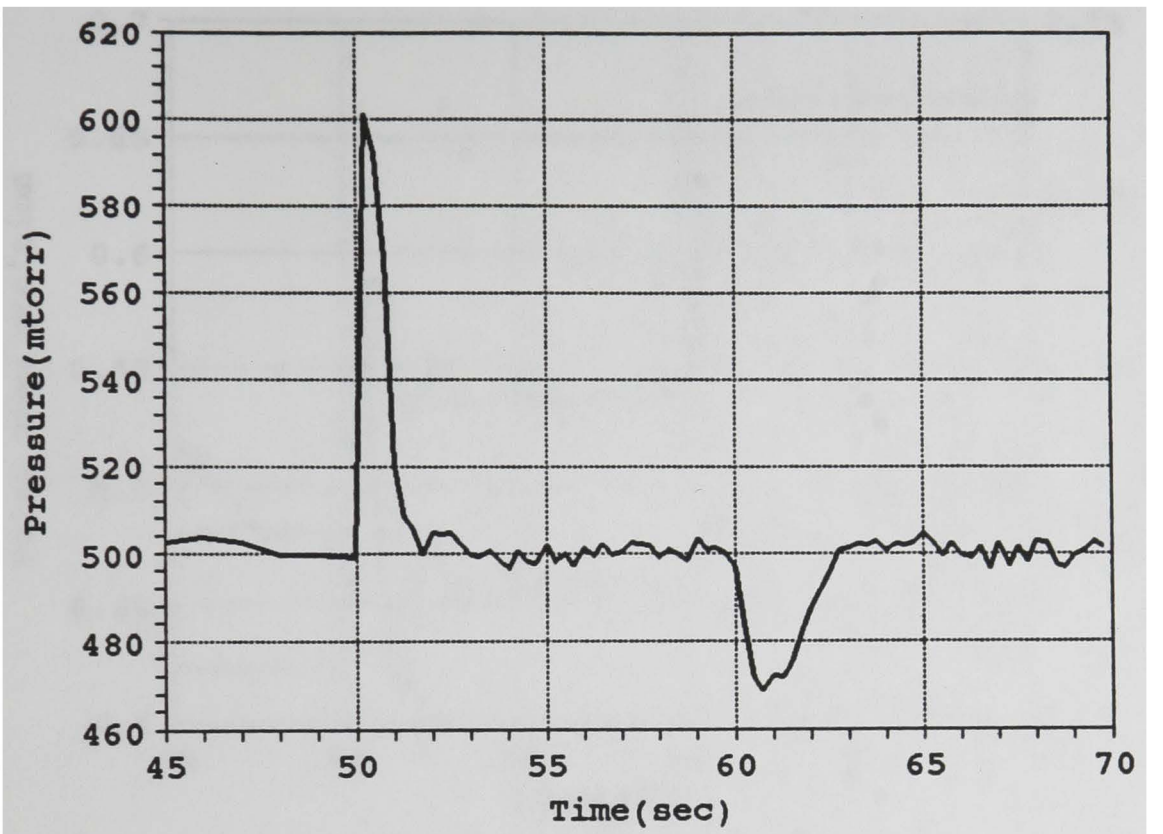

Figure 7.3 Pressure response for power and flow disturbance using PMBC.

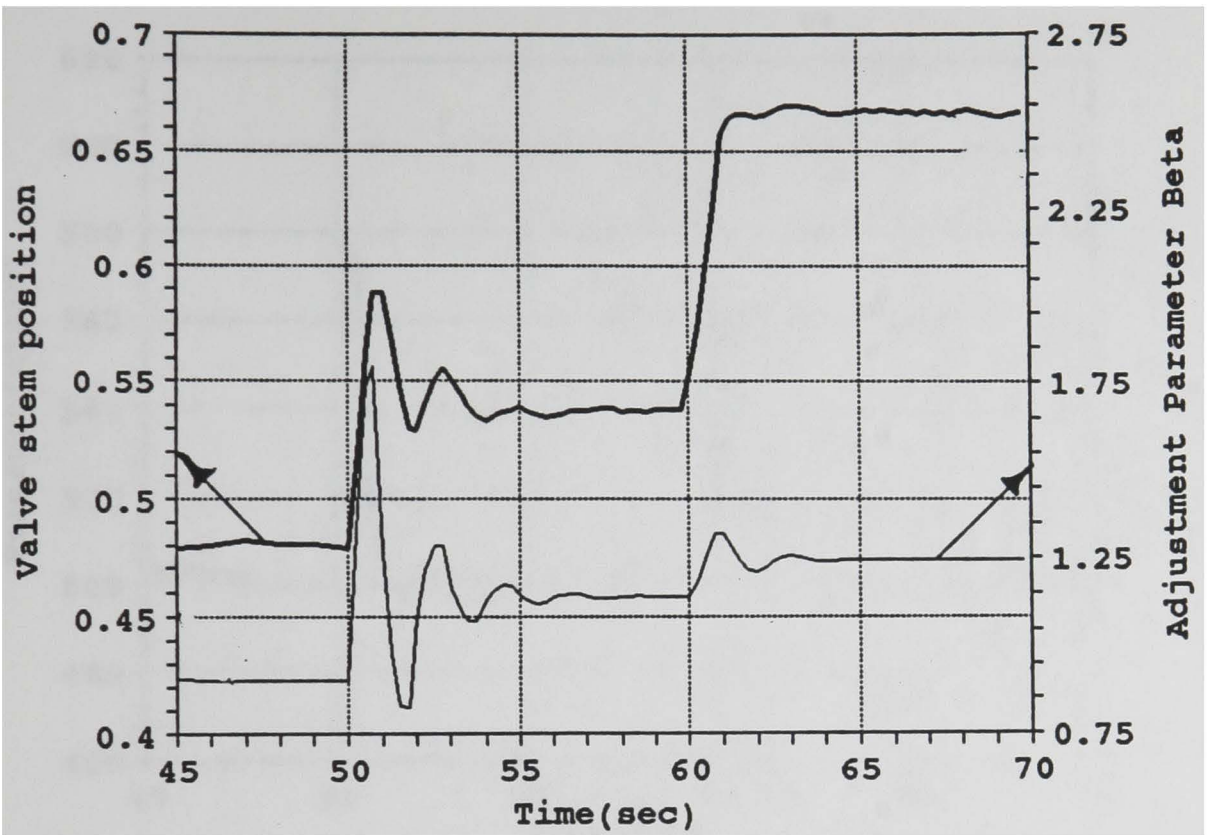

Figure 7.4 Change in valve position and adjustable parameter for power disturbance and increase in flow using PMBC.

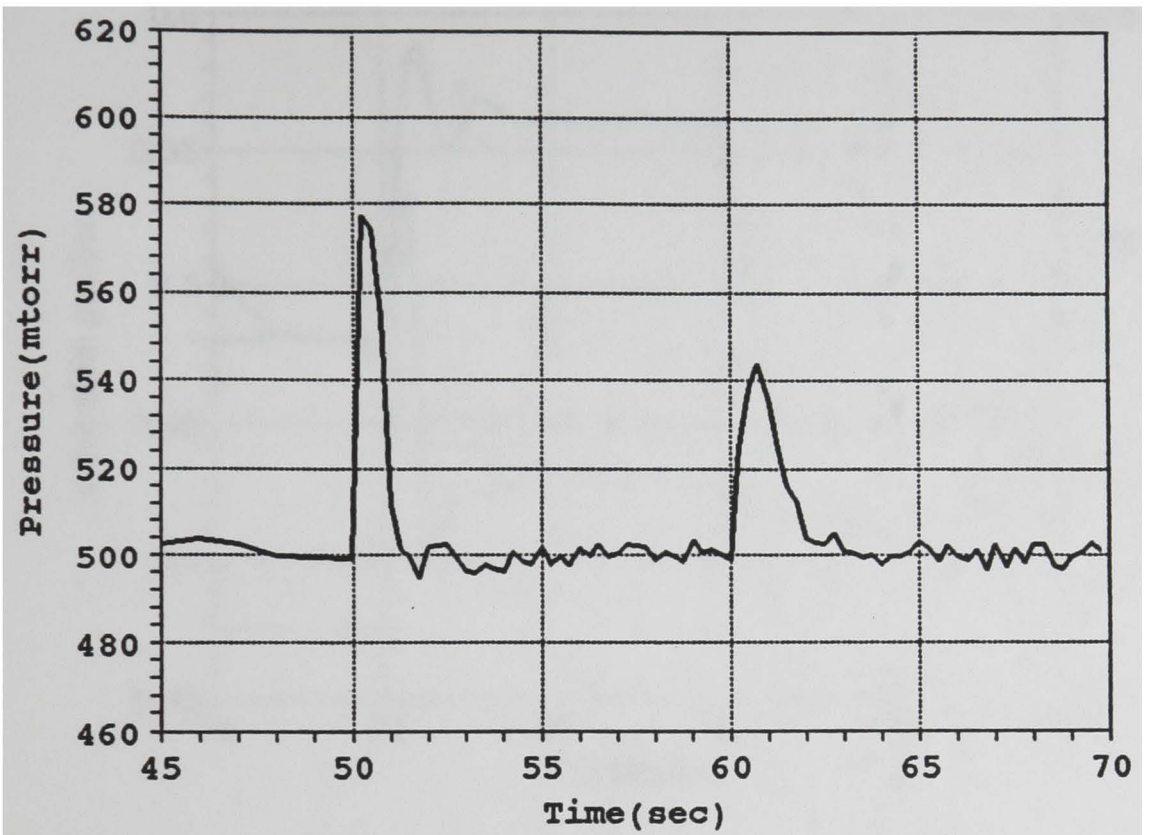

Figure 7.5 Pressure response for power and flow disturbance using PMBC.

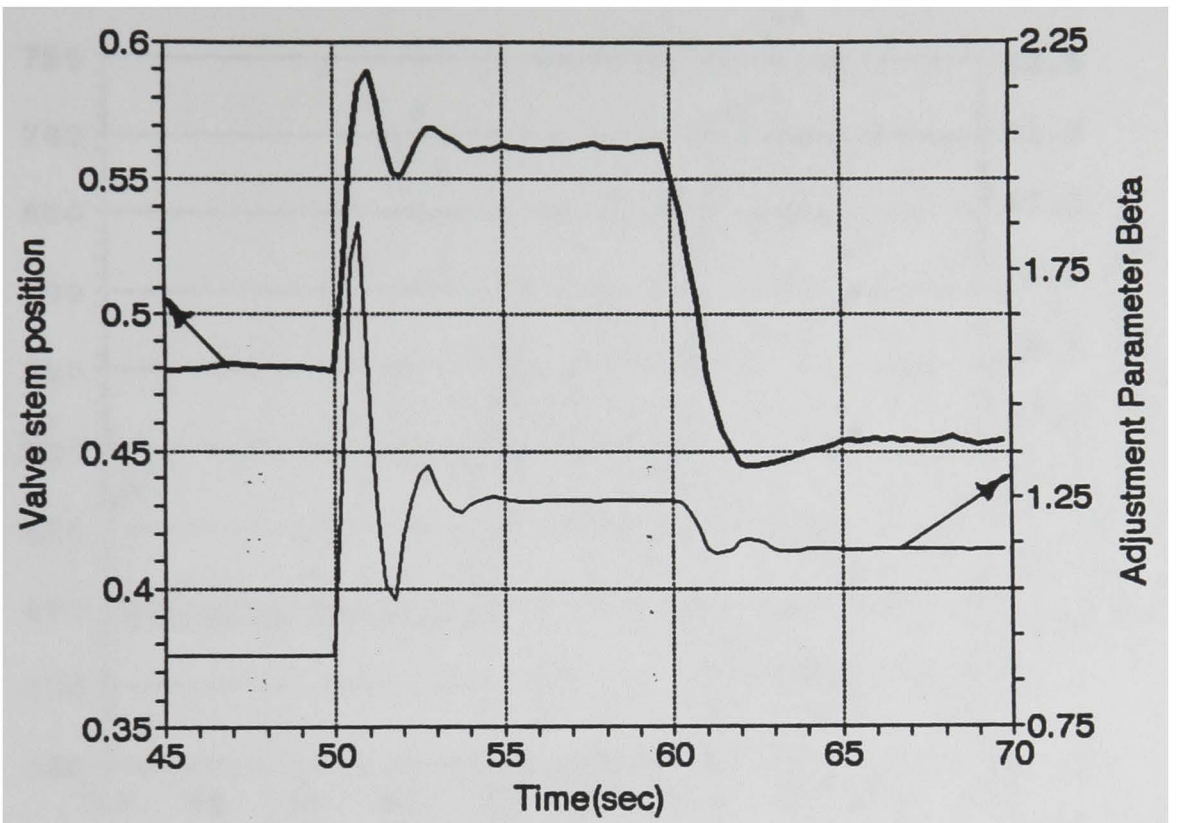

Figure 7.6 Change in valve position and adjustable parameter for power disturbance and decrease in flow using PMBC.

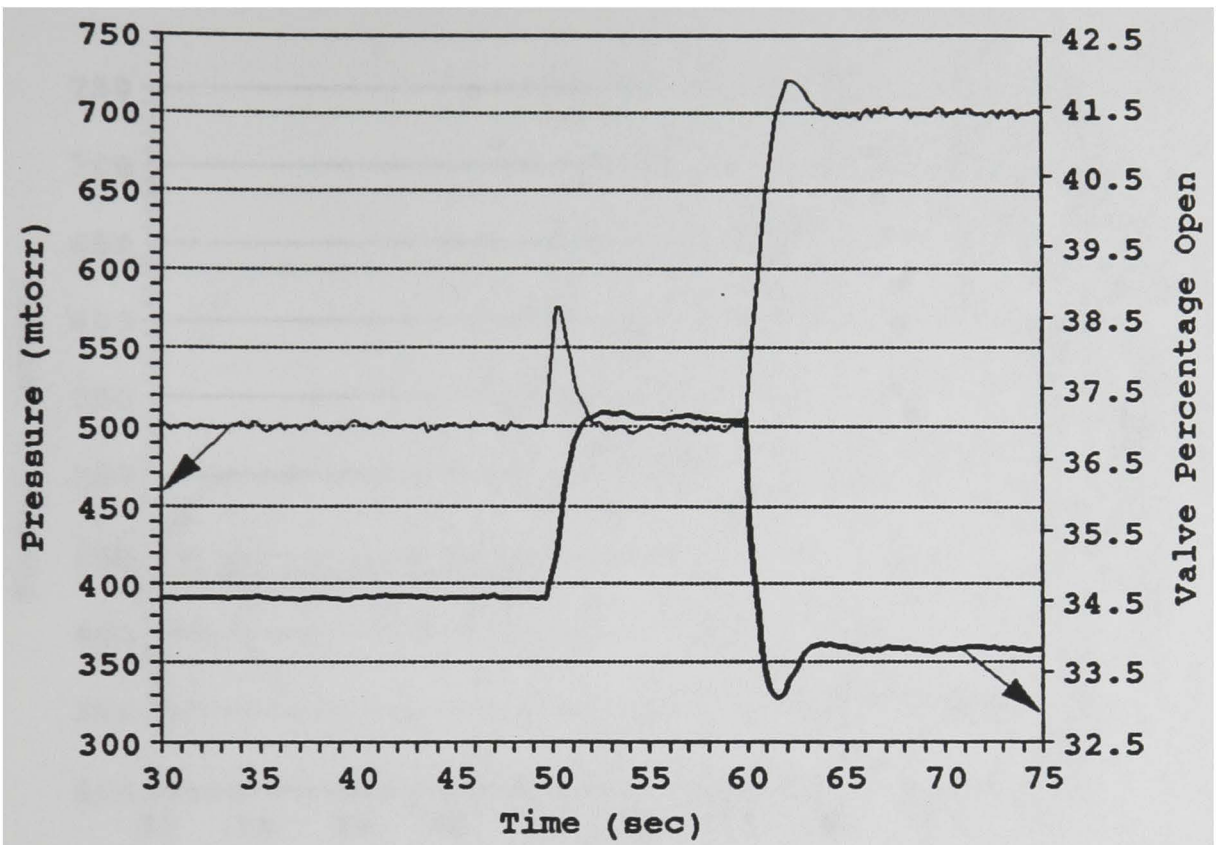

Figure 7.7 Pressure response and change in valve position for power disturbance and setpoint change using IMC.

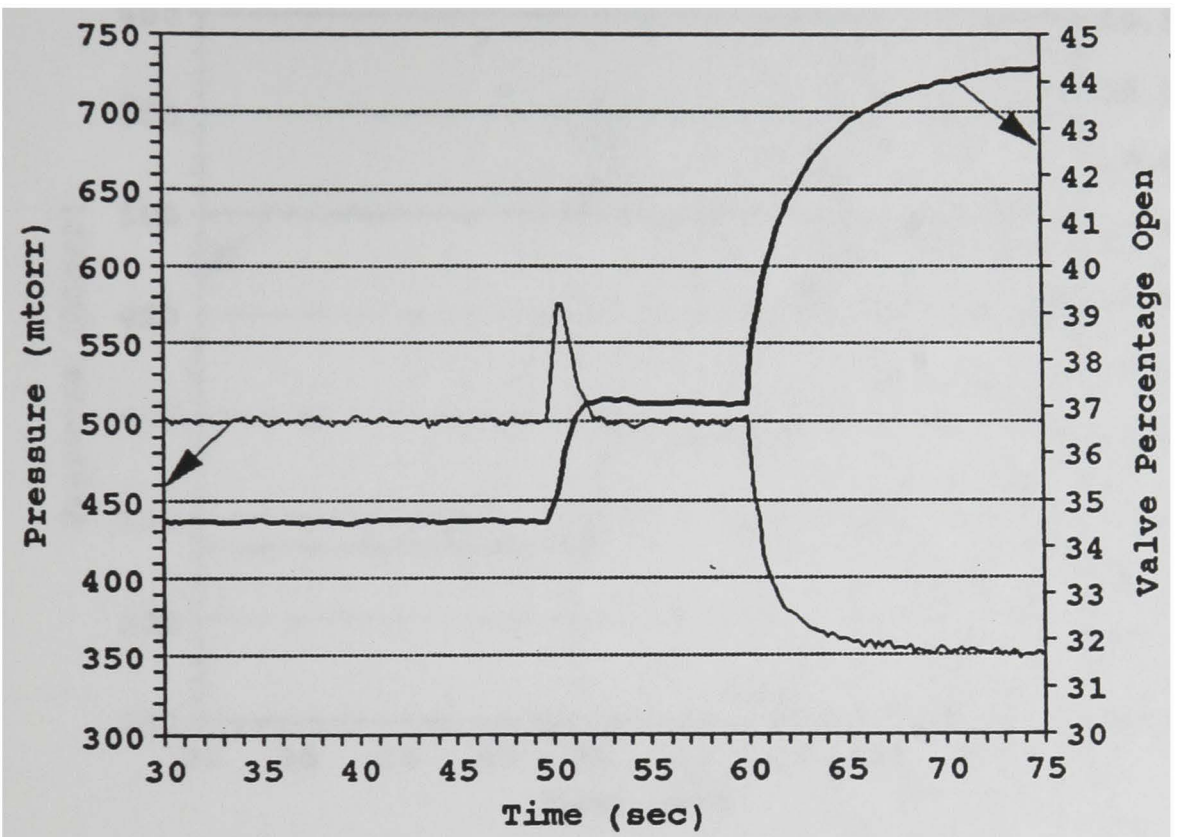

Figure 7.8 Pressure response and change in valve position for power disturbance and setpoint change using IMC.

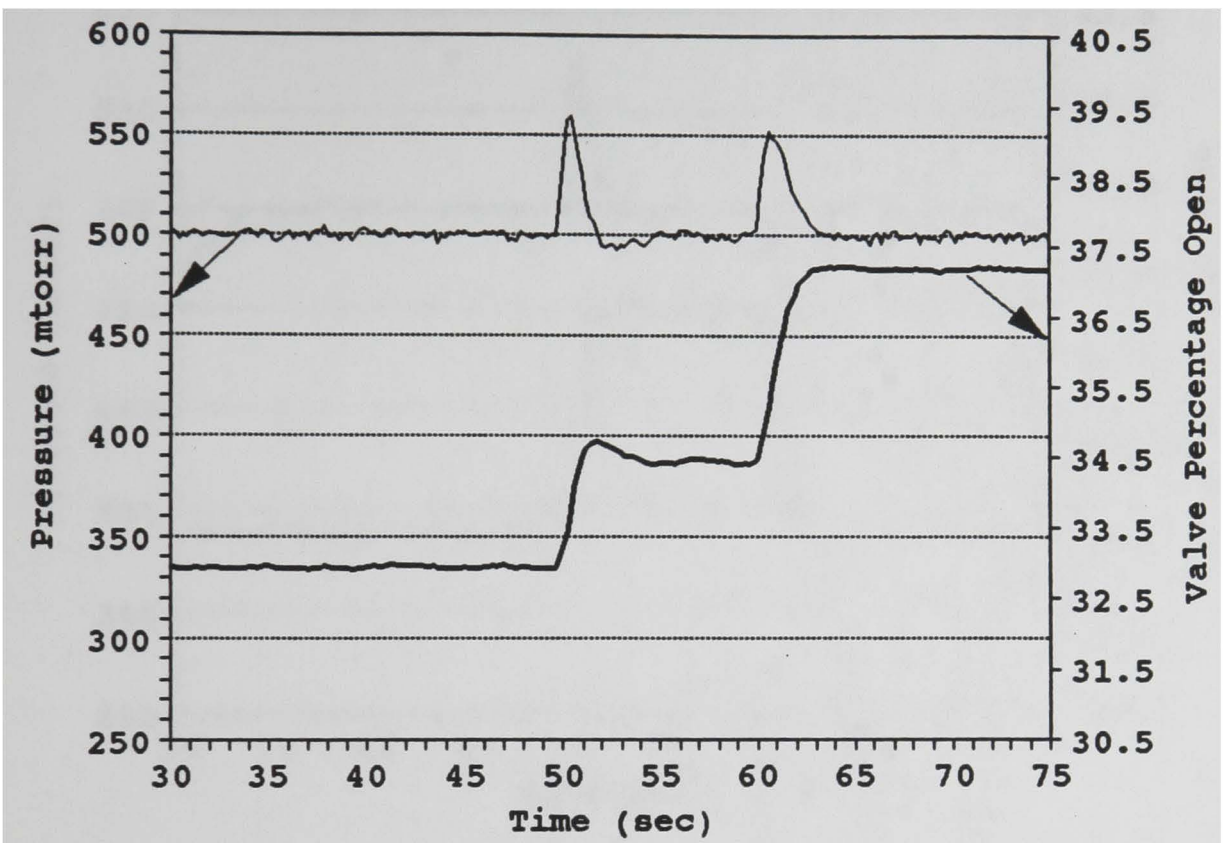

Figure 7.9 Pressure response and change in valve position for power disturbance and flow increase using IMC.

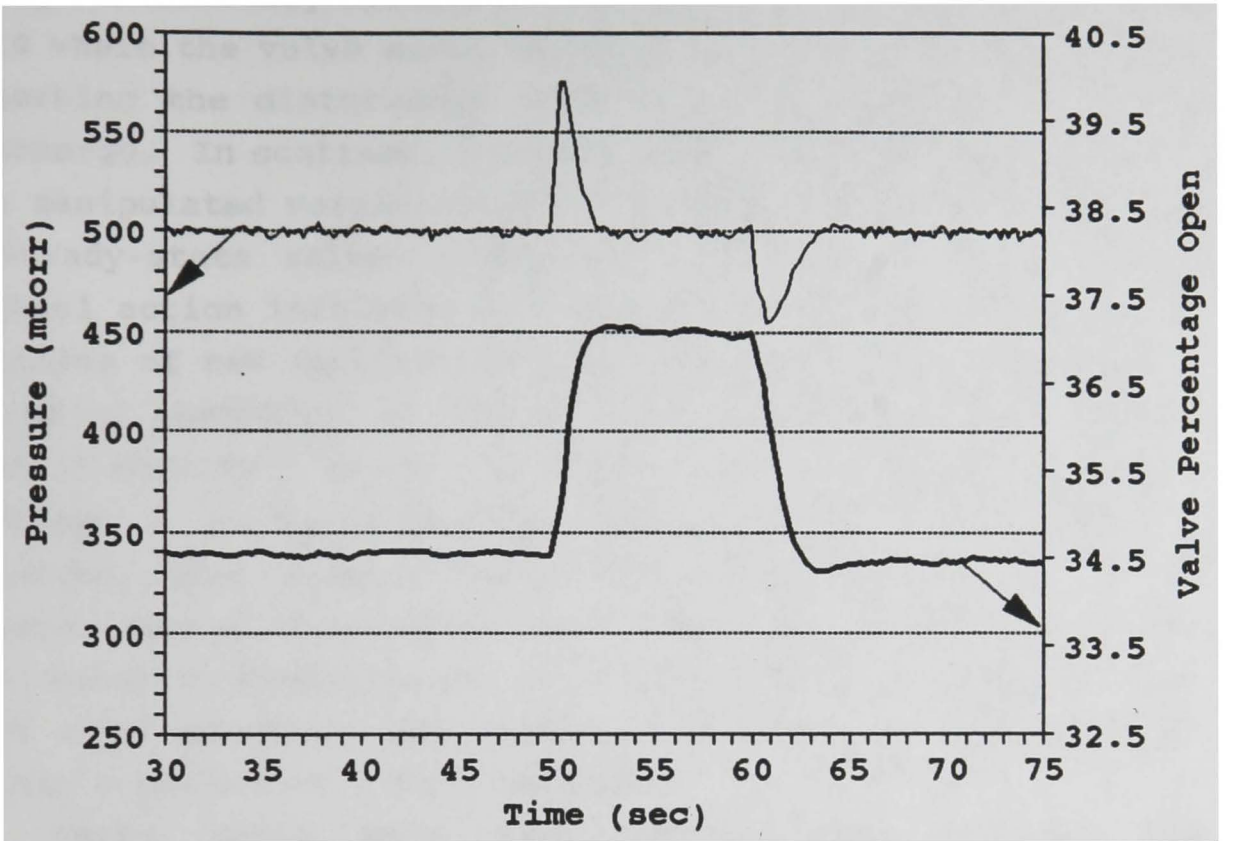

Figure 7.10 Pressure response and change in valve position for power disturbance and flow decrease using IMC.

criteria such as ITAE, IAE and the rate of change of manipulated variable. In the case of disturbance rejection, the performance of the IMC algorithm was superior to that of PMBC algorithm, with the rate of change of valve position being considerably smaller. This is seen from Figures 7.9 and 7.10 where the valve moved smoothly to its new position after absorbing the disturbance created by the initiation of the discharge. In contrast, when the PMBC algorithm was employed, the manipulated variable tended to oscillate before reaching a steady-state value. This was on account of the robust control action initiated by the model parameter. The sudden creation of new species was reflected in the sharp change in the model parameter, β, which initially, rapidly increased as seen in Figures 7.4 and 7.6. This caused the model to predict a change in the valve position, considerably larger than that required, thus causing the initial oscillation of the valve. However, the process model-based controller was able to handle the change in dissociation, as a result of the change in flow, much more smoothly and pressure returned to its setpoint within a period of 3 to 4 seconds.

Servo tests were also carried out on both the controllers. The IMC-based controller displayed an extremely sluggish response when the setpoint was changed from 500 mtorr to 350 mtorr as seen from Figure 7.8. This phenomena was later observed on the experimental system as well and was attributed to the inherent deficiency of a linear model when operating in a nonlinear region of operation. A setpoint change from 500 mtorr to 700 mtorr displayed a slight overshoot as the controller tuning was too aggressive in this region of operation.

Tuning parameters employed for the nonlinear dynamic model-based controller ranged from 0.75 to 1.5 s^{-1}. For the steady-state nonlinear model-based controller the tuning parameter was maintained at 1. The value of the relaxation coefficient employed in the parameterization relationship

ranged from 0.5 to 1.25. It was observed that maintaining this parameter at the ideal value of unity, led to over-aggressive parameterization and caused large changes in the manipulated variable. The range of filter time constants employed by the IMC algorithm ranged from 0.6 to 1.3 seconds. It was observed that, in general, the IMC algorithm was less dependent on changes in tuning parameters as compared to the process model-based control strategies.

CHAPTER 8
EXPERIMENTAL IMPLEMENTATION ISSUES

8.1 Introduction

Experimental issues can be very different from implementation of the control algorithms on the simulator. Though the algorithm remains the same, issues such as the rate of change of the valve, noisy data, time coordination and system lags and delays very often have a significant effect on controller performance. Some of the important issues are discussed in the following sections.

8.2 Sampling Interval and Valve Travel

In order to maintain a constant sampling and control interval of .22 seconds and ensure accuracy in controller performance, the rate of change of the valve was restricted to a maximum of one degree at any one control step. This ensured that the sequence of steps, namely data sampling, calculation of control action required, sending of the signal from the computer to the valve and the eventual movement of the final control element was achieved in .22 seconds. As a heuristic, at least twenty control actions, desirably thirty, within the transient are needed to ensure good control.

The extremely quick process dynamics of the process, lead to very small settling times in the range of 4.5 to 6 seconds. A sampling frequency of .22 seconds was needed to achieve at least twenty control actions. The controller signal to the valve was sent such that the valve moved in pulses of .2 degree. This was the smallest amount of resolution achievable without sacrificing on the accuracy of valve movement. A repetitive structure in the algorithm was employed to transmit these pulses for a fixed count of iterations depending on the change in valve position desired. The rate of change of the valve was restricted to one degree by restricting the number of pulses. Hence the total amount

of time elapsed in sending the signal and in the movement of the valve, remained almost constant, thus allowing for regular sampling.

For valve movement less than one degree the control interval was slightly smaller as the number of pulses transmitted decreased. However the error was insignificant compared to the resolution of the in-built clock in the computer. The maximum accuracy the computer clock could achieve was .055 seconds. Since the minimum amount of valve travel that could be handled was .2 degree, any change in valve position that calculated that was less than .2 degrees would not cause any pulses to be sent and hence the valve would remain at its original position. Therefore, till the control action calculated was sufficiently large to cause a change in the valve position, it had to be ensured that the controller algorithm "knew" that the valve position had not changed.

8.3 Time Coordination

This problem arose when employing the steady-state model in association with the GMC law for control. The steady-state model normally assumes that the process is at or near steady conditions before reparameterizing. However for extremely rapid responding processes, where a new steady state is achieved extremely rapidly, a pseudo steady state is assumed to occur at each sampling interval. The model is parameterized at this pseudo steady state based on the measured value of the controlled variable and the estimated value of the manipulated variable, as the actual valve position was not a measurable quantity. The only time the actual valve position was known was when the valve was at its two extreme positions, that is, open or close. These two positions were indicated by a lamp on the front panel of the pressure controller which was supplied with the reactor assembly.

Based on the steady-state target and the reparameterized model, a desired manipulated variable action was calculated. The initial change in the manipulated variable predicted by the controller model was very large. This was offset by restraining valve travel to a maximum of 1 degree as explained in the previous section. The controller model assumed that the desired valve position was attained immediately after the control action was calculated. However the valve moves only fractionally toward its new position and hence the pressure change is also insignificant. If the controller model were to employ the assumed valve position and the sampled pressure measurement to calculate the control action for the next interval, it would have led to a wrong control action being calculated. This was because the model was using a measured value of pressure and an assumed valve position which did not correspond.

To offset this problem the valve position employed by the controller model was filtered. As described in Chapter 6, a filter basically adjusts the extent to which a current measurement of a process variable, is used for subsequent calculations. By filtering the valve position used by the model during parameterization, it was ensured that the controller model used a valve position that was lagged and represented, to a large extent, the actual valve position at that instant. The amount of filtering required was not constant and changed depending on the process conditions. An accurate relationship relating the filter factor to either pressure or valve position could not be established and employing a constant filter factor was meaningless as it changed by a factor of four. Hence a self adjusting filter factor was employed.

For any filter, the filter factor is a ratio of the simulation, or alternately the control interval, and the approximate time constant for the process as given by,

$$f = \frac{t}{\tau}, \tag{8.1}$$

where, f = filter factor,

τ = time constant of the process,

t = simulation or control interval.

The process may be represented by a lumped parameter model based on a perfectly mixed tank or what is termed as a Continuous Stirred Tank Reactor (CSTR). A material balance, over the system, with time as the independent variable gives,

$$Q \cdot C_i(t) - Q \cdot C_o(t) = \frac{d}{dt} \cdot [V \cdot C_o(t)], \tag{8.2}$$

where, Q = volumetric flow rate,

C_i = concentration at inlet,

C_o = concentration at outlet,

V = volume of the reactor.

or,

$$C_i(t) - C_o(t) = \tau \cdot \frac{dC_o(t)}{dt}, \tag{8.3}$$

where the time constant for the process is given by the ratio of the volume of the reactor to the flow out of the reactor. Based on an approximate measurement of reactor volume and the calculated flow rate out of the reactor, the time constant was obtained for each sampling interval. The flow rate used to calculate the filter factor corresponds to actual reactor conditions, and is obtained from the flow rate at standard conditions using,

$$Q_r = Q_{std} \cdot \frac{P_{std}}{P_r}, \tag{8.4}$$

where the suffixes "r" and "std" denote reactor and standard conditions respectively. Thus, the filter factor was continuously adjusted based on process conditions. This

approach helped the model keep an accurate track of the process and the changing valve position. The filter factor changes appreciably during start-up and tracks process changes efficiently.

8.4 Noisy Data

Any process measurement is normally corrupted by a random error on account of the measuring instrument. This random error is termed as "noise". When the noise levels are too high the value of the actual measurement is meaningless as the error in measurement may be very large. Noisy data can lead to a variety of other problems such as large changes in model parameters on account of noise being transmitted to the parameters through the measured process variable. It may also cause the same effect on the manipulated variable thus causing wear and tear of the final control element. To counter the effect of random noise, a first order filter is normally employed to filter either the measured process variable, the adjustable parameter or the controller output signal. The filter factor chosen is small when the noise levels are high and vice-versa. However filtering has its disadvantages in that it introduces an artificial lag in the process thus slowing down the response of the process to a change in the manipulated variable.

During the experiments, noise on the measurements generally varied from 3 to 7 mtorr. This amount represented approximately 1 to 2% of the actual measured value. After considering all the filtering options, it was found that the effect of filtering was more of a detriment than a benefit, as the process response was considerably sluggish specially near the setpoint. The latter characteristic hampered offset removal, particularly in the case of PMBC, as filtering caused smaller changes in the adjustable parameter leading to even smaller changes in the manipulated variable. The change in manipulated variable was often less than .2 degrees and hence

there would be no change in the valve position causing the pressure also to remain unchanged. In addition, the filter used for time coordination in PMBC in process model based control helps to reduce noise as well. During the experiments with and without filtering it was found that the choice of filtered variable was crucial. Reduction in noise was maximum when filtering the controller output signal. The lag caused by this filter was the same as that caused by filtering the measured pressure signal or the adjustable parameter. However as stated previously the use of a filter for noise reduction was not made off.

CHAPTER 9
RESULTS AND DISCUSSION

9.1 Introduction

This chapter summarizes the results obtained and compares the performance of various controllers. The integral of the absolute error (IAE) was used as a basis for comparison. The performance of the manipulated variable was also employed as a means of comparison as suggested by Bequette (1991). There are no available criteria to compare manipulated variable responses. A criterion which may be employed, however, is termed valve travel and given by,

$$Travel = \sum |S_i - S_{i-1}|, \qquad (9.1)$$

where, S_i = valve stem position at the ith control interval.

This criterion was used to compare performance of the manipulated variable. Within the framework of each control strategy there existed certain differences such as the use of a dynamic vis-a-vis a steady-state model for process model-based control or the use of gain scheduling and feedforward action with internal model control (IMC) as compared to IMC without any modifications or additions. The difference in performance as a result of these variations have also been summarized. A brief paragraph under each controller sub-heading has been included on the rationale employed when selecting values for tuning parameters.

9.2 Controller Testing

The control algorithms used included those for Process Model Based Control (PMBC), Internal Model Control (IMC), and conventional Proportional Integral (PI) control. These controllers represented the three basic types used. In addition some internal differences existed in each type. For example, the PMBC algorithm was tested using both a steady

state model as well as a dynamic model, the IMC algorithm tested using gain-scheduling and feedforward characteristics and the conventional PI controller had gain scheduling characteristics tacked on as well. These algorithms were tested for both the servo and regulatory cases including setpoint changes in pressure and flow disturbances while the glow discharge was in progress. Control action was demonstrated in two main stages, the initial start-up and power disturbance; and subsequent flow disturbances or setpoint changes. The process commenced with the valve fully open and the chamber pumped down to the minimum pressure possible at that particular flow rate. The controller then brought the reactor chamber to the operating pressure, which was normally 500 mtorr. Once steady conditions had been attained, the power was turned on. This created a sudden increase in pressure owing to the large amount of dissociation. The speed of rejection to this unmodelled disturbance was one of the factors on controller performance evaluation. After the pressure had once again stabilized either setpoint changes or artificial disturbances were initiated. Two sets of servo tests, one in each direction, were carried out. The setpoint was first changed to 800 mtorr and then brought back to 500 mtorr. In another test the setpoint was changed to 200 mtorr and brought back to 500 mtorr. This wide range of test conditions from 200 to 800 mtorr was used in order to exploit the nonlinear behavior of the process. A flow rate of 100 sccm was normally maintained with either pure CF_4 or a mixture of CF_4 and O_2 containing 25% O_2 being employed. Flow disturbances were created by either increasing or decreasing the CF_4 flow rate by 25 sccm. Other cases tested for include setpoint changes varying from 200 to 900 mtorr with flow rates ranging from 75 to 125 sccm. Larger disturbances of the order of 50 sccm were also employed to test the robustness of the control algorithms employed.

9.3 Nonlinear Process Model-Based Control

The performance of the nonlinear model-based controller was as good or better than the other controllers for both servo and regulatory performance. The dynamic model performed better than the steady-state model for both setpoint changes as well as disturbance rejection. The servo performance using either controller model was better than the other controllers. The dynamic model was more robust than the steady-state model in the face of process-model mismatch. This was attributed to the fact that, the assumption of a pseudo steady state in the steady-state model was not a good one. Parameter tracking was also more efficient when the dynamic model was employed. This is evident from Figures 9.1 to 9.14 which show the performance of the two process model-based controllers for different cases. The controlled variable is pushed to its new setpoint without any oscillations and the manipulated variable moves to its new value almost instantaneously with little oscillation. The IAE was slightly larger when the steady-state model was employed. The valve travel, however, was smaller in the case of the steady-state model. These values are provided in Table 9-1 and the legend included in Tables 9.2 and 9.3.

Disturbance rejection in the case of both models was efficient though the IAE in the case of the dynamic model was about 10% lesser than that of the steady-state model. However, this improved performance was achieved at the expense of an increase in valve travel as is evident from Figure 9.4 which shows the oscillation of the manipulated variable. The valve travel in the case of the dynamic model increased by almost 39%. Disturbance rejection in the case of both process model-based controllers compared adversely with the IMC algorithm which incorporated feedforward action. The IAE increased by about 3% for the dynamic model and by about 10% for the steady-state model.

The trend displayed by the model parameter for both models was essentially the same. When oxygen was used, both

Table 9.1 IAE and Valve Travel for Servo and Regulatory Performance

Controller Number	Test Case	IAE	Valve Travel
1	A	8481	201
	B	5194	133
	C	5335	79
2	A	8771	279
	B	5185	128
	C	5099	129
3	A	10325	153
	B	5731	73
	C	5783	68
4	A	8930	189
	B	5635	68
	C	5750	63
5	A	9192	286
	B	5789	121
	C	5535	144

Table 9.2 Legend for Controller Identification.

Number	Controller Identification
1	Nonlinear PMBC (Dynamic Model)
2	IMC with gain scheduling and feedforward action
3	PI Control (Position Mode)
4	Nonlinear PMBC (Steady State Model)
5	IMC without gain-scheduling and feedforward action

Table 9.3 Legend for Test Case Identification.

Case	Test Case Identification
A	Start-up, power disturbance and setpoint changes
B	Start-up, power disturbance and increase in flow rate
C	Start-up, power disturbance and decrease in flow rate

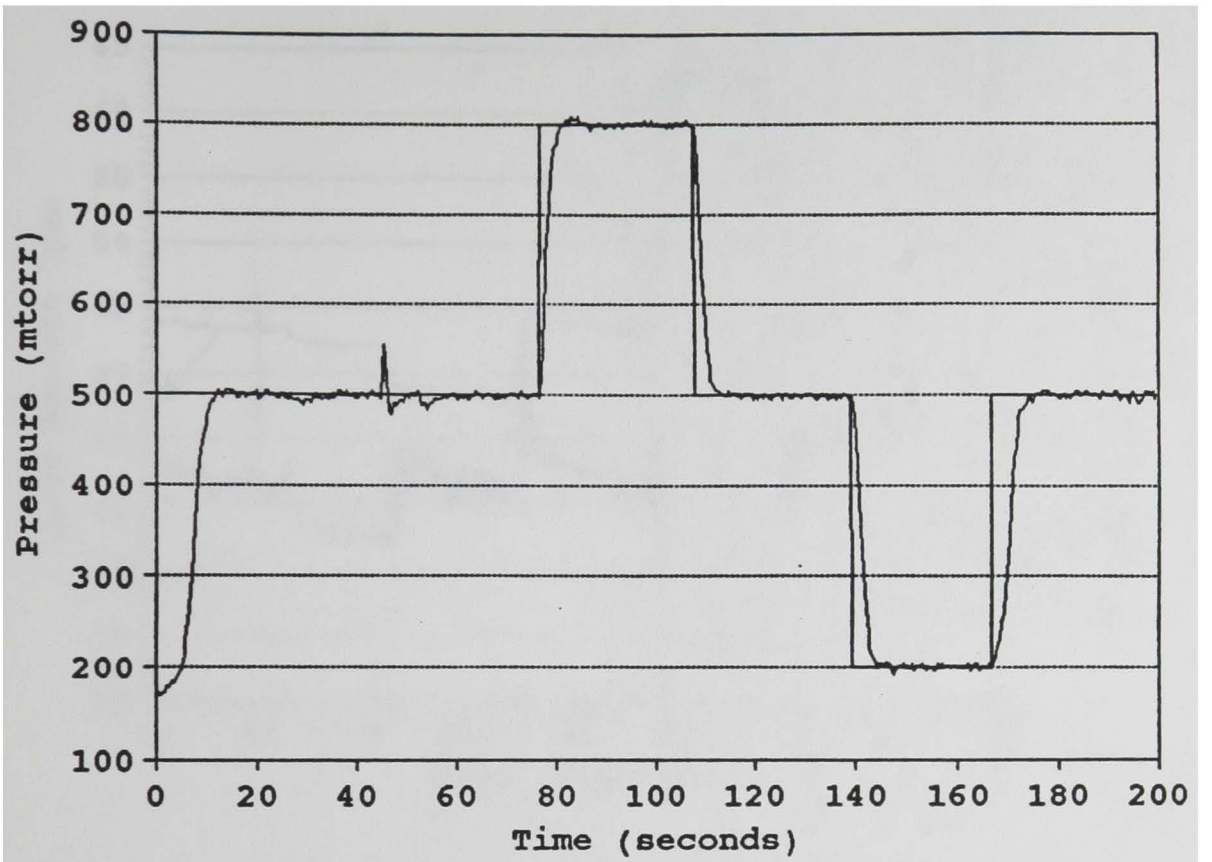

Figure 9.1 Pressure response for setpoint change using PMBC (Dynamic model).

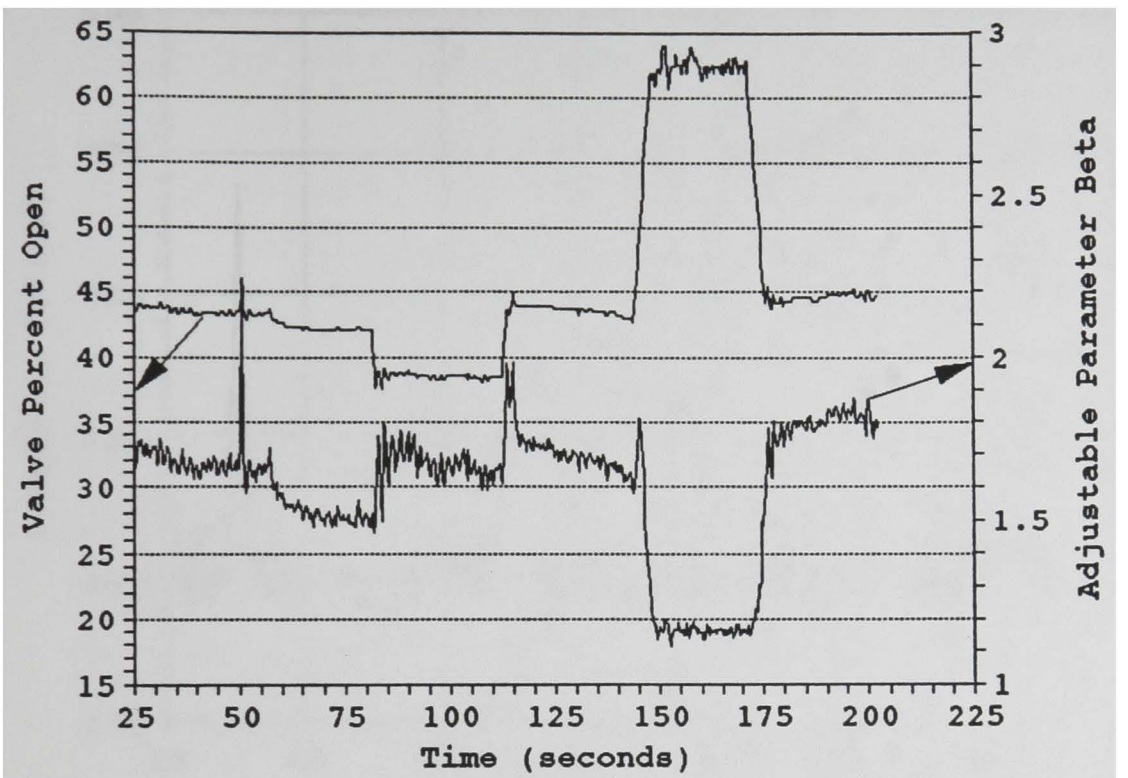

Figure 9.2 Change in valve opening and adjustable parameter for setpoint changes using PMBC (Dynamic model).

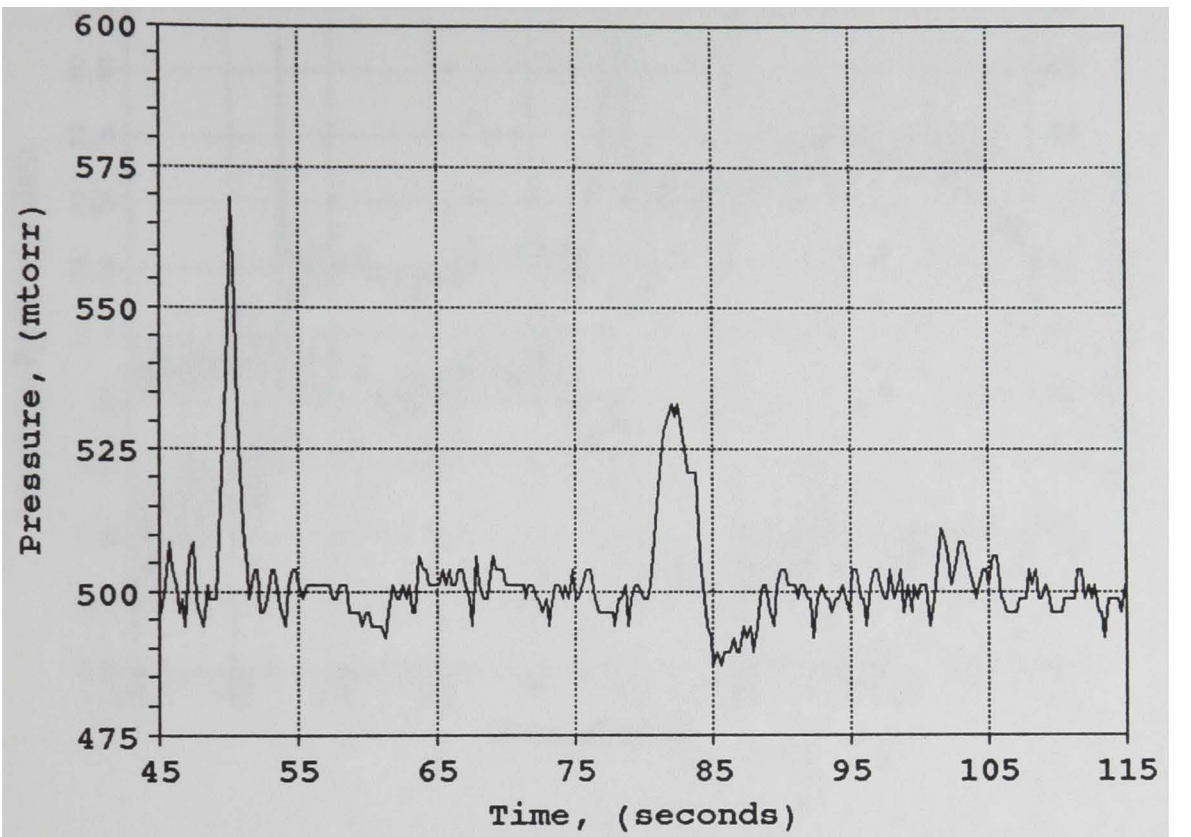

Figure 9.3 Pressure response for inlet flow rate increase using PMBC (Dynamic model).

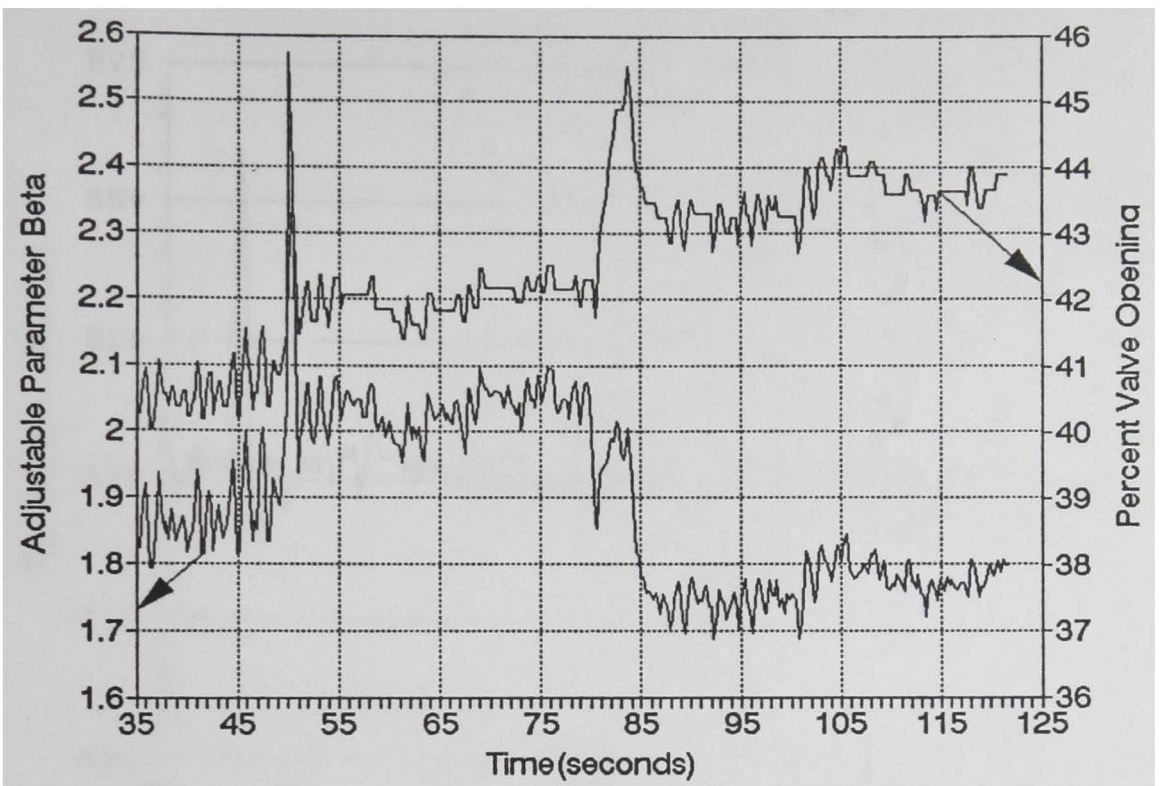

Figure 9.4 Change in valve opening and adjustable parameter for inlet flow rate increase using PMBC (Dynamic model).

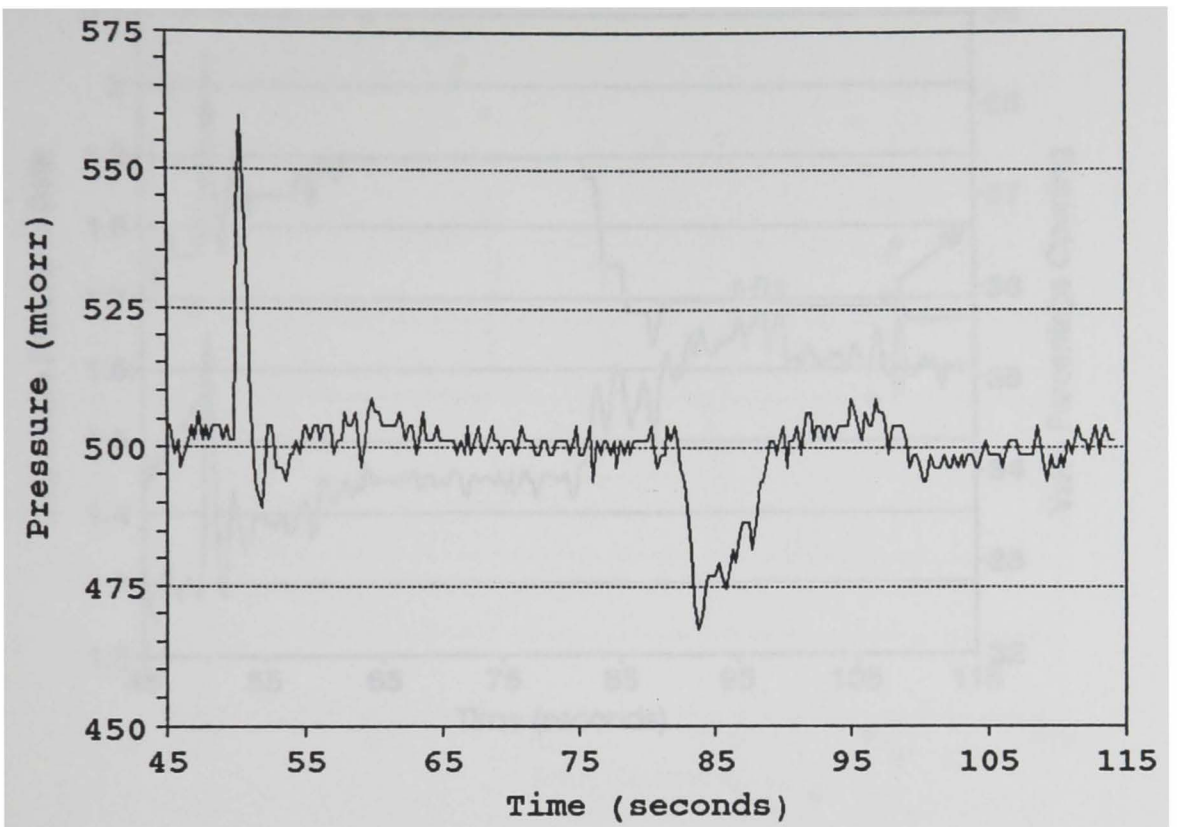

Figure 9.5 Pressure response for inlet flow rate decrease using PMBC (Dynamic model).

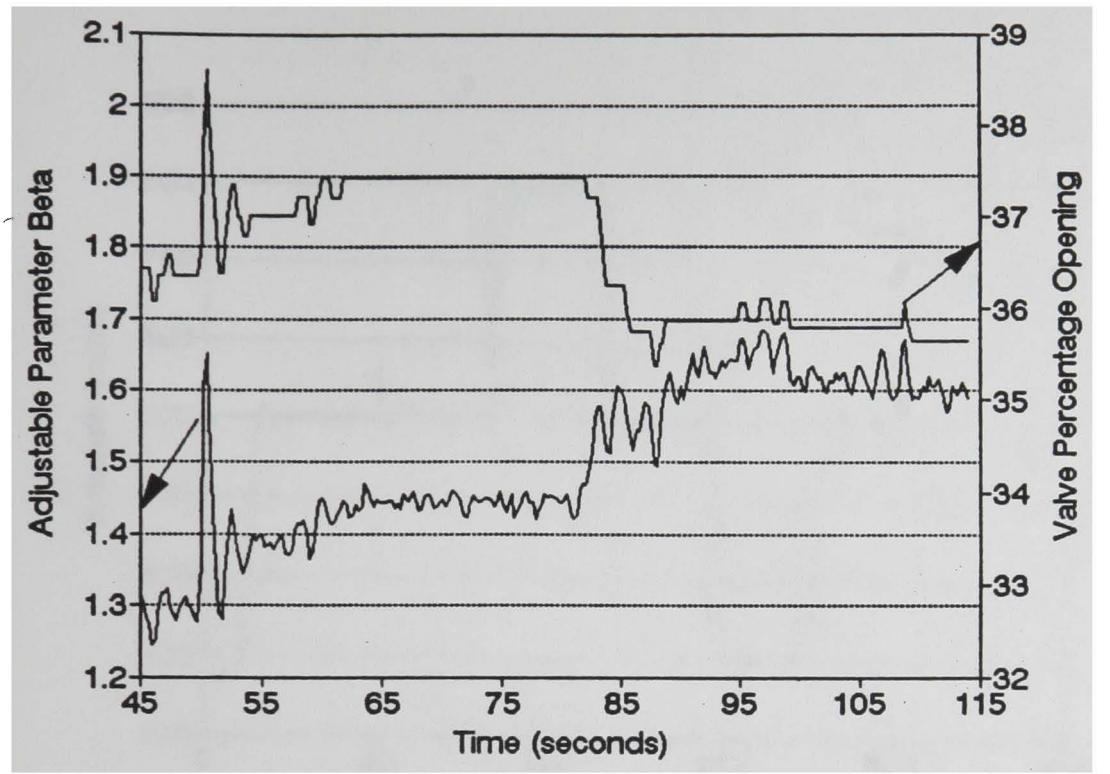

Figure 9.6 Change in valve opening and adjustable parameter for inlet flow rate decrease using PMBC (dynamic model).

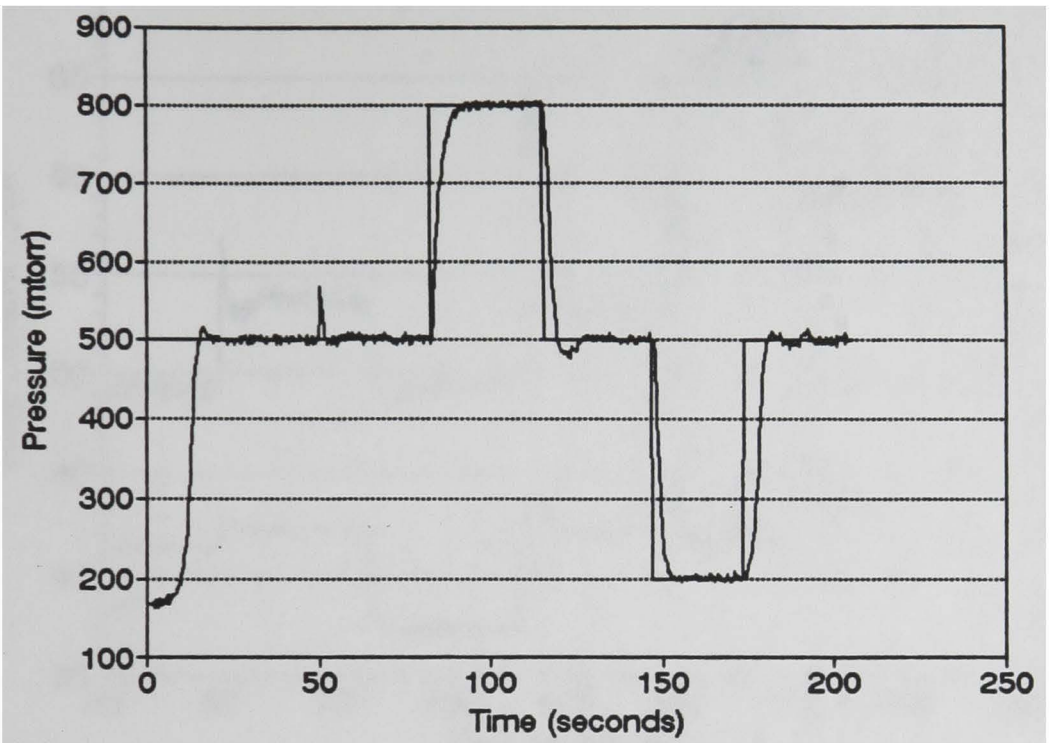

Figure 9.7 Pressure response for setpoint changes using PMBC (Steady-state model).

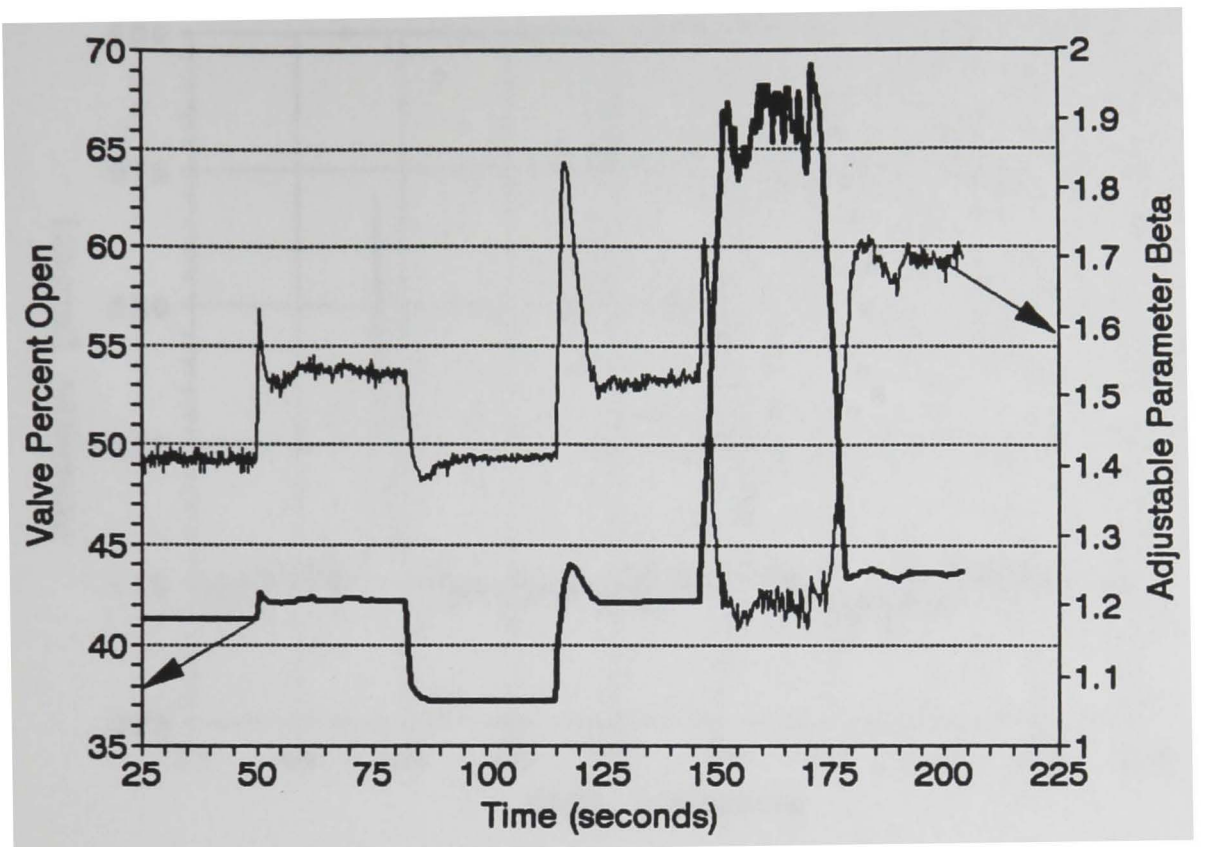

Figure 9.8 Change in valve opening and adjustable parameter for setpoint changes using PMBC (Steady-state model).

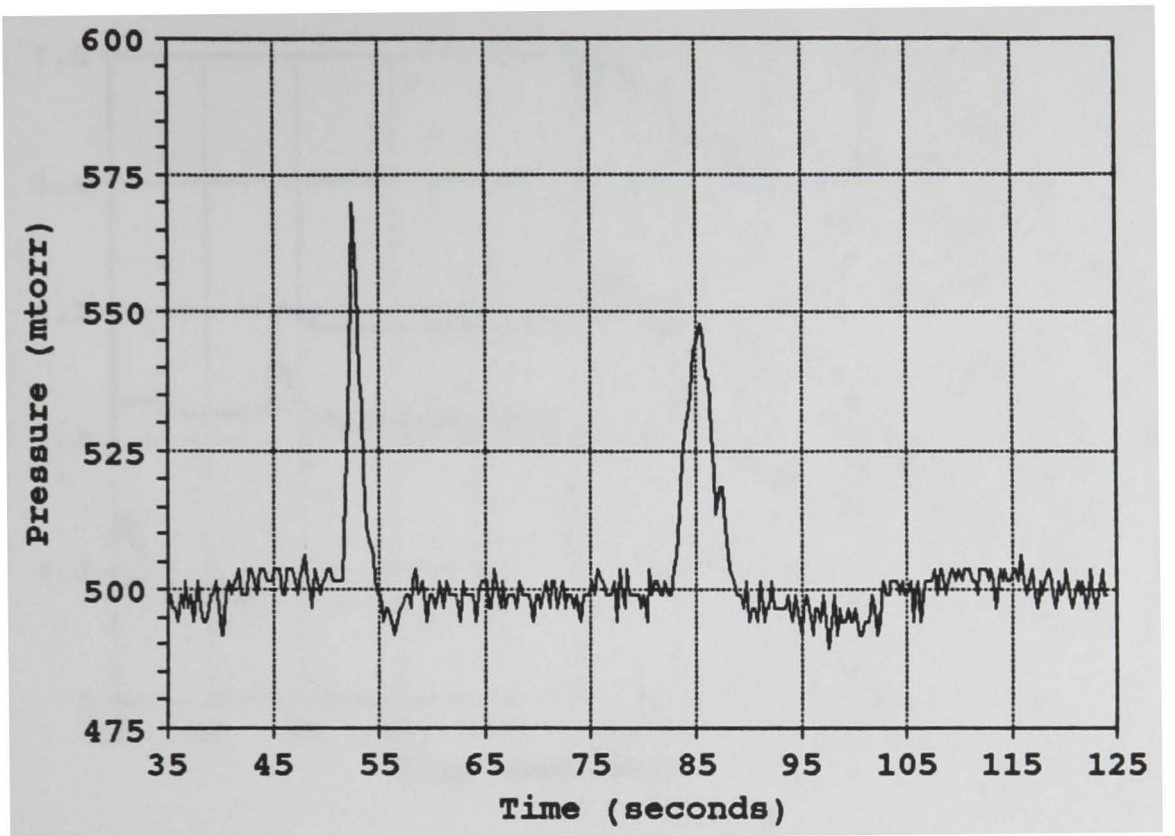

Figure 9.9 Pressure response for inlet flow rate increase using PMBC (Steady-state model).

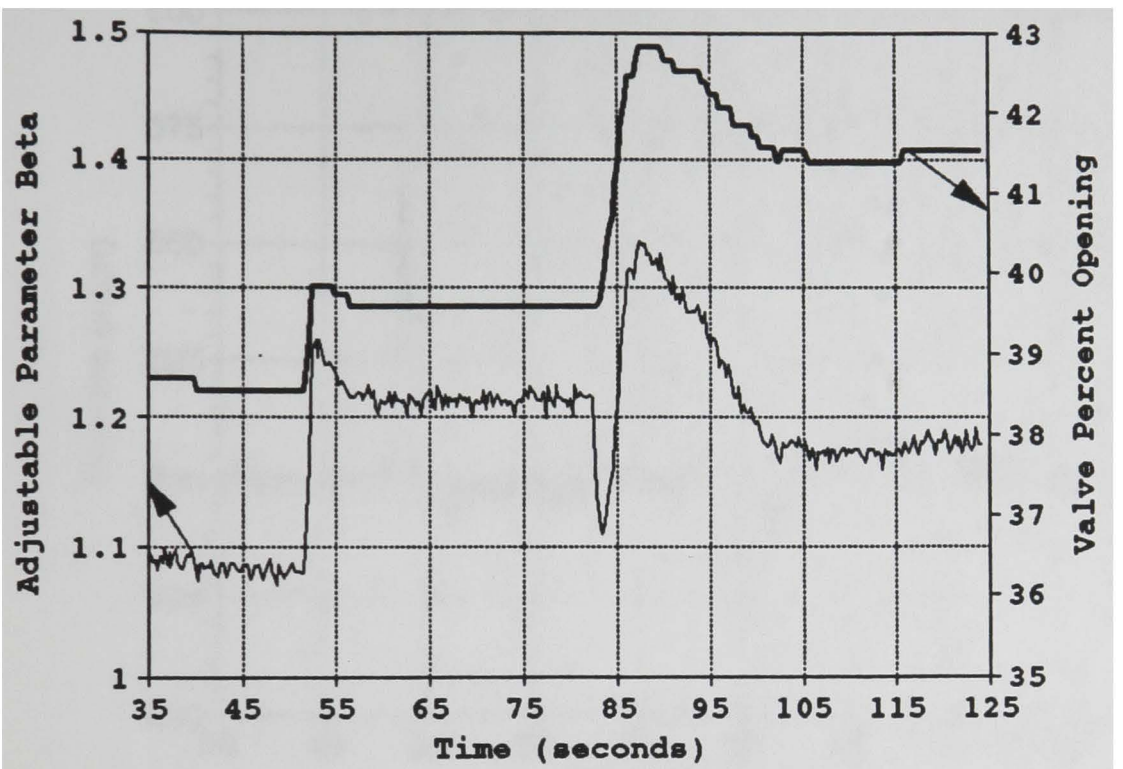

Figure 9.10 Change in valve opening and adjustable parameter for inlet flow rate increase using PMBC (Steady-state model).

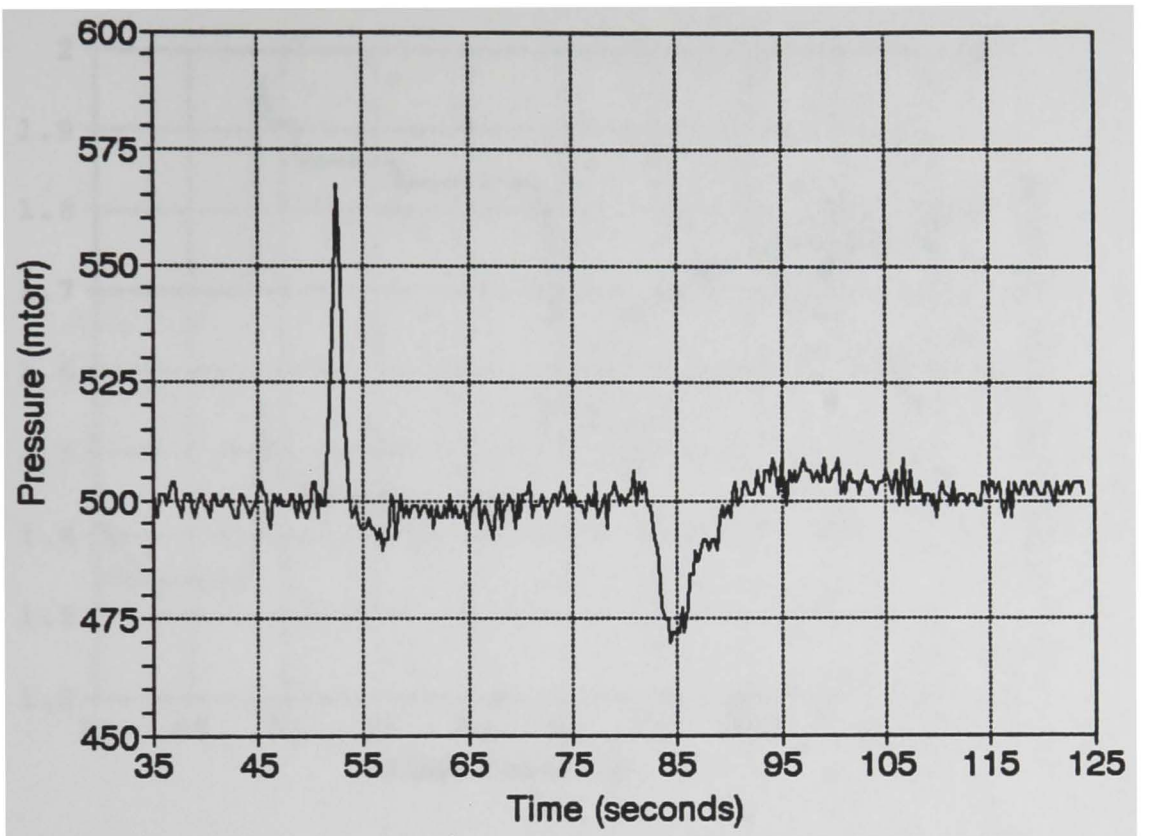

Figure 9.11 Pressure response for inlet flow rate decrease using PMBC (Steady-state model).

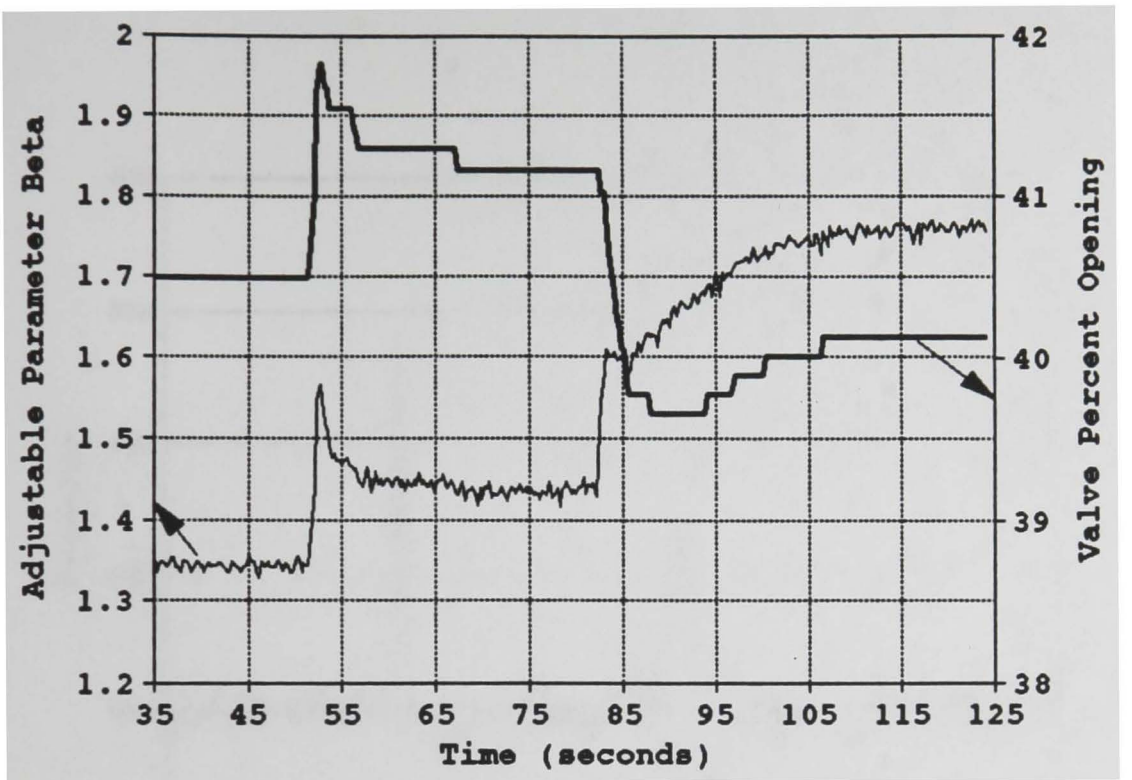

Figure 9.12 Change in valve opening and adjustable parameter for inlet flow rate decrease using PMBC (Steady-state model).

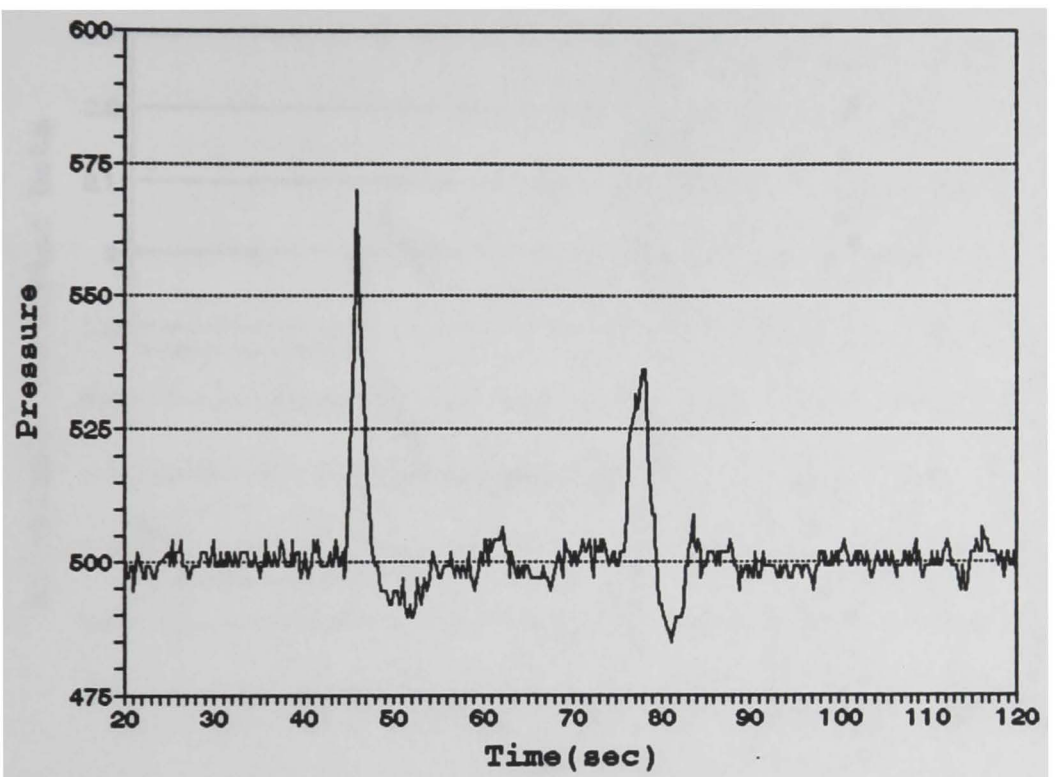

Figure 9.13 Pressure response for inlet flow rate increase using PMBC (Dynamic Model) for a mixture of CF_4 and O_2

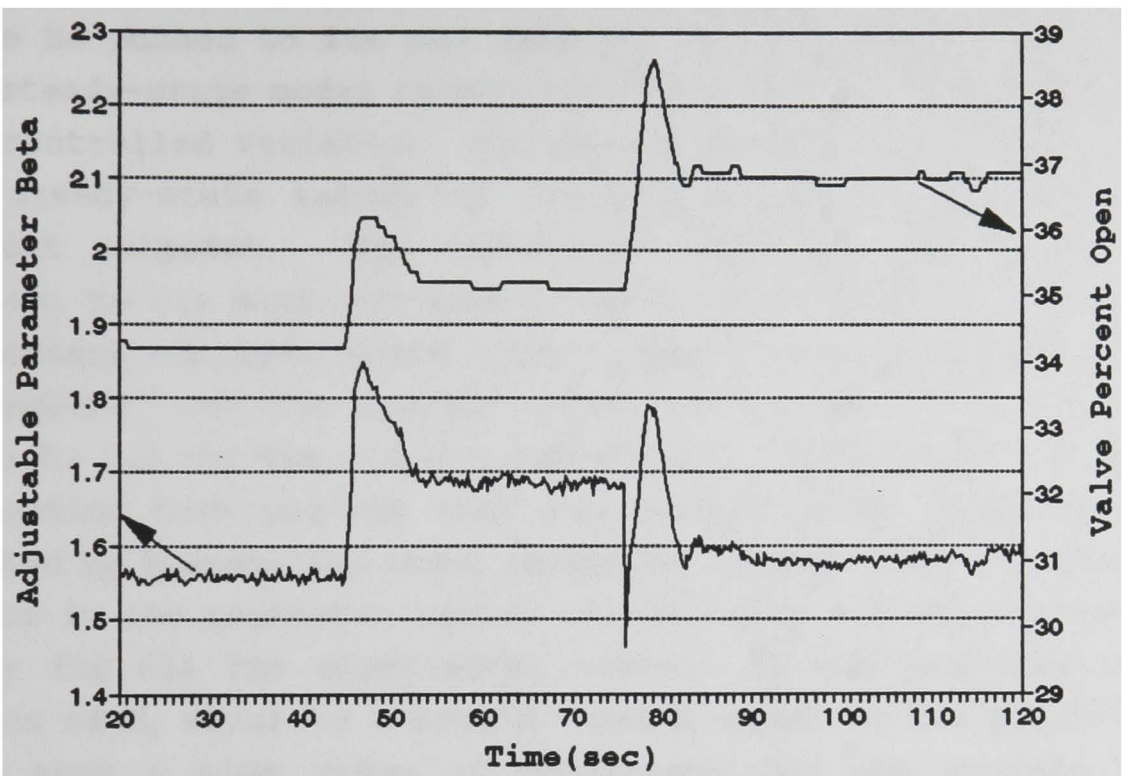

Figure 9.14 Change in valve opening and adjustable parameter for inlet flow rate increase using PMBC (Dynamic Model) for a mixture of CF_4 and O_2

models predicted an increased dissociation as is evident from Figure 9.14 which shows the difference between the values of the model parameter, before and after the power is turned on.

The physical significance of the tuning parameter, K_1, is different in the case of the dynamic and steady-state models. K_1, for the dynamic model represents the inverse of the time taken by the controller to drive the process to its setpoint. Thus a value of K_1 equal to 2 would indicate that the process is to be pushed to its new setpoint in 0.5 seconds. K_1, for the steady-state model determines the steady-state target for the controlled variable. A value of K_1 equal to 1 would set the steady-state target of the controlled variable at its current setpoint. The controller would try to drive the process to its setpoint within one control interval. Tuning parameters employed ranged from K_1 equal to 0.8 to K_1 equal to 1.2 $second^{-1}$ for the dynamic model and K_1 equal to 0.7 to K_1 equal to 1.0 for the steady- state model. The integral offset correction term was not used and process-model mismatch was handled by incremental model parameterization. The relaxation factor in the parameterization relationship was maintained at unity for all the experiental tests. It was observed that values of K_1 equal to 1 $second^{-1}$ and K_1 equal to 0.8 performed well over a wide range of conditions for the dynamic and steady- state models, respectively. The steady-state model in most controller tests required that K_1 be less than one as pushing the process to its new setpoint in one control interval was found to be too aggressive.

9.4 Internal Model Control

The results for both modes of IMC, that is with and without gain-scheduling are shown in Figures 9.15 to 9.22. The servo performance of the controller with gain scheduling added was better than that of the controller without gain-scheduling which is reflected in the values for IAE and Valve Travel in Table 9.1. Servo performance during the first set of setpoint

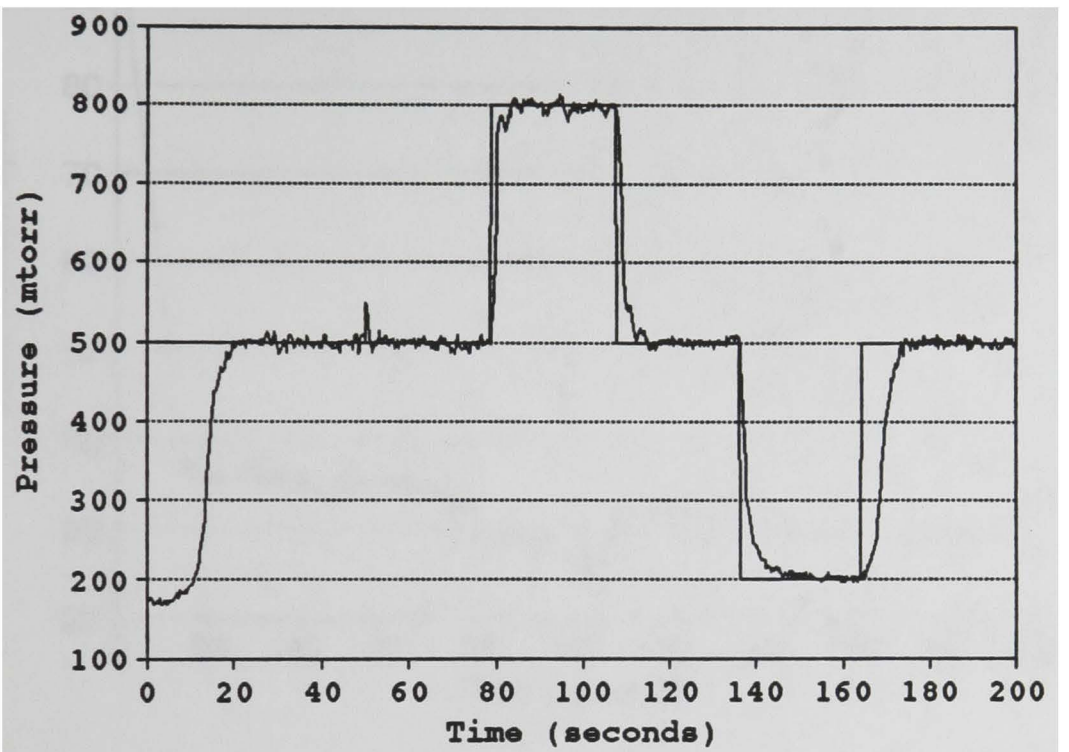

Figure 9.15 Pressure response for setpoint change for IMC with gain scheduling

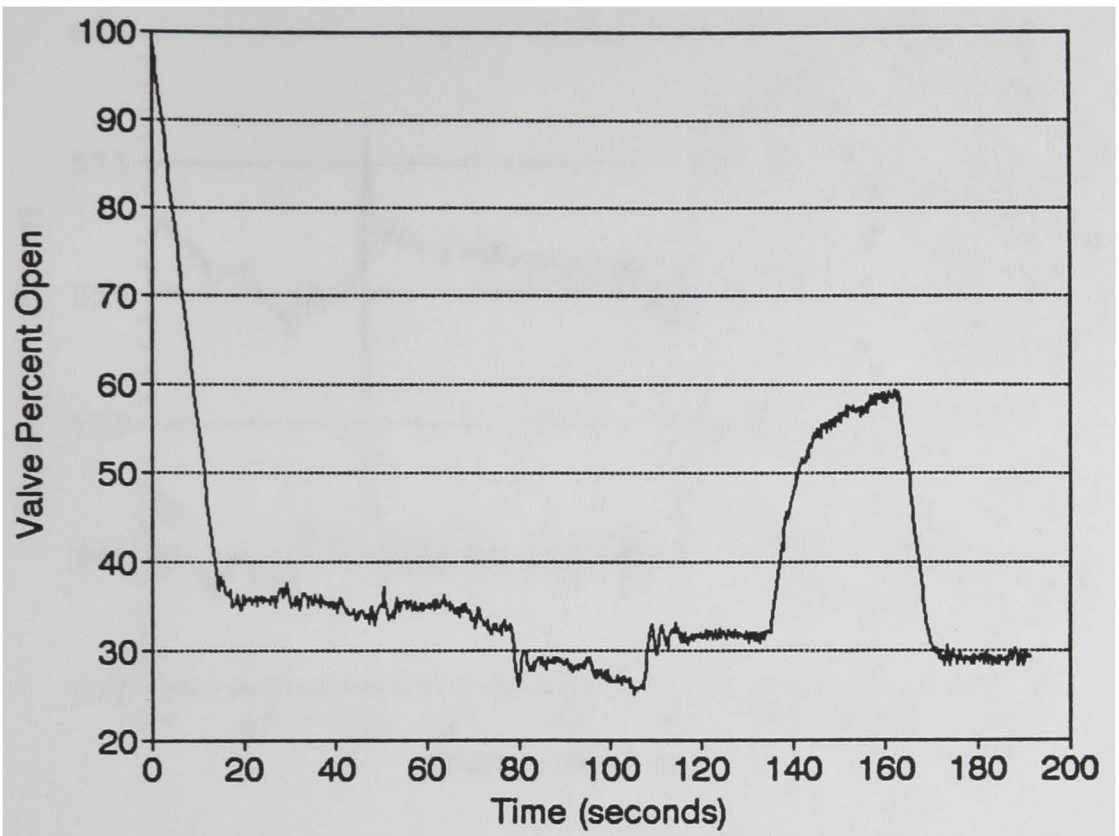

Figure 9.16 Change in valve opening for setpoint change using IMC with gain-scheduling.

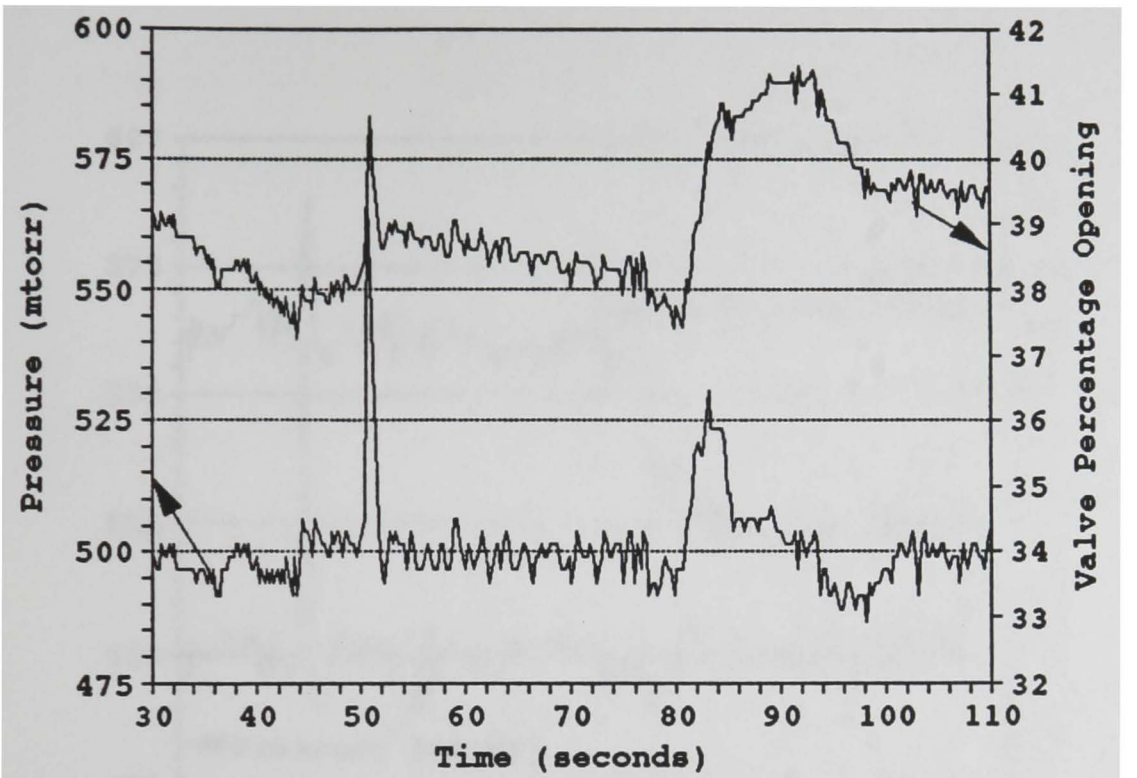

Figure 9.17 Pressure response and change in valve opening for inlet flow increase using IMC with feedforward action.

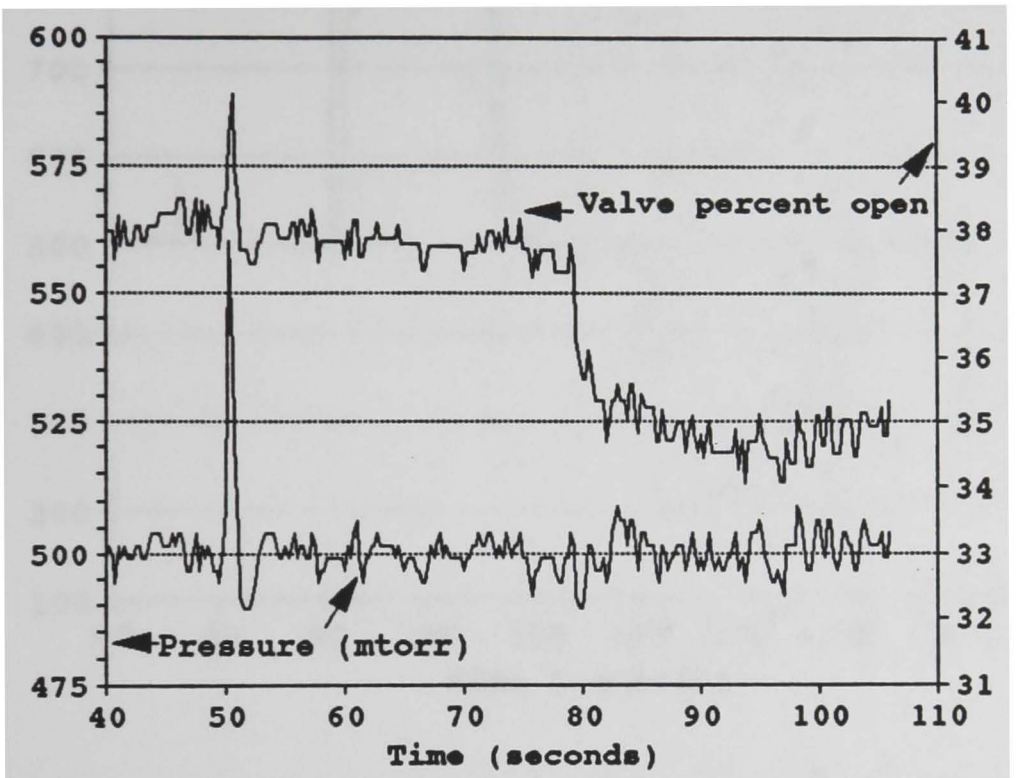

Figure 9.18 Pressure response and change in valve opening for inlet flow rate decrease using IMC with feedforward action

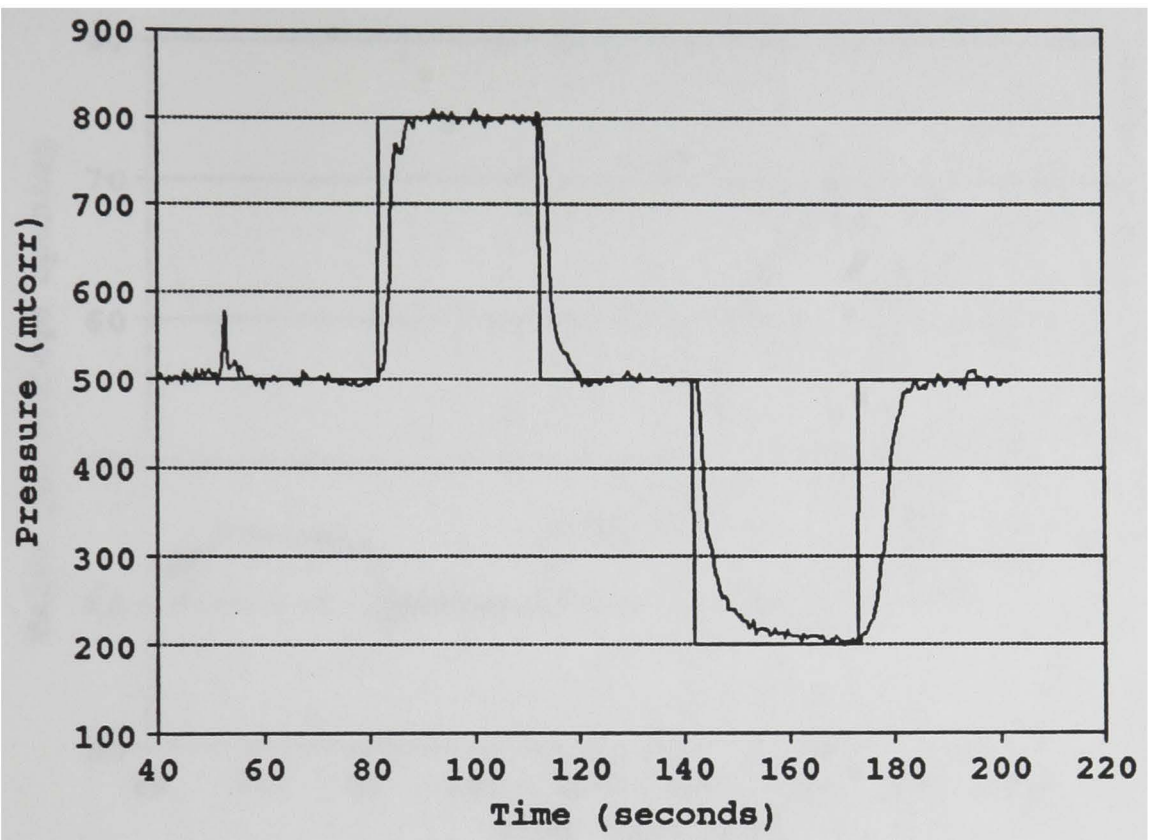

Figure 9.19 Pressure response for setpoint change for IMC without gain-scheduling.

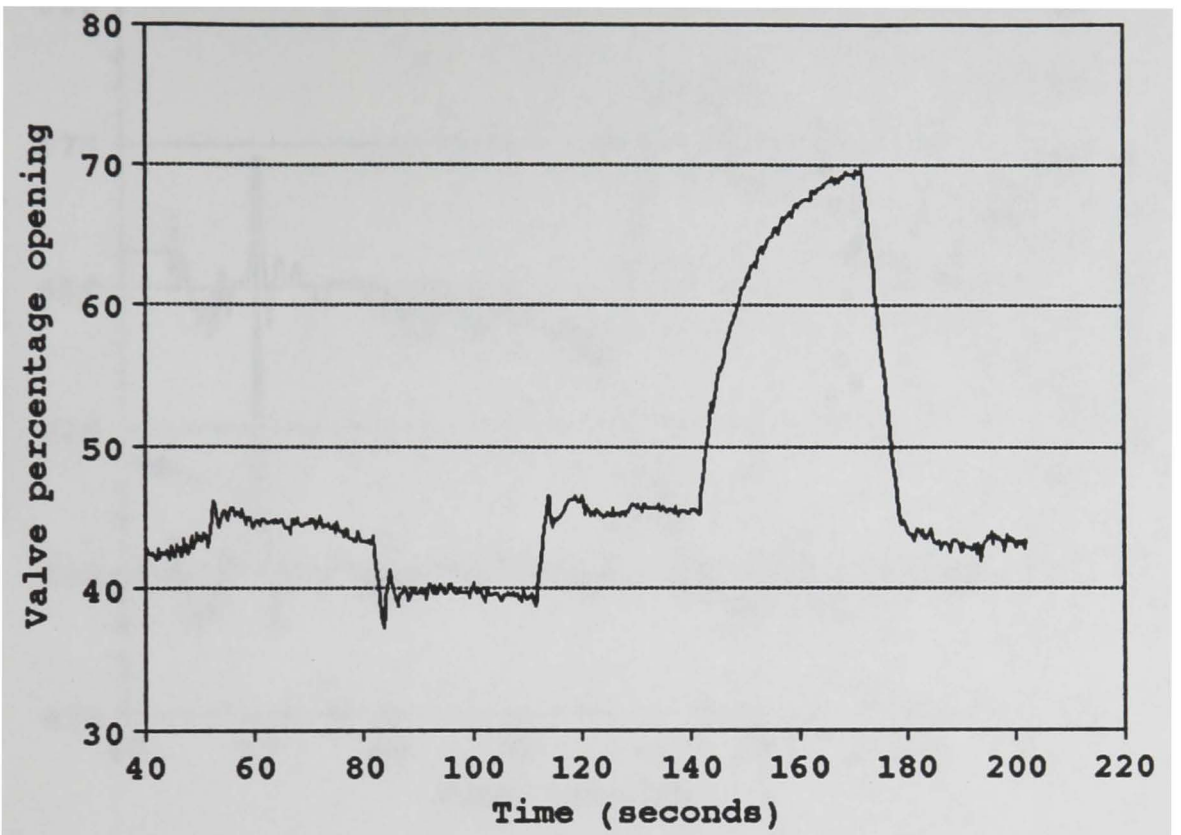

Figure 9.20 Change in valve opening for setpoint change using IMC without gain-scheduling.

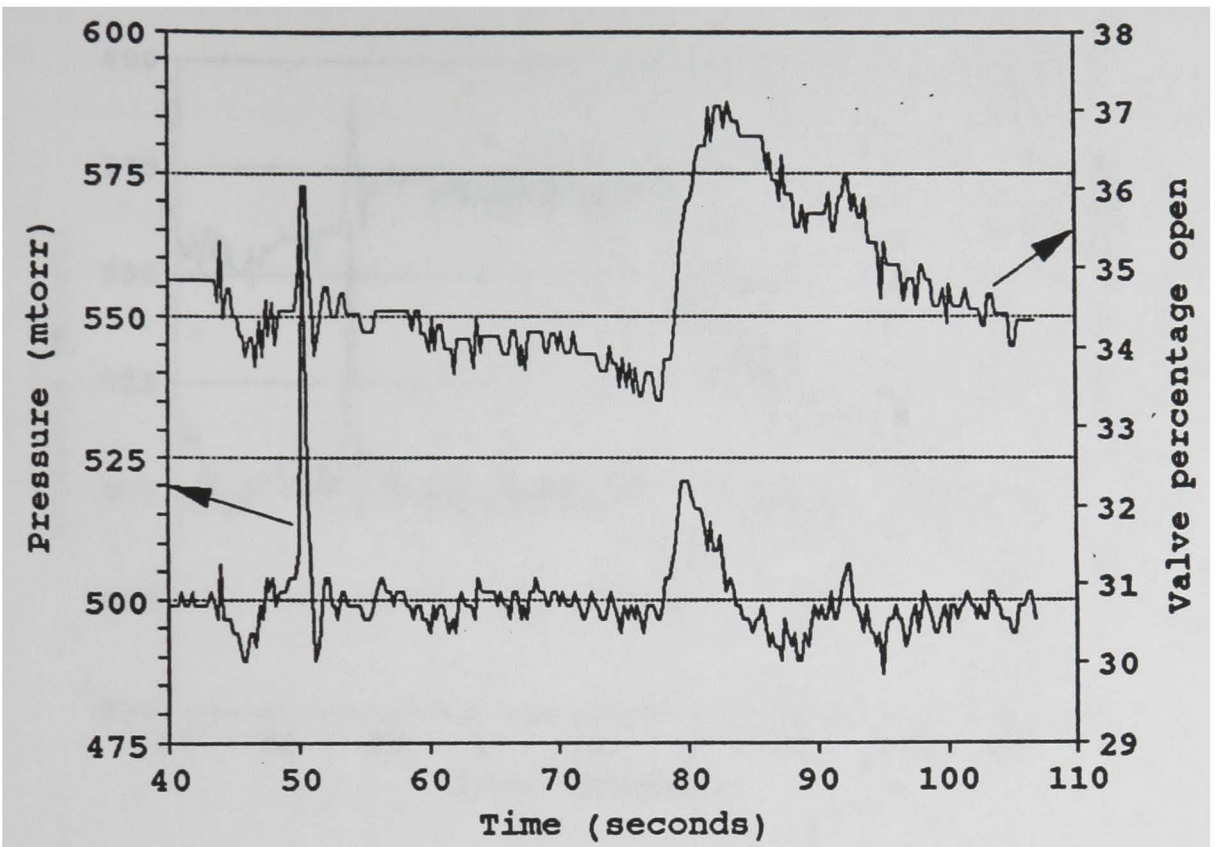

Figure 9.21 Pressure response and change in valve opening for inlet flow-rate increase using IMC without feedforward action.

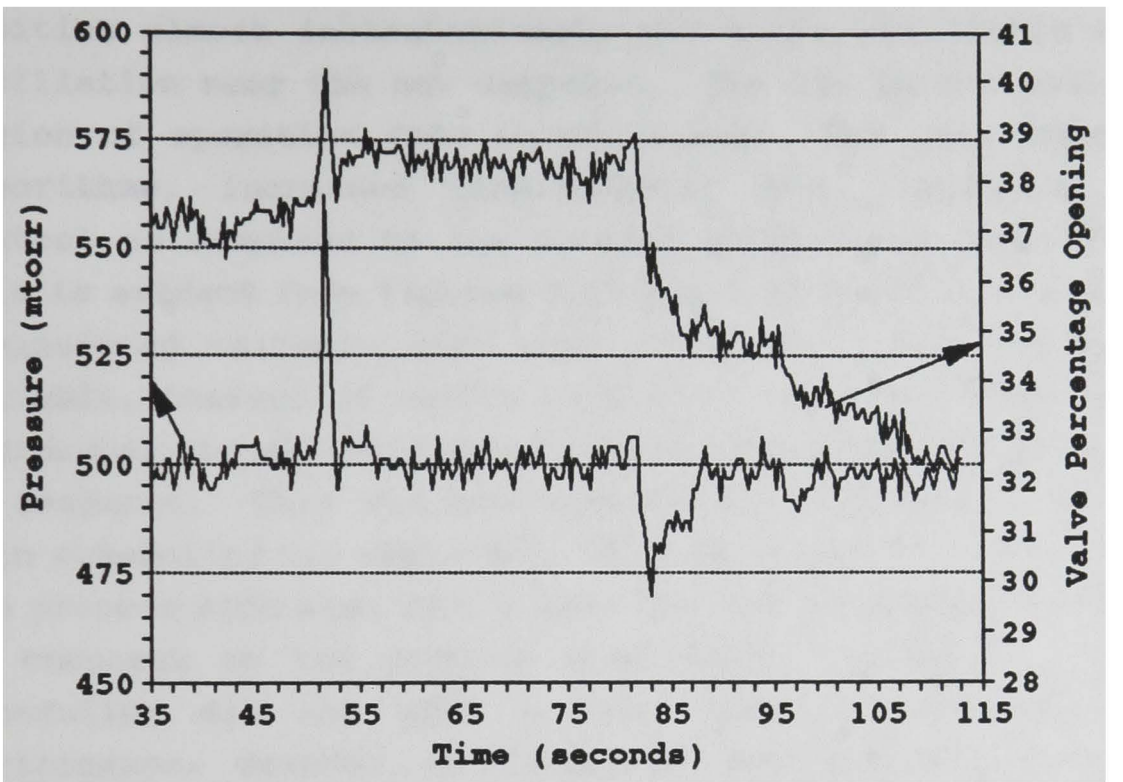

Figure 9.22 Pressure response and change in valve opening for decrease in inlet flow rate, using IMC without feedforward action.

changes, in the region of operation varying from 500 to 800 mtorr, compared favorably to that observed when using process model-based control. The IAE for this part of the process was equal or at times even smaller than the IAE for the nonlinear model-based control algorithms. The valve moved to its new position almost instantaneously and there was little or no oscillation near the new setpoint. The IAE in the nonlinear region of operation (200 to 500 mtorr), for both IMC-based algorithms, increased considerably, thus indicating poor control as compared to the process model-based controllers. This is evident from Figures 9.15 and 9.19 where the change in manipulated variable with time is shown. The manipulated variable, instead of moving to its new position immediately, approaches its ultimate value with a distinct first-order type of response. This was more pronounced in the case where no gain scheduling was employed. The IAE values for this part of the process were also much higher for the IMC-based strategies as compared to the process model-based strategies. Gain-scheduling did not show a very distinct improvement in performance. However, it did improve performance to a certain extent.

IMC, when used in combination with a feedforward strategy, was more effective in rejecting flow disturbances than PMBC. The disturbance was rejected faster and the absolute deviation from setpoint was smaller in the case of IMC with feedforward action. The IAE values for this case were at least 2 to 10 % smaller than that of the process model-based controllers. IMC without feedforward action had an IAE comparable to that obtained using the steady-state nonlinear model-based controller.

The significance of the single tuning parameter, τ_f, the IMC filter time constant has a physival significance. It determines the time taken by the process to return to its setpoint. Within the context of the IMC structure, the filter is used to adjust the effect of the biased setpoint on the

reference trajectory. Lower values of this parameter leads to more aggressive action while higher values cause smaller changes in the process variable. As a rule of thumb the filter time constant should be half the approximate time constant for the process. Based on this heuristic a time constant, τ_f = .75 seconds was initially employed. To make control more aggressive the value of τ_f was subsequently decreased to 0.6. A filter time constant in the range 0.6 to 0.8 seconds was normally employed. Both IMC-based controllers showed the largest amount of valve travel among the controllers tested. This was on account of the light filtering carried out by the IMC filter. The process-model mismatch at each control step was transmitted to the manipulated variable and caused the oscillatory action of the valve.

9.5 Proportional Integral (PI) Control

PI control in general could not reproduce the results obtained using model-based controllers. Servo performance in particular deteriorated considerably. Figures 9.23 to 9.26 show the results obtained using PI control. The control action taken was too aggressive in the region of low gain (500 to 800 mtorr) which is evident from the overshoot. On the other hand the PI controller was able to remove offset only after a long period of time. The IAE values from Table 9.1 reflect these results. The valve travel, however, was considerably less as compared to IMC and equivalent to that of PMBC.

The regulatory performance of the PI controller was better than its servo performance. Though it could not match the performance of the model-based controllers, the disparity between the PI controller and the model-based controllers was less as compared to the disparity observed for servo performance. The absolute deviation from setpoint was slightly greater than that observed for the model-based

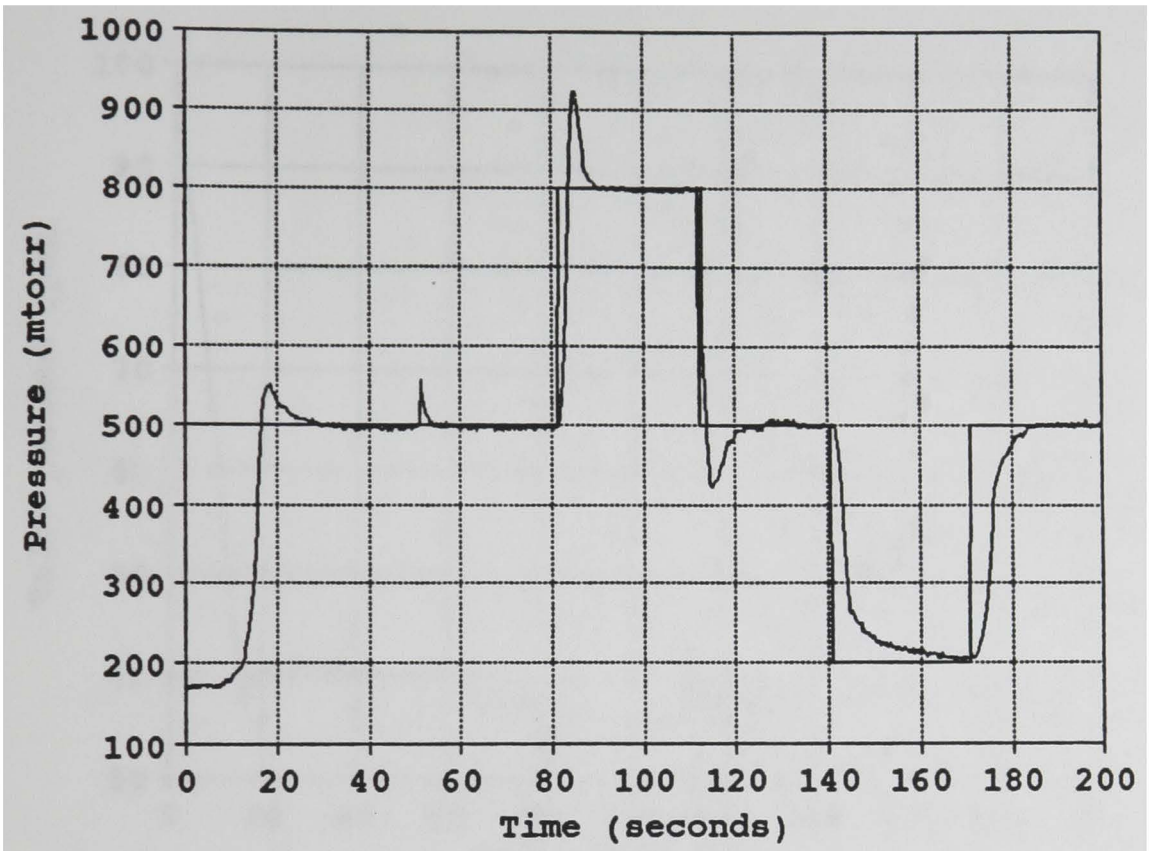

Figure 9.23 Pressure response for setpoint change, using PI control.

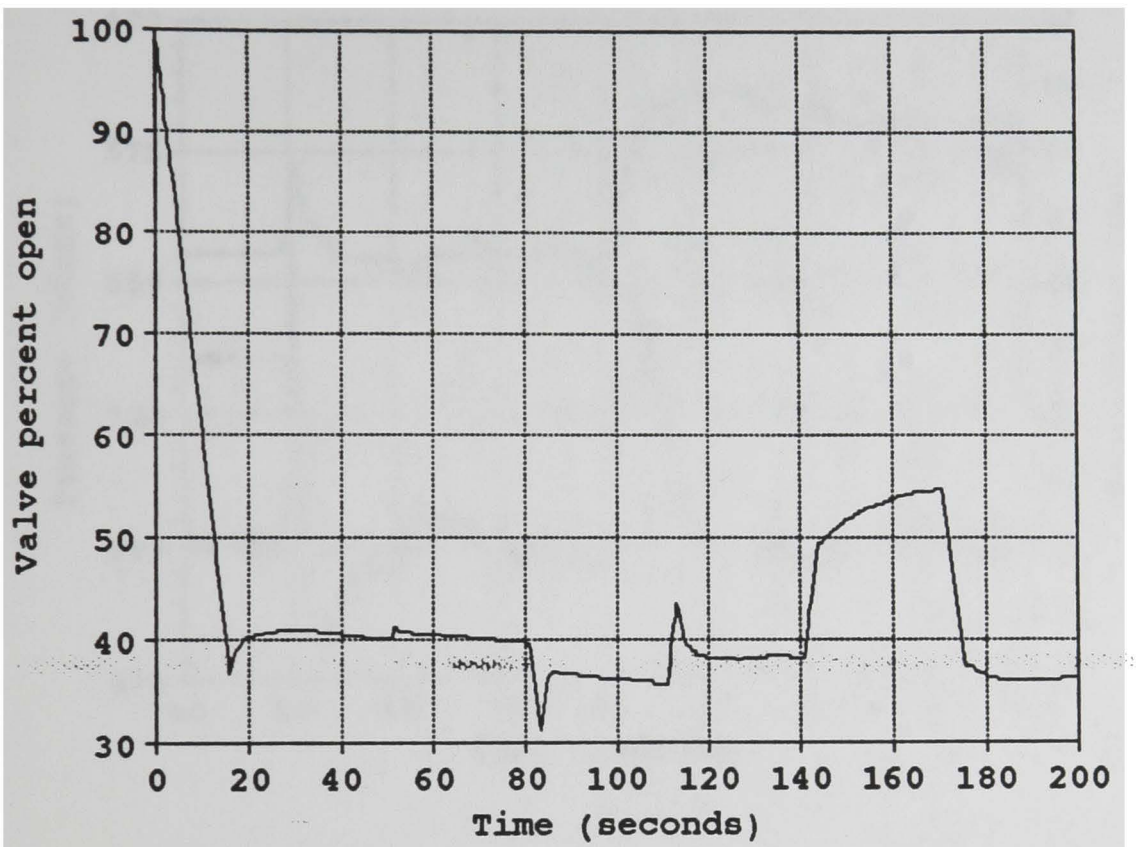

Figure 9.24 Change in valve opening for setpoint change, using PI control.

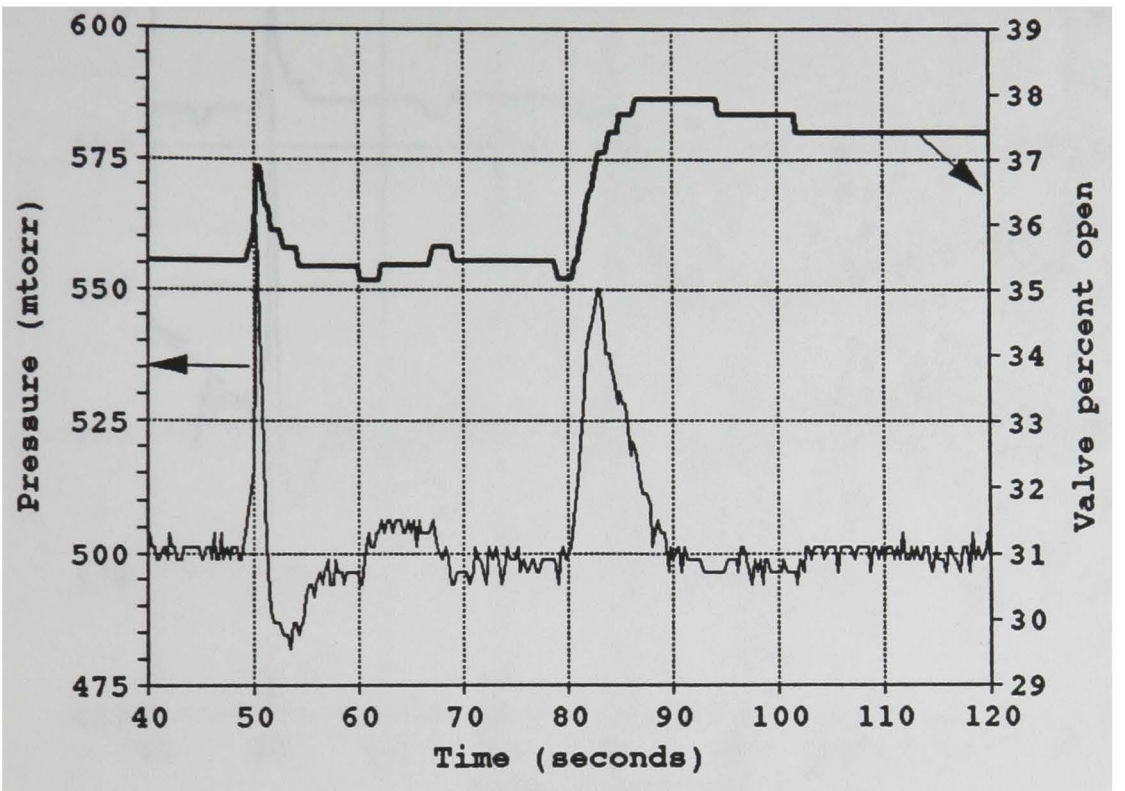

Figure 9.25 Pressure response and change in valve opening for increase in inlet flow rate, using PI control.

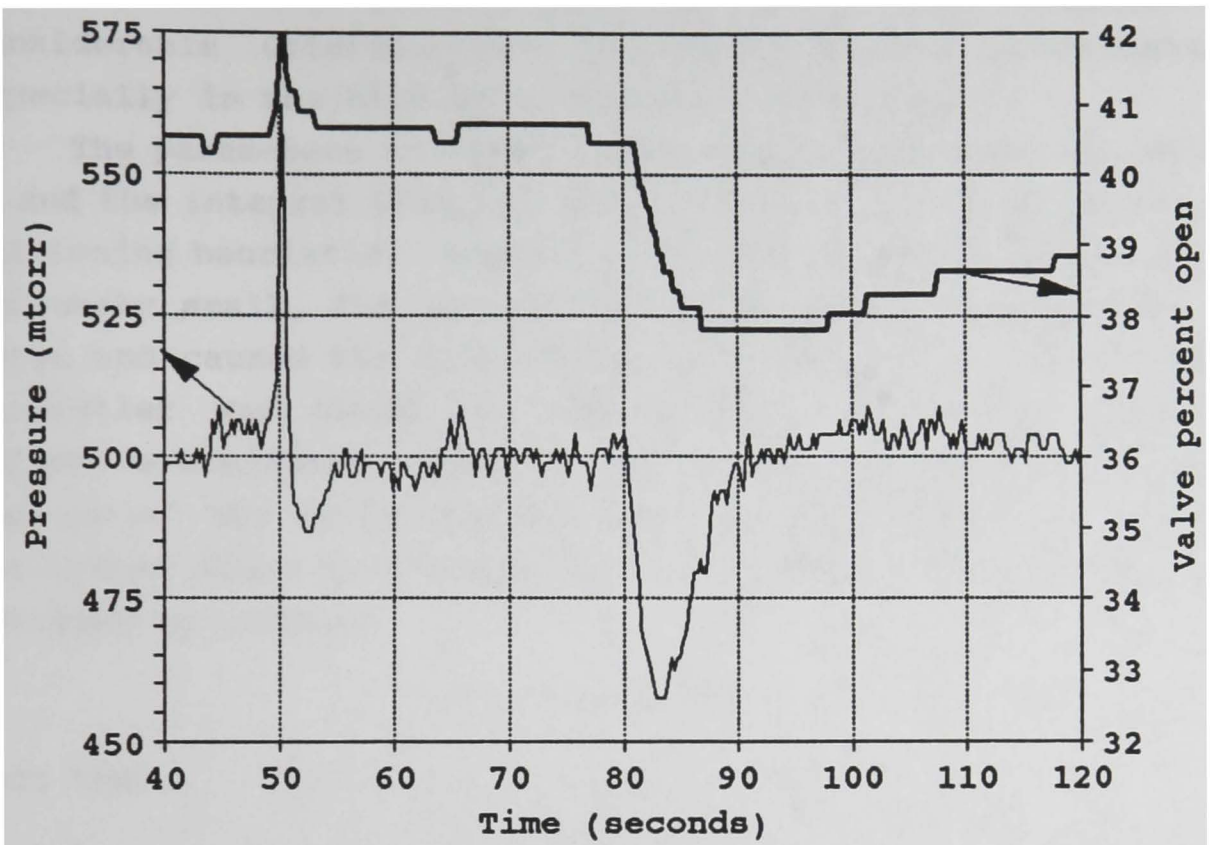

Figure 9.26 Pressure response and change in valve opening for decrease in inlet flow rate, using PI control.

controllers. The PI controller also took a slightly larger amount of time to reject the disturbances. However the valve travel in the case of disturbance rejection was smaller as compared to IMC and PMBC. Increasing the gain would have improved control performance but would have caused a considerable deterioration in servo control performance especially in the high gain region of operation.

The parameters involved in the tuning exercise, the gain K_c and the integral time, τ_i, were estimated using the minimum IAE tuning heuristic. However since the process deadtime was extremely small, the estimate obtained for K_c was extremely large and caused the process to become unstable. Hence the controller was tuned by selecting a desired first-order reference trajectory having a specified time constant, which was one of the tuning parameters. The PI controller drives the system along this trajectory. The tuning parameters were obtained by setting,

$$\tau_i = \tau_w = 1.5s, \tag{9.2}$$

such that,

$$K_c = \frac{1}{K_p} \cdot \frac{\tau_p}{\tau_w}, \tag{9.3}$$

where, τ_i = integral time constant,
τ_w = time constant for the desired reference trajectory,
K_c = controller gain,
K_p = process gain,
τ_p = process time constant.

The ratio τ_p/τ_w determined the rate at which the process was driven to its setpoint. A value of two suggests that the controller pushes the process at twice its normal rate. This value when employed in Equation (9.3) gave K_c = - 0.018 degrees/mtorr.

9.6 Critique

The servo performance of PMBC was better than IMC, because the nonlinear model was able to account for the large gain changes that take place, especially in the extremely nonlinear region (200 - 500 mtorr). The nonlinear conditions are evident from the response of the manipulated variable. The change in the manipulated variable for a pressure setpoint change in the negative direction, that is below the nominal operating point, as compared to the same change in the positive direction from the nominal operating point, was approximately six times larger. Though gain scheduling was added to the IMC strategy it could not exactly account for the nonlinearity of the process, as the gain changes substantially in a very small operating region.

The dynamic model was found to give better performance than the steady-state model because the model was adjusted using the pressure calculated from a dynamic relationship rather than a steady state relationship, which better represented the process at hand. This led to more robust model parameterization.

The superior performance of IMC with feedforward action added was due to the fact that the controller was tested within the region of operation used to develop the model. The nonlinear process model-based controller had inherent feedforward action as the inlet flow term was accounted for in the equation representing the nonlinear model. This framework was more global and hence was effective for any modelled flow disturbance. The IMC-based controller rejected the disturbances aggressively but at the expense of greater valve travel.

In model-based control the performance of the manipulated variable was distinctly different from that observed in conventional controllers particularly during setpoint changes. During setpoint changes the model "knows" the desired value of the manipulated variable required to move the controlled

variable to its new setpoint. Hence the change in the manipulated variable to its new position was almost immediate with very little oscillation or time lag. In contrast the conventional PI controller had to "find" the correct manipulated variable action to obtain the desired change in the controlled variable. This was particularly observed in the case of PMBC, which has inherent gain-scheduling characteristics and hence was able to determine the correct amount of manipulated variable action required

PI controller performance improved in all respects for disturbance rejection because the tuning parameters obtained at the nominal operating conditions were appropriate for the flow disturbances, as these disturbances represented small deviations from the normal region of operation, when compared to setpoint changes. The local gain near the nominal operating point does not change appreciably and hence the controller gain determined was valid over the range of the disturbances.

The rejection of the unmodelled disturbances, caused due to the sudden dissociation of species, was another criteria in controller performance evaluation. The performance of all the controllers was almost equivalent with IMC and PMBC having a slight edge over the PI controller. The model parameter β, was able to track the dissociation taking place which led to improved disturbance rejection.

9.7 Variation of the Adjustable Parameter

Ideally β accounts for the dissociation only, that is, it assumes that measured quantities such as the valve inherent characteristics, the reactor volume and the vacuum pressure are known with great certainty. If this was true then the value of β would be unity before the discharge was turned on. Any setpoint changes and disturbances would cause changes in β that were on account of changes in net dissociation and independent of other factors. However the valve functional

relationship, the reactor volume and the vacuum pressure were quantities whose values were not exactly known. Thus β also accounted for errors in measurement. Hence, certain trends in the model were phenomenologically explicable but not all were. For example, it was known that the net dissociation when using a CF_4/O_2 mixture was greater than when only CF_4 was employed. This effect can be seen in Figures 9.20 and 9.21 The model parameter value increased sharply when power was turned on and then settled at a steady-state value. The difference between the value of β before and after power was turned on was greater when oxygen was part of the reaction mixture.

The trend in β was the same for both models. When pressure was increased from 500 mtorr to 800 mtorr the value of β decreased thus indicating decreased dissociation. This was due to the decreased electron density as electron density decreases with increasing pressure. Recombination reactions are also favored at higher pressures. However, when the pressure was decreased from 500 mtorr to 200 mtorr, the model parameter did not behave as expected, that is, dissociation did not increase with decreasing pressure. Ideally, if the flow, pressure and power were identical, then the valve should attain the same position each time the experiment was performed. However, experimental irregularities such as valves not opening by the amount expected caused the valve to attain a new steady state location. This mismatch was reflected in the change in β.

9.8 Computational Efficiency and Engineering Effort

Computational efficiency of implementation was also examined. Linear IMC without the addition of gain-scheduling or feedforward action was easy to implement on the computer as the lead, lag, delay and summation functions could easily be digitally programmed. The nonlinear model determined the

manipulated action explicitly, by solving a set of equations, and did not require an iterative nonlinear equation solver. The manipulated variable was related to a variable in the model for the output. The algorithms developed were able to measure the process variable, calculate the required control action and implement it within a time interval of 0.22 seconds. The models developed had to be as computationally simple as possible. The process dynamics were extremely rapid and they dictated the sampling and control interval employed. Using a computationally intensive model would have caused the sampling interval to be larger than that required thus leading to a deterioration in control performance.

The time and effort in adding such features as gain-scheduling and feedforward action to either IMC or PI control was the same as that taken to develop a nonlinear model. Additionally, the adjustable model parameter had a phenomenological significance and was used as a tool for process diagnosis.

CHAPTER 10
CONCLUSIONS AND RECOMMENDATIONS

10.1 Introduction

The scope of this work included the development and validation of a dynamic simulator to represent the process, and subsequent development and testing of various control algorithms on the simulator as well as the process. The aim was to experimentally compare various control strategies using the plasma reactor system as a vehicle. This chapter summarizes the conclusions drawn from this work. Some of these were expected based on previous knowledge and experience. A few suggestions for future work in this area are presented.

10.2 Conclusions

Plasma reactors are notorious for their lack of reproducibility of experimental conditions. Experimental results may vary based on reactor geometry and the recipe employed. Reactor conditions vary from run to run based on changes in vacuum suction, power input, leak rate, wafer conditions, etc. Normally industrial reactors are allowed to operate for at least three to four hours and process one or two initial wafers before the commencement of the etch process. This time allows the reactor to reach a given stable operating condition. At any given time a variety of factors affect the plasma and it is difficult to isolate each of these. The dynamics of the reactor system are affected by both plasma chemistry as well as the system flow characteristics. These process characteristics make plasma process control extremely difficult. Models developed for control need to be exceptionally robust.

It was found in general that model-based control strategies were superior to conventional control techniques. This difference in performance was especially evident during

setpoint changes. The "intelligent" control action of the model-based controllers could not be reproduced by the PI controller. However, in the case of disturbance rejection the difference in performance was not that large. The absolute deviation from setpoint was larger than that observed when model-based controllers were employed. However, the manipulated variable action was less aggressive than some of the model-based control strategies tested. The gain remains about the same when small perturbations are made from the nominal operating conditions, as in the case of disturbances. The tuning parameters determined at the nominal operating point, hence, gave better control performance for disturbance rejection than setpoint changes where the process gain changes considerably.

The difference between the linear and nonlinear model-based controllers was observed only when operating in an extremely nonlinear region of operation. In all other cases tested their performance was about the same with the variation in manipulated variable being greater in the case of the linear model-based controller. The improvement in performance with the addition of gain-scheduling to the IMC algorithm was better observed when operating in a nonlinear region. However, this "tack-on" mechanism to handle nonlinearity could not match the performance of the nonlinear model-based controller. IMC, with feedforward action added to it, performed better than all the other controllers for disturbance rejection. This was due to the local tuning being better for the particular case, where the process operating conditions are similar to those used when developing the model. The nonlinear process model-based controller was however more generic in its outlook and could handle flow disturbances in any region of operation.

It was concluded that the engineering effort required to develop the nonlinear models was approximately the same as that required to develop models for gain-scheduling and

feedforward action. With the time and effort involved in adding nonlinear characteristics to a linear model-based control being about the same, it would be better to develop nonlinear phenomenological models as they are more global in their application. Additionally the adjustable parameter or parameters in the model can be used as a tool for process diagnosis. This is advantageous for processes which are ill-defined as in the case of plasma processes. By running the model parallel to the process and evaluating the trends in the adjustable parameter, one can gather considerable information about the process, which can then be used for control purposes.

Among the important aspects of this work has been the emphasis on the performance of the manipulated variable. Better control performance (smaller IAE, less overshoot etc) at the expense of large variations in manipulated variable are not considered conducive to "good" control. Economics dictate that the wear and tear of final control elements be reduced to a minimum. Hence, the variation in manipulated variable was compared for the controllers tested. Including this criterion as part of the controller performance evaluation criteria, considerably affected some of the conclusions drawn. This was especially true of the IMC-based controller which displayed the largest amount of valve travel.

The computational effort required was also determined. All the algorithms used were easy to implement and did not require any iterative calculations. The only differential equation in the dynamic nonlinear model was integrated using the explicit Euler method. The linear IMC algorithm was easy to implement as the terms evaluated included leads, lags, delays and summations. A start-up routine was developed as part of the implementation procedure. This involved opening the valve completely, pumping down the reactor to its minimum pressure, turning on the gas flow and then bringing the reactor to its operating pressure. This entire operation when

automated could be performed in less than a minute. This work also critically examined some of the implementation issues such as time coordination when using steady-state models and the limitation of valve travel, in a given control interval, to a fixed amount. It was concluded that for processes with extremely fast dynamics, nonlinear dynamic models were generally more robust than steady-state models. Model parameterization was another issue examined. Time coordination was absolutely essential for the steady state models to ensure accurate parameterization. A filter used for time coordination employed a time constant developed from a knowledge of the process. Valve dynamics played an important in actual implementation. Valve travel was limited to one degree at a maximum, in order to ensure a regular control and parameterization interval, based on the operation of the valve. The conclusions drawn are summarized in Table 10.1. The controllers tested are given a rank from 1 (best) to 5 (worst). Tables 10.2 and 10.3 summarize the controller types employed and the categories used for performance evaluation.

These issues were examined on the simulator before their experimental implementation. The simulator also helped to observe the response of the process to changes in various parameters as well as the dynamics of the process. In addition it served as a vehicle for the testing of the controller algorithms before their actual implementation. In this work more computationally involved models were also experimented with. The models included using a scaled version of the simulator as the controller model. However, the benefits were minimal as compared to the increase in computational time, a luxury that could not be afforded on account of the extremely fast dynamics of the system.

Table 10.1 Summary of Controller Evaluation.

Category	A	B	C	D	E	F
Controller Type						
1	2	1	1	1	3	5
2	1	2	2	2	4	4
3	5	5	5	5	2	1
4	4	3	3	3	1	3
5	3	4	4	4	5	2

Table 10.2 Legend for Controller Identification.

Number	Controller Identification
1	Nonlinear PMBC (Dynamic Model)
2	IMC with gain scheduling and feedforward action
3	PI Control (Position Mode)
4	Nonlinear PMBC (Steady State Model)
5	IMC without gain-scheduling and feedforward action

Table 10.3 Legend for Performance Category.

Category	Identification
A	Local regulatory performance.
B	Global regulatory performance.
C	Local servo performance.
D	Global servo performance.
E	Valve Travel.
F	Ease of implementation.

10.3 Recommendations

The recommendations presented here are of two types; those which are more specific and related to process control of plasma processes and those which look at the field of process control from a larger view-point.

This work examined pressure control from an independent perspective. It was assumed based on previous work (Butler et al., 1989; McLaughlin et al., 1989) that better pressure control led to better uniformity. Elta et al. (1993) have shown how the process can be distinctly divided into two sections: the plasma factory and the etch factory. They have indicated that the manipulated variable action calculated for the etch factory be used as a setpoint for the plasma factory. A similar concept was employed in this work. Though the effect of pressure control on the uniformity of the etch was not measured, a means for maintaining pressure at its setpoint was demonstrated. However uniformity is also affected by manipulated variables other than pressure and pressure in turn affects parameters such as etch rate. A study which examines more manipulated-controlled variable pairings and the interaction between them would, lead to improved etch performance.

Models developed for real-time control in plasma reactor systems have mainly been empirical in nature. The classical method employed is termed as response surface methodology (Rashap et al., 1993). It employs static steady-state nonlinear output models. Dynamic empirical transfer function models developed from step tests (Butler et al., 1989, McLaughlin et al., 1989) have also been employed. The role of nonlinear phenomenological models has been limited so far. The complexity of the models developed has been an important factor. Another important factor has been the lack of reliable on-line process measurements. The cause and effect relationships, such as that between pressure and uniformity, are also difficult to establish. A knowledge of these

relationships would help in the development of nonlinear models relating manipulated and performance variables. Phenomenological models have the ability to account for multi-variable interaction. This capability makes them ideal candidates for use in plasma systems where the interaction between various parameters is considerable. A model which employed fluorine concentration and dc bias measurements to control etch rate as well as other selected parameters, by manipulating power, pressure and oxygen content would prove extremely useful. The challenge lies in developing a model that is sufficiently generic, that is, it can account for the various electrical and chemical phenomena while retaining its simplicity and computational efficiency. A good place to start would be the to develop a nonlinear model to relate fluorine concentration measurements to power input and the etch rate. This can then be expanded to include other manipulated-performance variable pairings.

From a control stand-point, comparison of controllers especially model-based controllers is best done using multiple-input-multiple-output (MIMO) processes. Multi-variable inter-action adds a new dimension of complexity to control problems. IMC performs as well as NPMBC for single-input-single-output (SISO) processes in terms of engineering effort required to develop the models. Additionally, the difference in performance between conventional control techniques, such as proportional-integral (PI) control, and model-based control is not that obvious unless one uses multivariable processes to test the algorithms. One of the biggest advantages of using nonlinear phenomenological models is their ability to handle multivariable interactions as part of the representation of the process. Linear model-based controllers are also able to handle interaction between variables, by using process data which reflects multivariable interaction to develop the model. Conventional controllers normally employ some form of decoupling mechanism. Comparison

of the various algorithms on a multivariable process would enable the performance of the model-based controllers to be seen in their true light. In addition the effort required to develop nonlinear control models could be compared with the effort required to add features such as decoupling and gain-scheduling. An experimental two-input-two-output system would prove more useful than a SISO system. Nonlinear coupled processes also serve as an ideal testing ground for the comparison of nonlinear model-based controllers with linear model-based controllers. The robustness of controller models can be determined better by using MIMO processes.

This work developed a nonlinear phenomenological model and used it in conjunction with the Generic Model Control (GMC) law. GMC is a single-time-step-ahead control formulation. It is a powerful technique except when it comes to handling constraints or ill-behaved dynamics such as inverse responses or large process deadtime. In these cases its ability to "look" only one step further into the process is inherently limiting. Model predictive control (MPC) strategies on the other hand are able to handle constraints on line and can "visualize" inverse response behavior due to their time-horizon characteristics. In preliminary studies carried out on the simulator it was observed that the MPC algorithm compared well with the other control algorithms tested. The models used were developed from elementary step response data. This algorithm was not tested on the experimental system because the obtaining the process responses was difficult based on the limitations in valve travel. Additionally, the experimental process did not have any constraints or ill-behaved dynamics. Hence the true advantages of model predictive control, vis-a vis other control strategies, would not be clearly visible. It is recommended that any comparative study, especially on a process that has constraints or ill-behaved dynamics, consider linear MPC as a viable alternative.

A control criteria often important in model-based control is the ability to handle process-model mismatch or what is termed as robustness. Models which better represent the process exhibit better control. Selection of a model parameter which periodically updates the model is an important step in the effort to reduce the process-model mismatch. This work used a phenomenological model parameter which represented the net dissociation taking place. It is recommended that other model parameters such as one of the constants in the valve functional relationship or the valve flow coefficient be experimented with for use as a model parameter.

BIBLIOGRAPHY

Arkun, Y., J. Hollet., W. M. Canney and M. Morari; "Experimental Study of Internal Model Control," Ind Eng. Chem. Process Des. Dev. 1986, 25, 102-108

Balchen, J. G., B. Lie, and I Solberg, "Internal Decoupling in Nonlinear Process Control," Modelling, Identification and Control, 9(3), 137-148 (1988).

Bequette, B. W.; "Nonlinear Control of Chemical Processes: A Review," Ind. Eng. Chem. Res., 1991, 30, 1391-1413

Bushman, S., T. F. Edgar, and I. Trachtenberg, "Process Control and Modelling of Plasma Etching Reactors," Proceedings of the AICHE Conference, Miami, 1992.

Butler, S. W., K. J. McLaughlin, T. F. Edgar, and I. Trachtenberg; "Development of Techniques for Real-Time Monitoring and Control in Plasma Etching," J. Electrochem. Soc., 1981, 138, 2727 - 2735

Coburn, J. W., and M. Chen, "Optical emission spectroscopy of reactive plasmas: A method for correlating emission intensities to reactive particle density," J. Appl. Phys. 51(6), 3134, June 1980.

Cott, B. J. and S. Macchietto,"Temperature Control of Exothermic Batch Reactors Using Generic Model Control," Ind. Eng. Chem. Res. 1989, 28, 1177-1184.

Cutler, C. R., and B. L. Ramaker, "Dynamic Matrix Control - A Computer Control Algorithm," Automatic Control Conference, Paper WP5-B, San Francisco, 1980.

Dalvie, M. and K. F. Jensen, "Combined Experimental and Modeling Study of Spatial Effects in Plasma Etching: CF_4/O_2 etching of Silicon," J. Electrochem. Soc., 1990, 137, 1062.

Donnelly, V. M., D. L. Flamm, and W. C. Dantremont-Smith, "Anisotropic Etching of SiO_2 in a low-frequency CF_4/O_2 and NH_3/Ar Plasmas," J. Appl. Phys. 55(1), January 1984.

Economou, C. G., M. Morari, and B. O. Palsson; "Internal Model Control 5: Extension to Nonlinear Systems," Ind. Eng. Chem. Process Des. Dev. 1986, 25, 403-411

Edelson, D., and D. L. Flamm, "Computer simulation of a CF_4 plasma etching silicon," J. Appl. Phys., 56(5), 1522, September 1984.

Elta, M., H. Etemad, J. S. Freudenberg, M. D. Giles, J. W. Grizzle, P. T. Kabamba, P. P. Khargonekar, S. Lafortune, S. M. Meerkov, J. R. Moyne, B. A. Rashap, D. Teneketzis, and F. L. Terry, Jr., "Applications of Control to Semiconductor Manufacturing: Reactive Ion Etching," Proceedings of the American Control Conference, San Francisco, California, June 1993.

Garcia, C. E., and M. Morari; "Internal Model Control 1: A Unifying Review and some New Results," Ind. Eng. Chem. Process Des. Dev. 1982, 21, 308-323

Henson, M. A., and D. E. Seborg; "A Unified Differential Geometric Approach to Nonlinear Process Control," Presented at the 1989 AICHE Annual Meeting, San Francisco, CA, 1989.

Keithley Metrabyte DDA-06 analog/digital expansion board manual, Keithley Metrabyte Corporation, Taunton, MA 02780, 1985.

Lee, P. L., and G. R. Sullivan; "Generic Model Control (GMC)," Comput. Chem. Eng. 1988, 12, 573-580

Lee, P. L., R. B. Newell, and G. R. Sullivan; "Generic Model Control-A Case Study," Can. J. Chem. Eng. 1989, 67, 478-484

Mahuli, S., R. R. Rhinehart and J. B. Riggs; "Experimental Demonstration of Nonlinear Model Based In-Line Control of pH," Journal of Process Control, 1992, Vol 2,No. 3, 145-153

Masoneilian Handbook for Control Valve Sizing, Dresser Industries, Houston, Texas 77084, 1989

McLaughlin, K. J., T. F. Edgar, and I. Trachtenberg; "Real Time Monitoring and Control in Plasma Etching," IEEE Control Systems Magazine, 1991

Mogab, C. J., A. C. Adams, and D. L. Flamm, "Plasma etching of Si and SiO_2-The effect of oxygen additions to CF_4 plasmas," J. Appl. Phys. 49(7), 3796, July 1978.

Pandit, H. G., and R. R. Rhinehart; "Experimental Demonstration of Constrained Process-Model-Based Control of a Nonideal Distillation Column," Proceedings of the American Control Conference, Chicago, IL, June, 1992

Patwardhan, A. A., J. B. Rawlings, and T. F. Edgar; "Nonlinear Model Predictive Control Using Solution and Optimization," Presented at the 1988 AICHE Annual Meeting, Washington D.C.

Plumb, I. C. and K. R. Ryan, "A model of the Chemical Processes Occurring in CF_4/O_2 Discharges Used in Plasma Etching," Plasma Chemistry and Plasma Processing, 6(3), 205-229, 1986.

Rashap, B. A., P. P. Khargonekar, J. W. Grizzle, M. E. Elta, J. S. Freudenberg, and F. L. Terry, Jr.,"Real-Time Control of Reactive Ion Etching: Identification and Disturbance Rejection," To be presented at the IEEE conference on Decision and Control, San Antonio, Texas, December 1993.

Rhinehart, R. R., Personal communication, May 1993, Department of Chemical Engineering, Texas Tech University.

Rhinehart, R. R., "Model-Based Control," Instrument Engineer's Handbook: Process Control and Analysis, 3rd Edition, Bela Liptak, Editor, Chilton Book Company, Rodmore, PA.

Rhinehart, R. R., and J. B. Riggs; "Two Simple Methods For On-Line Incremental Model Parameterization," Comput. Chem. Engg., 1991, 15, 3, 181-189

Rhinehart, R. R. and J. B. Riggs, " Process Control Through Nonlinear Modelling," Control, July, 1990, 86-90.

Richalet, J., A. Rault, J. L. Testud, and J. Papon,"Model Predictive Heuristic Control: Application to Industrial Process," Automatica, 14, 413-418, 1979.

Riggs, J. B., An Introduction To Numerical Methods For Chemical Engineers , Texas Tech University Press, Lubbock, Texas, 1988.

Riggs, J. B. and R. R. Rhinehart, "Comparison Between Process Model Based Controllers," Proceedings of the American Control Conference, 1591 (1988).

Riggs, J. B., J. Watts, and M. Beauford; Adv Instrum. Control 1990, 45, Part 2

Ryan, K. R. and I. C. Plumb, "A Model for the Etching of Si in CF_4 Plasmas: Comparison with Experimental Measurements," Plasma Chemistry and Plasma Processing, 6(3), 231, 1986.

Schoenborn, P., R. Patrick, and H. P. Baltes, "Numerical Simulation of a CF_4/O_2 Plasma and Correlation with Spectroscopic and Etch Rate Data," J. Electrochem. Soc., 136(1), 199-205, January 1989.

Singh V., "Fluid Flow and Concentration Distribution in a Radial Flow Plasma Etch reactor," Masters's Thesis, Texas Tech University, 1990.

Smolinsky, G. and D. L. Flamm, "The plasma oxidation of CF_4 in a tubular-alumina fast-flow reactor," J. Appl. Phys. 50(7), 4982, July 1979.

Texas Instruments, "ASPR plasma reactor manual," Dallas, Texas, 1980.

APPENDIX A
DEVELOPMENT OF VALVE CHARACTERISTICS

Step 1

The vacuum pressure and the valve flow coefficient, C_v were determined using data obtained with the valve full open. The value of vacuum pressure, P_v, in column 5 of Table A.1 was adjusted till the X coefficient (the slope) in the regression output was approximately equal to unity. Table A.2 shows the regressed output and Table A.1 lists the volume and pressure data used to obtain the regression relationship. The results from the regression output are obtained using a value of P_v = 63.5 mtorr and give a value of a = 0.608.

Step 2

The values of P_v and C_v determined were used to obtain the inherent valve characteristic for each set of pressure-valve position data corresponding to a particular flow rate. Table A.3 lists the inherent valve characteristic for 3 different flow rates along with the averaged characteristic for those three data sets. The regressed relationship is shown in column 5 of the same table.

Step 3

The average of the three data sets was regressed and used to obtain the model parameters A and B as shown in Table A.4. The nonlinear relationship employed is described in Chapter 3.

Table A.1 Flow and Pressure Data Used to Calculate Vacuum Pressure P_v and the Constant "a"

Flowrate (Q) (sccm)	Pressure (P) (mtorr)	$\log(P^2 - P_v^2)$	$\log(Q^2)$
25	72	7.049038	6.437752
50	116	9.150988	7.824046
75	149	9.807458	8.634976
100	179	10.24027	9.210340
125	203	10.52344	9.656627
150	233	10.82490	10.02127
175	260	11.05986	10.32957
200	283	11.23924	10.59663

Table A.2 Regressed Data Used to Obtain Vacuum Pressure P_v and the Constant "a"

Definition	Value
Constant (log a^2)	- 0.99506
Standard error of Y estimate	0.277169
R squared	0.966728
Number of observations	8
Degrees of freedom	6
X coefficient (m)	1.009719
Standard error of coefficient	0.076474

Table A.3 Inherent Valve Characteristics

Valve Open(%)	Flow = 75 sccm	Flow = 100 sccm	Flow = 125 sccm	Averaged Data	Curve Fit
100	0.905377	0.973061	1.03845	0.972296	0.96942
88.89	0.900124	0.967895	1.03298	0.971243	0.95776
77.78	0.889968	0.959858	1.020609	0.956812	0.93645
66.67	0.853727	0.916141	0.986738	0.918959	0.89243
55.56	0.750465	0.798217	0.871394	0.806692	0.78777
51.11	0.649599	0.674186	0.770448	0.698077	0.70928
46.67	0.544005	0.548324	0.585390	0.55924	0.59685
42.22	0.446956	0.365479	0.391712	0.401382	0.44710
37.78	0.304013	0.211591	0.247894	0.254499	0.27699
33.33	0.176699	0.137293	0.130028	0.148006	0.12947
28.89	0.088092	0.089063	0.087251	0.088135	0.04136

Table A.4 Determination of Regressed Curve Fit Parameters

Definition	Value
Constant	6.13736
Standard error of Y estimate	0.330607
R squared	0.976714
Number of observations	22
Degrees of freedom	20
X coefficient	-259.1
Standard error of X coefficient	8.945693
Regressed parameter A = exp(constant)	462.83
Regressed parameter B = X coefficient	-259.1

APPENDIX B
CALCULATION OF REACTOR VOLUME AND LEAK RATE

The ideal gas law gives,

$$P \cdot V = n \cdot R \cdot T, \tag{B.1}$$

where, P = pressure in the reactor,
V = volume in the reactor,
n = number of moles in the reactor,
R = Ideal gas constant,
T = temperature in the reactor.

Differentiating Equation (B.1) with respect to time, and assuming that the reactor volume and temperature remain constant, gives,

$$V \cdot \frac{dP}{dt} = R \cdot T \cdot \frac{dn}{dt}. \tag{B.2}$$

The molar flow rate may be expressed in terms of volumetric flow rate by using the ideal gas law to give,

$$\frac{dn}{dt} = \frac{d}{dt}(Q \cdot C) = \frac{P}{R \cdot T} \cdot \frac{dQ}{dt}, \tag{B.3}$$

where, C = concentration of the gas at standard conditions before its entry in to the reactor,
Q = volumetric flow in to the reactor,
P = standard pressure (760 mm Hg).

Substituting Equation (B.3) into Equation (B.2) and rearranging gives,

$$V_R = \frac{P \cdot \frac{dQ}{dt}}{\frac{dp}{dt}}, \tag{B.4}$$

where, V_R is the volume of the reactor.

Equation (B.4) was used to estimate the volume of the reactor. It can also be rearranged to give,

$$\frac{dQ}{dt} = \frac{V_R \cdot \frac{dp}{dt}}{P}, \qquad \text{(B.5)}$$

from which the leak rate can be computed. The term dQ/dt represents the volumetric flow rate into the reactor at standard conditions and dp/dt represents the slope of the line obtained by measuring the pressure at constant intervals of time. Four sets of data were obtained for flow rates of 0, 10, 15 and 20 sccm (standard cubic centimeter per minute). The slope of the line relating pressure to time for no flow (0 sccm) corresponded to the increase in pressure due to reactor leaks. This slope was subtracted from the slope calculated for each of the subsequent data sets before using Equation (B.4) to calculate the volume.

Table B.1 shows the pressure versus time data used to compute the volume and the leak rate. Table B.2 summarizes the slope (dp/dt) for each data set corresponding to a particular flow rate and the volume of the reactor calculated for that flow rate. Using an averaged approximate volume (*) of 2800 cc, the leak rate determined using Equation (B.5) is,

$$\frac{2800\ cc \cdot 0.006882\ torr/s \cdot 60\ s/\text{min}}{760 torr} = 1.52\ sccm. \qquad \text{(B.6)}$$

Table B.1 Pressure-Time Data Used to Estimate Volume

Time(s)	Flow = 0 sccm	10 sccm	15 sccm
0	0	28	39
10	69	350	604
20	141	926	1290
30	209	1466	2007
40	279	1976	2763
50	350	2523	3504
60	416	3042	4253
70	482	3563	4966
80	544	4144	5684
90	620	4699	6446
100	689	5227	7170
110	759	5787	7974
120	824	6349	8631

Table B.2 Calculation of Volume of the Reactor

Slope (mtorr/s)	Flow rate (sccm)	Volume (cc)
6.882	0 (leak rate)	2800.00 (*)
53.737	10	2703.38
73.216	15	2864.29
92.950	20	2943.44

APPENDIX C
DEVELOPMENT OF SIMULATOR EQUATIONS

These equations were developed using the mole balance over each species. They were developed using the nomenclature given in Table C.1. In these equations V_1 and V_2 represent the volumes of the dissociation region and the recombination region respectively. Q_1 represents the volumetric flow rate from the dissociation region (region 1) to the recombination region while Q_2 represents the flow rate out of the reactor from the recombination region (region 2). F_I represents the total molar flow rate into the reactor. Y_i represents the concentration of species i in the dissociation and recombination regions respectively.

C.1 Equations for the Dissociation Region

$$\frac{dY_1}{dt} = \frac{F_I \cdot f_{CF_4}}{V_1} - (k_1 + k_2)\cdot Y_1 + k_6 \cdot Y_2 \cdot Y_4 - \frac{Q_1 \cdot Y_1}{V_1}. \qquad (C.1)$$

$$\frac{dY_2}{dt} = k_1 \cdot Y_1 - k_6 \cdot Y_2 \cdot Y_4 + k_7 \cdot Y_3 \cdot Y_4 - k_8 \cdot Y_2 \cdot y_{10} - \frac{Q_1 \cdot Y_2}{V_1}. \qquad (C.2)$$

$$\frac{dY_3}{dt} = k_2 \cdot Y_1 - k_7 \cdot Y_3 \cdot Y_4 - (k_9 + k_{10}) \cdot Y_3 \cdot Y_{10} - \frac{Q_1 \cdot Y_3}{V_1}. \qquad (C.3)$$

$$\frac{dY_4}{dt} = a + b + c, \qquad (C.4a)$$

where,

$$a = k_4 \cdot Y_7 - k_6 \cdot Y_2 \cdot Y_4 - k_7 \cdot Y_3 \cdot Y_4 + k_8 \cdot Y_2 \cdot Y_{10}, \qquad (C.4b)$$

Table C.1 Nomenclature for Simulator Equations

Identity of Species	Dissociation Region	'Fall-off' Region
CF_4	Y_1	Y_{11}
CF_3	Y_2	Y_{12}
CF_2	Y_3	Y_{13}
F	Y_4	Y_{14}
O_2	Y_5	Y_{15}
CO_2	Y_6	Y_{16}
COF_2	Y_7	Y_{17}
COF	Y_8	Y_{18}
CO	Y_9	Y_{19}
O	Y_{10}	Y_{20}

$$b = k_1 \cdot Y_1 + k_9 \cdot Y_3 \cdot Y_{10} + 2 \cdot k_{10} \cdot Y_3 \cdot Y_{10} + k_{11} \cdot Y_8 \cdot Y_{10}, \qquad \text{(C.4c)}$$

and,

$$c = 2 \cdot k_2 \cdot Y_1 - k_{12} \cdot Y_8 \cdot Y_4 - k_{13} \cdot Y_4 \cdot Y_9 - \frac{Q_1 \cdot Y_4}{V_1}. \qquad \text{(C.4d)}$$

$$\frac{dY_5}{dt} = f_{O_2} \cdot \frac{F_I}{V_1} - k_3 \cdot Y_5 - \frac{Q_1 \cdot Y_5}{V_1}. \qquad \text{(C.5)}$$

$$\frac{dY_6}{dt} = -k_5 \cdot Y_6 + k_{11} \cdot Y_8 \cdot Y_{10} - \frac{Q_1 \cdot Y_6}{V_1}. \qquad \text{(C.6)}$$

$$\frac{dY_7}{dt} = -k_4 \cdot Y_7 + k_8 \cdot Y_2 \cdot Y_{10} + k_{12} \cdot Y_4 \cdot Y_8 - \frac{Q_1 \cdot Y_7}{V_1}. \qquad \text{(C.7)}$$

$$\frac{dY_8}{dt} = a + b, \qquad \text{(C.8a)}$$

where,

$$a = k_4 \cdot Y_7 + k_9 \cdot Y_3 \cdot Y_{10} - k_{11} \cdot Y_8 \cdot Y_{10}, \qquad \text{(C.8b)}$$

and,

$$b = -k_{12} \cdot Y_4 \cdot Y_8 + k_{13} \cdot Y_4 \cdot Y_9 - \frac{Q_1 \cdot Y_8}{V_1}. \qquad \text{(C.8c)}$$

$$\frac{dY_9}{dt} = k_5 \cdot Y_6 + k_{10} \cdot Y_3 \cdot Y_{10} - k_{13} \cdot Y_4 \cdot Y_9 - \frac{Q_1 \cdot Y_9}{V_1}. \qquad \text{(C.9)}$$

$$\frac{dY_{10}}{dt} = a + b, \qquad \text{(C.10a)}$$

where,

$$a = 2 \cdot k_3 \cdot Y_5 + k_5 \cdot Y_6 - k_8 \cdot Y_2 \cdot Y_{10} - k_9 \cdot Y_3 \cdot Y_{10}, \qquad \text{(C.10b)}$$

and,

$$b = -k_{10} \cdot Y_3 \cdot Y_{10} - k_{11} \cdot Y_8 \cdot Y_{10} - \frac{Q_1 \cdot Y_{10}}{V_1}. \qquad \text{(C.10c)}$$

C.2 Equations for the Recombination Region

$$\frac{dY_{11}}{dt} = \frac{Q_1 \cdot Y_1}{V_2} - + k_6 \cdot Y_{12} \cdot Y_{14} - \frac{Q_2 \cdot Y_{11}}{V_2}. \qquad \text{(C.11)}$$

$$\frac{dY_{12}}{dt} = \frac{Q_1 \cdot Y_2}{V_2} - k_6 \cdot Y_{12} \cdot Y_{14} + k_7 \cdot Y_{13} \cdot Y_{14} - k_8 \cdot Y_{12} \cdot y_{20} - \frac{Q_2 \cdot Y_{12}}{V_2}. \qquad \text{(C.12)}$$

$$\frac{dY_{13}}{dt} = \frac{Q_1 \cdot Y_3}{V_2} - k_7 \cdot Y_{13} \cdot Y_{14} - (k_9 + k_{10}) \cdot Y_{13} \cdot Y_{20} - \frac{Q_2 \cdot Y_{13}}{V_2}. \qquad \text{(C.13)}$$

$$\frac{dY_{14}}{dt} = a + b + c, \qquad \text{(C.14a)}$$

where,

$$a = \frac{Q_1 \cdot Y_4}{V_2} - k_6 \cdot Y_{12} \cdot Y_{14} - k_7 \cdot Y_{13} \cdot Y_{14} + k_8 \cdot Y_{12} \cdot Y_{20}, \qquad \text{(C.14b)}$$

$$b = + k_9 \cdot Y_{13} \cdot Y_{20} + 2 \cdot k_{10} \cdot Y_{13} \cdot Y_{20} + k_{11} \cdot Y_{18} \cdot Y_{20}, \qquad \text{(C.14c)}$$

and,

$$c = -k_{12} \cdot Y_{18} \cdot Y_{14} - k_{13} \cdot Y_{14} \cdot Y_{19} - \frac{Q_2 \cdot Y_{14}}{V_2}. \qquad \text{(C.14d)}$$

$$\frac{dY_{15}}{dt} = \frac{Q_1 \cdot Y_5}{V_2} - \frac{Q_2 \cdot Y_{15}}{V_2}. \qquad \text{(C.15)}$$

$$\frac{dY_{16}}{dt} = \frac{Q_1 \cdot Y_6}{V_2} + k_{11} \cdot Y_{18} \cdot Y_{20} - \frac{Q_2 \cdot Y_{16}}{V_2}. \qquad \text{(C.16)}$$

$$\frac{dY_{17}}{dt} = \frac{Q_1 \cdot Y_7}{V_2} + k_8 \cdot Y_{12} \cdot Y_{20} + k_{12} \cdot Y_{14} \cdot Y_{18} - \frac{Q_2 \cdot Y_{17}}{V_2}. \qquad \text{(C.17)}$$

$$\frac{dY_{18}}{dt} = a + b, \qquad \text{(C.18a)}$$

where,

$$a = \frac{Q_1 \cdot Y_8}{V_2} + k_9 \cdot Y_{13} \cdot Y_{20} - k_{11} \cdot Y_{18} \cdot Y_{20}, \qquad \text{(C.18b)}$$

and,

$$b = -k_{12} \cdot Y_{14} \cdot Y_{18} + k_{13} \cdot Y_{14} \cdot Y_{19} - \frac{Q_2 \cdot Y_{18}}{V_2}. \qquad \text{(C.18c)}$$

$$\frac{dY_{19}}{dt} = k_{10} \cdot Y_{13} \cdot Y_{20} - k_{13} \cdot Y_{14} \cdot Y_{19} - \frac{Q_2 \cdot Y_{19}}{V_2}. \qquad \text{(C.19)}$$

$$\frac{dY_{20}}{dt} = a + b, \qquad \text{(C.20a)}$$

where,

$$a = \frac{Q_1 \cdot Y_{10}}{V_2} - k_8 \cdot Y_{12} \cdot Y_{20} - k_9 \cdot Y_{13} \cdot Y_{20}, \qquad \text{(C.20b)}$$

and,

$$b = -k_{10} \cdot Y_{13} \cdot Y_{20} - k_{11} \cdot Y_{18} \cdot Y_{20} - \frac{Q_2 \cdot Y_{20}}{V_2}. \qquad \text{(C.20c)}$$

The flow rate Q_1 was obtained by summing the equations for each region to obtain the total change in concentration with time for each region. The sums were then equated to each other based on the assumption that the concentration in each region was the same. The final equation for Q_1 is given by,

$$Q_1 = \frac{a + b + c + d}{e}, \qquad \text{(C.21a)}$$

where,

$$a = \frac{F_I}{V_1} + (k_1 + 2 \cdot k_2) \cdot Y_1 + k_4 \cdot Y_7, \qquad \text{(C.21b)}$$

$$b = -k_6 \cdot (Y_2 \cdot Y_4 - Y_{12} \cdot Y_{14}) - k_7 \cdot (Y_3 \cdot Y_4 - Y_{13} \cdot Y_{14}), \qquad \text{(C.21c)}$$

$$c = -k_{13}\cdot(Y_4\cdot Y_9 - Y_{14}\cdot Y_{19}) + k_5\cdot Y_6 + \frac{Q_2\cdot Y_{tot}}{V_2}, \qquad \text{(C.21d)}$$

$$d = k_{10}\cdot(Y_3\cdot Y_{10} - Y_{13}\cdot Y_{20}) - k_{12}\cdot(Y_4\cdot Y_8 - Y_{14}\cdot Y_{18}), \qquad \text{(C.21e)}$$

and,

$$e = Y_{tot}\cdot(\frac{1}{V_1} + \frac{1}{V_2}). \qquad \text{(C.21f)}$$

In Equation (C.21d) and (C.21f), Y_{tot} represents the total concentration of all species.

APPENDIX D
ESTIMATION OF ELECTRON DENSITY

A self-sustained plasma must require a specific area per volume ratio, and hence essentially a specific value of,

$$\frac{\pi \cdot R^2 + 4 \cdot \pi \cdot R \cdot L}{2 \cdot \pi \cdot R^2 \cdot L} = \frac{1}{2 \cdot L} \cdot (1 + \frac{4 \cdot L}{R}), \qquad (D.1)$$

where, R is the radius of the electrodes and 2L is the inter-electrode spacing. The exact constraint is determined from the steady-state electron-diffusion-production balance. When the electron balance is combined with the specific area per volume ratio, the relationship obtained is,

$$(\frac{2.405}{R})^2 + (\frac{\pi}{2L})^2 = \frac{K_i}{D_a} = \frac{1}{\Lambda^2}. \qquad (D.2)$$

The parameter Λ represents the electron diffusion length and has the units of length. Another important dimensionless quantity is the Dahmkohler number ($K_i L^2/D_a$). For a plasma to be self sustained this parameter must have the value,

$$(\frac{L}{\Lambda})^2 = \frac{K_i \cdot L^2}{D_a} \geq \frac{\pi^2}{4} + \frac{5.78 \cdot L^2}{R^2}. \qquad (D.3)$$

For most plasma reactors the ratio L/R is normally much smaller than 1, which means that the only criterion to be satisfied is that of,

$$\frac{L}{\Lambda} \geq \frac{\pi}{2}. \qquad (D.4)$$

Λ depends on the coefficient K_i, which is controlled through the power input to the reactor. This necessarily means that for a self-sustained plasma the electrode spacing, L, is related to the power input.

The rate constant associated with the production of etchant species by electron impact is a function only of the

electron temperature. The electron temperature, T_e, depends on the electric field strength, E_e, and the gas pressure, p. The ratio, E_e/p, is in turn dependent only on the product $p\Lambda$, where Λ is the electron diffusion length. Similarly the average electron density, n_e, can be determined from the $p\Lambda$ product of the reactor. This follows from a relationship of the power dissipated per unit of reactor volume, p/V, to the field strength, E_e, and the electron drift velocity v_d:

$$\frac{p}{V} = n_e \cdot q \cdot v_d \cdot E_e, \qquad (D.5)$$

where P is the power input, V is the volume of the reactor and q is the charge of a single electron. Equation (D.5) when rearranged gives,

$$\frac{n_e}{\Lambda \cdot (\frac{p}{V})} = [q \cdot v_d \cdot p \cdot \Lambda \cdot (\frac{E_e}{p})]^{-1}. \qquad (D.6)$$

It is known that v_d is a function only of E_e/p and hence of $p\Lambda$. It follows then, that the left hand side of Equation (D.5) is a function only of $p\Lambda$. Figure D.1 displays this relationship.

The reactor used for this work had electrodes 8 inches (20 cm.) in diameter separated by an inter-electrode space of 2 cm.. The power input was 100 W (watts) and the average pressure maintained in the reactor was 500 mtorr. Using R = 20 cm., L = 2 cm. and p = .5 torr in Equation (D.2) gives $p\Lambda$ = .315. For this value of $p\Lambda$, the corresponding value of $n_e/\Lambda(P/V)$ from Figure D.1 is 7.3 W^{-1} cm^{-1}. Using a reactor volume of,

$$V = \pi \cdot R^2 \cdot 2L = 3.1416 \cdot 10^2 \cdot 4 = 1256.64 cc., \qquad (D.7)$$

gives,

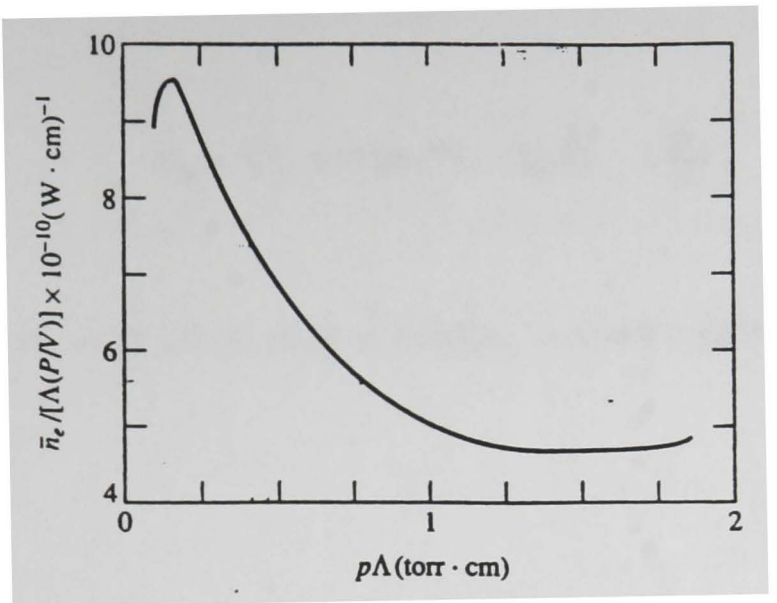

Figure D.1: Electron density as a function of pΛ

$$\frac{P}{V} = \frac{100}{1256.6} = 0.07958 W/cc. \qquad (D.8)$$

Hence,

$$n_e = (7.3 W^{-1} cm^{-1}) \cdot (p\Lambda) \cdot (\frac{P}{V}), \qquad (D.9)$$

or,

$$n_e = (7.3) \cdot (.315) \cdot (.07985) = 1.83 \cdot 10^{10}\ cc^{-1}. \qquad (D.10)$$

APPENDIX E

BASIC SUBROUTINES USED FOR CONTROL

E.1 Subroutines Used to Implement PMBC

E.1.1 Dynamic Model

```
2100  'SUBROUTINE TO IMPLEMENT PMBC USING A DYNAMIC MODEL.
2105  'INITIALIZING VARIABLES
2110  IF N% > 0 THEN GOTO 2170 ELSE GOTO 2120
2120  D = 90!
2130  DE1OLD = 100!
2135  BETAOLD = 1!
2136  BETA = 1!
2140  AC = 462.93
2145  VOL = 2750!
2150  BC = 268.1
2152  CMPOLD = FL(5)
2155  ERCALOLD = ERCAL
2160  FEX = .97
2170  N% = N% + 1
2172  'READING PRESSURE SIGNAL
2174  OUT BASADR% + 2, 5
2175  OUT BASADR% + 1, 0
2176  XL%(5) = INP(BASADR%): XH%(5) = INP(BASADR% + 1)
2177  D%(5) = 16 * XH%(5) + XL%(5) / 16
2178  V(5) = (D%(5) * (10 / 4096) - 5) * 100
2179  FL(5) = (V(5) + 3.5) * 10
2180  'TIME COORDINATION SEQUENCE
2185  FLOW = FEX * CV * ((FL(5) ^ 2 - PVAC ^ 2) ^ .5)
2190  FLOW = (FLOW * 760! * 1000!) / (FL(5) * 60)
2195  TAU = VOL / FLOW
2197  SI = TIMER - CSTART: CSTART = TIMER
2200  FDE1 = (1! - EXP(-SI / TAU))
2210  DE1 = (D * 100 / 90)
2212  DE1 = DE1 * FDE1 + (1! - FDE1) * DE1OLD
2214  DE1OLD = DE1
```

```
2215  'PREDICTION OF PRESSURE USING THE DYNAMIC MODEL
2220  TM = AC * EXP(-BC / DE1)
2230  FEX = TM / (1! + TM)
2240  LOCATE 11, 10: PRINT " PRESSURE IS "; FL(5); "MTORR";
2250  ER = FL(5) - SET
2260  FIN = (FL(1) * 760! * 1000!) / (FL(5) * 60!)
2270  PT = (CMPOLD ^ 2 - PVAC ^ 2) ^ .5
2275  QOUT = (CV * FEX * PT) / 60!
2277  FOUT = (QOUT * 760! * 1000) / FL(5)
2280  DPDT = (FIN*CMPOLD*BETA)/VOL - (CMPOLD * FOUT)/ VOL
2285  CMP = CMPOLD + SI * DPDT
2290  CMPOLD = CMP
2292  'REPARAMETERIZING THE MODEL
2295  CMER = FL(5) - CMP
2300  BETA = BETAOLD + (CMER*VOL*ALFA) / (SI * FIN * CMP)
2302  BETAOLD = BETA
2303  'CALCULATING REQUIRED CONTROL ACTION
2304  TERM1 = (FIN * CMP * BETA) / VOL + PK1 * ER
2310  QOUT = (TERM1 * VOL) / CMP
2312  QOUT = (QOUT * FL(5) * 60!) / (1000! * 760!)
2320  CAL = 0!
2335  CALI = 0!
2340  PT1 = (FL(5) ^ 2 - PVAC ^ 2) ^ .5
2350  FEX1 = QOUT / (CV * PT1)
2354  IF FEX1 > 1! THEN FEX1 = .99
2355  IF FEX1 <= 0! THEN FEX1 = .01
2357  'IMPLEMENTING CONTROL ACTION CALCULATED
2360  DG = LOG(AC) - LOG(FEX1 / (1! - FEX1))
2370  DE = BC / DG: 'NEW VALVE POSITION REQUIRED
2372  ERCAL = ABS(ER)
2374  TIAE = TIAE + (SI * (ERCAL + EROLD) / 2!)
2376  EROLD = ERCAL
2380  SDE = (DE * 90!) / 100!
2385  DEG = ABS(D - SDE)
2387  LOCATE 18, 10: PRINT "INTEGRAL ABSOLUTE ERROR"; TIAE
```

```
2388  IF DEG < .2 THEN DEG = 0!
2389  IF DEG > 1! THEN DEG = 1!
2390  LOCATE 17, 10: PRINT "VALVE POSTION REQUIRED"; SDE;
      "DEGREES"
2400  IF D < SDE THEN D$ = "O" ELSE D$ = "C"
2410  LOCATE 19, 10: PRINT "VALVE TURNS BY"; DEG; "DEGREES"
2420  M = 28
2430  L = 31
2440  OUT &H330 + &HE, 128 'CLEARS O/P ON THE DDA BOARD
2470   LOCATE 21, 10: PRINT "BETA = "; BETA; "FEX1= "; FEX1;
     "CMP= "; CMP
2480  N = INT((DEG * 5) + .5)
2490  IF D$ = "O" THEN A = 4 ELSE GOTO 2570
2495  'SENDING PULSES TO VALVE
2500  FOR I = 1 TO N
2510   OUT &H330 + &HE, A: 'OPEN VALVE--26TH PIN IS LOW AND
      27TH IS HIGH
2520  FOR JJ = 1 TO L: NEXT JJ
2530  OUT &H330 + &HE, 128
2540  NEXT I
2550  CAL = DEG
2560  GOTO 2650
2570  B = 8
2580  FOR I = 1 TO N
2590  OUT &H330 + &HE, B: 'CLOSE VALVE--27TH PIN IS LOW AND
      26TH IS HIGH
2600  FOR KK = 1 TO M: NEXT KK
2610  OUT &H330 + &HE, 128
2620  NEXT I
2630  CALI = DEG
2640  GOTO 2660
2650  D = D + CAL: GOTO 2665
2660  D = D - CALI
2665   LOCATE 23, 10: PRINT " THE VALVE IS OPEN AT "; D;
     "DEGREES"
```

E.1.2 Steady-State Model

```
2100  'SUBROUTINE TO IMPLEMENT PMBC USING A STEADY-STATE
      MODEL.
2105  'INITIALIZING THE VARIABLES
2110  IF N% > 0 THEN GOTO 2170 ELSE GOTO 2120
2120  D = 90!
2130  DE1OLD = 100!
2135  BETAOLD = 1!
2140  AC = 462.93
2145  VOL = 2750!
2150  BC = 268.1
2155  EROLD = ERCAL
2160  FEX = .97
2170  N% = N% + 1
2172  'READING PRESSURE SIGNAL
2174  OUT BASADR% + 2, 5
2175  OUT BASADR% + 1, 0
2176  XL%(5) = INP(BASADR%): XH%(5) = INP(BASADR% + 1)
2177  D%(5) = 16 * XH%(5) + XL%(5) / 16
2178  V(5) = (D%(5) * (10 / 4096) - 5) * 100
2179  FL(5) = (V(5) + 4!) * 10
2180 'TIME COORDINATION PROCEDURE
2185  FLOW = FEX * CV * ((FL(5) ^ 2 - PVAC ^ 2) ^ .5)
2190  FLOW = (FLOW * 760! * 1000!) / (FL(5) * 60)
2195  TAU = VOL / FLOW
2197  SI = TIMER - CSTART: CSTART = TIMER
2200  FDE1 = (1! - EXP(-SI / TAU))
2210  DE1 = (D * 100! / 90!)
2212  DE1 = DE1 * FDE1 + (1! - FDE1) * DE1OLD
2214  DE1OLD = DE1
2215  'REPARAMETERIZING THE MODEL USING IMPOL
2220  TM = AC * EXP(-BC / DE1)
2230  FEX = TM / (1! + TM)
2240  FL(7) = FL(1) + FL(3)
2250  LOCATE 11, 10: PRINT " PRESSURE IS "; FL(5); "MTORR";
```

```
2270  FL(6) = SET - FL(5)
2280  FIN = FL(7)
2290  PT = (FL(5) ^ 2 - PVAC ^ 2) ^ .5
2292  QSTERM = ((FIN * BETAOLD) / (CV * FEX)) ^ 2!
2294  T1 = (FIN / (CV * FEX)) ^ 2!
2296  DERB = (T1 * BETAOLD) / SQR(PVAC ^ 2! + QSTERM)
2298  CMP = SQR(QSTERM + PVAC ^ 2!)
2300  CMER = FL(5) - CMP
2301  BETA = BETAOLD + CMER / DERB
2302  BETAOLD = BETA
2304  FOUT = FIN * BETA
2305  'CALCULATING THE STEADY-STATE TARGET PRESSURE
2310  PST = FL(5) + PK1 * FL(6)
2315  FL6OLD = FL(6)
2320  CAL = 0!
2335  CALI = 0!
2337  'CALCULATING REQUIRED CONTROL ACTION
2340  PT1 = (PST ^ 2 - PVAC ^ 2) ^ .5
2350  FEX1 = FOUT / (CV * PT1)
2354  IF FEX1 > 1! THEN FEX1 = .99
2360  DG = LOG(AC) - LOG(FEX1 / (1! - FEX1))
2370  DE = BC / DG: 'NEW VALVE POSITION REQUIRED
2372  ERCAL = ABS(FL(6))
2374  TIAE = TIAE + (SI * (ERCAL + EROLD) / 2!)
2376  EROLD = ERCAL
2378  'IMPLEMENTING REQUIRED CONTROL ACTION
2380  SDE = (DE * 90!) / 100!
2385  DEG = ABS(D - SDE)
2387  LOCATE 18, 10: PRINT "INTEGRAL ABSOLUTE ERROR"; TIAE
2388  IF DEG < .1 THEN DEG = 0!
2389  IF DEG > 1! THEN DEG = 1!
2390  LOCATE 17, 10: PRINT "VALVE POSTION REQUIRED"; SDE;
      "DEGREES"
2400  IF D < SDE THEN D$ = "O" ELSE D$ = "C"
2410  LOCATE 19, 10: PRINT "VALVE TURNS BY"; DEG; "DEGREES"
```

```
2420  M = 28
2430  L = 31
2440  OUT &H330 + &HE, 128 'CLEARS O/P ON THE DDA BOARD
2470  LOCATE 21, 10: PRINT "BETA = "; BETA; " SS TARGET ";
      PST; "FEX1= "; FEX1
2480  N = INT((DEG * 5) + .5)
2490  IF D$ = "O" THEN A = 4 ELSE GOTO 2570
2495  'SENDING PULSES TO VALVE
2500  FOR I = 1 TO N
2510  OUT &H330 + &HE, A: 'OPEN VALVE--26TH PIN IS LOW AND
      27TH IS HIGH
2520  FOR JJ = 1 TO L: NEXT JJ
2530  OUT &H330 + &HE, 128
2540  NEXT I
2550  CAL = DEG
2560  GOTO 2650
2570  B = 8
2580  FOR I = 1 TO N
2590  OUT &H330 + &HE, B: 'CLOSE VALVE--27TH PIN IS LOW AND
      26TH IS HIGH
2600  FOR KK = 1 TO M: NEXT KK
2610  OUT &H330 + &HE, 128
2620  NEXT I
2630  CALI = DEG
2640  GOTO 2660
2650  D = D + CAL: GOTO 2665
2660  D = D - CALI
2665  LOCATE 23, 10: PRINT " THE VALVE IS OPEN AT "; D;
     "DEGREES"
2680  RETURN
```

E.2 Subroutine Used to Implement IMC

E.2.1 With Feedforward Action and Gain-Scheduling

```
2100  'THIS SUBROUTINE IMPLEMENTS AN IMC ALGORITHM WHICH HAS
      GAIN-SCHEDULING AND FEEDFORWARD ACTION INCORPORATED
2102  IF RTIME > 30! AND RTIME < 30.3 THEN GOTO 2103 ELSE
      GOTO 2108
2103  W4REF = 0!
2105  W5REF = 0!
2107  W6REF = 0!
2108  'FEED FORWARD INITIALIZATION COMPLETE
2109  'INITIALIZATION OF DEVIATION VARIABLES
2110  IF N% > 1 THEN GOTO 2160 ELSE GOTO 2120
2120  D = 90!
2130  W1REF = W1
2132  W2REF = W2
2134  W3REF = W3
2135  CSS = 90!
2136  SOLD = 90!
2137  FV = 1!
2138  TAUD = 3.5
2140  TAUP = 1.5
2150  W1OLD = W1
2155  W3OLD = W3
2157  FLOW = FL(1)
2160  N% = N% + 1
2162  SI = TIMER - CSTART
2163  CSTART = TIMER
2164  'CALCULATION OF FILTER FACTORS
2165  FF = (1! - EXP(-SI / TAUF))
2170  FP = (1! - EXP(-SI / TAUP))
2172  FD = (1! - EXP(-SI / TAUD))
2175  CAL = 0!
2176  PKD = 4!
2178  'GAIN-SCHEDULING IMPLEMENTED
```

```
2180  IF SET >= 150! AND SET < 350! THEN PKIMC = -30
2182  IF SET >= 350! AND SET < 600! THEN PKIMC = -35!
2184  IF SET >= 600! AND SET < 1000! THEN PKIMC = -45!
2185  'CALCULATION OF FEEDFORWARD ACTION
2186  FFGAIN = -(PKD / PKIMC)
2187  CALI = 0!
2188  DHAT = FL(1) - FLOW
2189  IF RTIME <= 30 THEN DHAT = 0!
2190  T1 = FP * PKIMC * VALOL
2195  T2 = (1! - FP) * (W1OLD - W1REF)
2200  W1 = W1REF + T1 + T2
2202  T5 = FD * PKD * DHATOLD
2204  T6 = (1! - FD) * (W4OLD - W4REF)
2206  W4 = W4REF + T5 + T6
2207  IF RTIME <= 30 THEN W4 = 0!
2208  W4OLD = W4
2210  W1OLD = W1
2215  'READING PRESSURE SIGNAL AND CALCULATING ERROR
2220  OUT BASADR% + 2, 5
2230  OUT BASADR% + 1, 0
2240  XL%(I) = INP(BASADR%): XH%(I) = INP(BASADR% + 1)
2250  D%(I) = 16 * XH%(I) + XL%(I) / 16
2260  V(5) = (D%(5) * (10 / 4096) - 5) * 100
2270  FL(5) = (V(5) + 4) * 10
2275  LOCATE 11, 10: PRINT " PRESSURE IS "; FL(5)
2280  ER = SET - FL(5)
2285  'CALCULATION OF CONTROL ACTION
2290  W2 = W2REF + (W1 - W1REF) + ER + (W4 - W4REF)
2300  W3 = W3REF + FF * (W2 - W2REF) + (1 - FF) * (W3OLD -
      W3REF)
2310  T3 = ((W3 - W3REF) / PKIMC)
2320  T4 = (TAUP / PKIMC) * ((W3 - W3OLD) / SI)
2322  T7 = FFGAIN * DHATOLD * FD
2324  T8 = (1! - FD) * (W5OLD - W5REF)
2326  W5 = W5REF + T7 + T8
```

```
2327  IF RTIME <= 30 THEN W5 = 0!
2328  W6 = W6REF + TAUP * ((W5 - W5OLD) / SI) + (W5 - W5REF)
2329  IF RTIME <= 30 THEN W6 = 0!
2330  CS = T3 + T4 + (W6 - W6REF)
2334  IF N% < 2 THEN CS = 0!
2336  S = CSS + CS
2340  SD = S - SOLD
2345  DEG = ABS(S - D)
2347  IF DEG > 1 AND S - D > 0 THEN S = D + 1
2349  IF DEG > 1 AND S - D < 0 THEN S = D - 1
2351  CS = S - CSS
2353  IF DEG > 1 THEN DEG = 1!
2355  VALOL = CSOLD
2356  CSOLD = CS
2357  DHATOLD = DISOL1
2358  DISOL1 = DISOL2
2359  DISOL2 = DHAT
2360  W3OLD = W3
2362  W5OLD = W5
2370  SOLD = S
2372  'IMPLEMENTING CONTROL ACTION
2375  LOCATE 21, 10: PRINT "VALVE POSITION REQUIRED"; S
2388  IF DEG < .2 THEN DEG = 0!
2400  IF SD > 0 THEN D$ = "O" ELSE D$ = "C"
2410  LOCATE 19, 10: PRINT "VALVE TURNS BY"; DEG; "DEGREES"
2420  M = 26
2430  L = 31
2440  OUT &H330 + &HE, 128 'CLEARS O/P ON THE DDA BOARD
2445  'SENDING PULSES TO THE VALVE
2480  N = INT((DEG * 5) + .5)
2490  IF D$ = "O" THEN A = 4 ELSE GOTO 2570
2500  FOR I = 1 TO N
2510  OUT &H330 + &HE, A: 'OPEN VALVE--26TH PIN IS LOW AND
      27TH IS HIGH
2520  FOR JJ = 1 TO L: NEXT JJ
```

```
2530  OUT &H330 + &HE, 128
2540  NEXT I
2550  CAL = DEG
2560  GOTO 2650
2570  B = 8
2580  FOR I = 1 TO N
2590  OUT &H330 + &HE, B: 'CLOSE VALVE--27TH PIN IS LOW AND
      26TH IS HIGH
2600  FOR KK = 1 TO M: NEXT KK
2610  OUT &H330 + &HE, 128
2620  NEXT I
2630  CALI = DEG
2640  GOTO 2660
2650  D = D + CAL: GOTO 2665
2660  D = D - CALI
2665   LOCATE 23, 10: PRINT " THE VALVE IS OPEN AT "; D;
      "DEGREES"
2680  RETURN
```

E.2.2 Without Feedforward action and Gain-scheduling

```
2100  'THIS SUBROUTINE IMPLEMENTS A SIMPLE IMC ALGORITHM
2105  'INITIALIZATION OF DEVIATION VARIABLES
2110  IF N% > 1 THEN GOTO 2160 ELSE GOTO 2120
2120  D = 90!
2130  W1REF = W1
2132  W2REF = W2
2134  W3REF = W3
2135  CSS = 90!
2136  SOLD = 90!
2137  FV = 1!
2138  EROLD = ERCAL
2140  TAUP = 1.5
2150  W1OLD = W1
2155  W3OLD = W3
```

```
2160  N% = N% + 1
2162  SI = TIMER - CSTART
2163  CSTART = TIMER
2164  'CALCULATING FILTER FACTORS
2165  FF = (1! - EXP(-SI / TAUF))
2170  FP = (1! - EXP(-SI / TAUP))
2175  CAL = 0!
2186  CALI = 0!
2190  T1 = FP * PKIMC * VALOL
2195  T2 = (1! - FP) * (W1OLD - W1REF)
2200  W1 = W1REF + T1 + T2
2210  W1OLD = W1
2215  'READING PRESSURE SIGNAL
2220  OUT BASADR% + 2, 5
2230  OUT BASADR% + 1, 0
2240  XL%(I) = INP(BASADR%): XH%(I) = INP(BASADR% + 1)
2250  D%(I) = 16 * XH%(I) + XL%(I) / 16
2260  V(5) = (D%(5) * (10 / 4096) - 5) * 100
2270  FL(5) = (V(5) + 3.5) * 10
2275  LOCATE 11, 10: PRINT " PRESSURE IS "; FL(5)
2280  ER = SET - FL(5)
2281  ERCAL = ABS(ER)
2282  TIAE = TIAE + (SI * (ERCAL + EROLD) / 2!)
2284  EROLD = ERCAL
2285  'CALCULATING CONTROL ACTION
2290  W2 = W2REF + (W1 - W1REF) + ER + (W4 - W4REF)
2300  W3 = W3REF + FF * (W2 - W2REF) + (1 - FF) * (W3OLD -
      W3REF)
2310  T3 = ((W3 - W3REF) / PKIMC)
2320  T4 = (TAUP / PKIMC) * ((W3 - W3OLD) / SI)
2330  CS = T3 + T4
2334  IF N% < 2 THEN CS = 0!
2336  S = CSS + CS
2338  'IMPLEMENTING CONTROL ACTION CALCULATED
2340  SD = S - SOLD
```

```
2345  DEG = ABS(S - D)
2347  IF DEG > 1 AND S - D > 0 THEN S = D + 1
2349  IF DEG > 1 AND S - D < 0 THEN S = D - 1
2351  CS = S - CSS
2353  IF DEG > 1 THEN DEG = 1!
2355  VALOL = CSOLD
2356  CSOLD = CS
2360  W3OLD = W3
2370  SOLD = S
2375  LOCATE 21, 10: PRINT "VALVE POSITION REQUIRED"; S
2386  LOCATE 17, 10: PRINT "INTEGRAL ABSOLUTE ERROR"; TIAE
2387  'LOCATE 18, 10: INPUT "DEGREES"; DEG
2388  IF DEG < .1 THEN DEG = 0!
2400  IF SD > 0 THEN D$ = "O" ELSE D$ = "C"
2410  LOCATE 19, 10: PRINT "VALVE TURNS BY"; DEG; "DEGREES"
2420  M = 27
2430  L = 31
2440  OUT &H330 + &HE, 128 'CLEARS O/P ON THE DDA BOARD
2450  'SENDING PULSES TO THE VALVE
2480  N = INT((DEG * 5) + .5)
2490  IF D$ = "O" THEN A = 4 ELSE GOTO 2570
2500  FOR I = 1 TO N
2510  OUT &H330 + &HE, A: 'OPEN VALVE--26TH PIN IS LOW AND
      27TH IS HIGH
2520  FOR JJ = 1 TO L: NEXT JJ
2530  OUT &H330 + &HE, 128
2540  NEXT I
2550  CAL = DEG
2560  GOTO 2650
2570  B = 8
2580  FOR I = 1 TO N
2590  OUT &H330 + &HE, B: 'CLOSE VALVE--27TH PIN IS LOW AND
      26TH IS HIGH
2600  FOR KK = 1 TO M: NEXT KK
2610  OUT &H330 + &HE, 128
```

```
2620  NEXT I
2630  CALI = DEG
2640  GOTO 2660
2650  D = D + CAL: GOTO 2665
2660  D = D - CALI
2665   LOCATE 23, 10: PRINT " THE VALVE IS OPEN AT "; D;
     "DEGREES"
2669  IF DEG < 1 THEN ICT = 200 ELSE ICT = 150
2670  FOR I = 1 TO ICT: NEXT I
2680  RETURN
```

E.3 Subroutine to Implement a PI Controller

```
2100  'THIS SUBROUTINE IMPLEMENTS A PI CONTROLLER
2105  'INITIALIZING VARIABLES
2110  IF N% > 1 THEN GOTO 2136 ELSE GOTO 2112
2112  D = 90!
2122  SOLD = 90!
2123  EROLD = ER
2124  FV = 1!
2126  SBAS = S
2136  N% = N% + 1
2138  SI = TIMER - CSTART
2140  CSTART = TIMER
2148  CAL = 0!
2160  CALI = 0!
2170  'READING PRESSURE SIGNAL AND CALCULATING ERROR
2222  OUT BASADR% + 2, 5
2224  OUT BASADR% + 1, 0
2240  XL%(I) = INP(BASADR%): XH%(I) = INP(BASADR% + 1)
2250  D%(I) = 16 * XH%(I) + XL%(I) / 16
2260  V(5) = (D%(5) * (10 / 4096) - 5) * 100
2270  FL(5) = (V(5) + 3.5) * 10
2275  LOCATE 11, 10: PRINT " PRESSURE IS "; FL(5)
2280  ER = SET - FL(5)
2285  'CALCULATING CONTROL ACTION
```

```
2290  AINT = AINT + SI * ((ER + EROLD) / 2!)
2300  EROLD = ER
2310  SD = PKC * (ER + (AINT / TAUI))
2315  S = SBAS + SD
2320  SD = S - D
2325  ERT = ABS(ER)
2330  TIAE = TIAE + (SI * (ERT + ERCAL) / 2!)
2335  ERCAL = ERT
2340  'IMPLEMENTING CONTROL ACTION
2345  DEG = ABS(SD)
2347  IF DEG > 1 AND SD > 0 THEN S = D + 1
2349  IF DEG > 1 AND SD < 0 THEN S = D - 1
2353  IF DEG > 1 THEN DEG = 1!
2370  SOLD = S
2375  LOCATE 21, 10: PRINT "VALVE POSITION REQUIRED"; S
2387  LOCATE 18, 10: PRINT "INTEGRAL ABSOLUTE ERROR"; TIAE
2388  IF DEG < .2 THEN DEG = 0!
2400  IF S - D > 0! THEN D$ = "O" ELSE D$ = "C"
2410  LOCATE 19, 10: PRINT "VALVE TURNS BY"; DEG; "DEGREES"
2420  M = 27
2430  L = 31
2440  OUT &H330 + &HE, 128 'CLEARS O/P ON THE DDA BOARD
2450  'SENDING PULSES TO THE VALVE
2480  N = INT((DEG * 5) + .5)
2490  IF D$ = "O" THEN A = 4 ELSE GOTO 2570
2500  FOR I = 1 TO N
2510  OUT &H330 + &HE, A: 'OPEN VALVE--26TH PIN IS LOW AND
      27TH IS HIGH
2520  FOR JJ = 1 TO L: NEXT JJ
2530  OUT &H330 + &HE, 128
2540  NEXT I
2550  CAL = DEG
2560  GOTO 2650
2570  B = 8
2580  FOR I = 1 TO N
```

```
2590  OUT &H330 + &HE, B: 'CLOSE VALVE--27TH PIN IS LOW AND
      26TH IS HIGH
2600  FOR KK = 1 TO M: NEXT KK
2610  OUT &H330 + &HE, 128
2620  NEXT I
2630  CALI = DEG
2640  GOTO 2660
2650  D = D + CAL: GOTO 2665
2660  D = D - CALI
2665   LOCATE 23, 10: PRINT " THE VALVE IS OPEN AT "; D;
      "DEGREES"
2668  PRINT #1, FL(5), D, TIMER
2670  IF DEG < 1! THEN ICT = 250 ELSE ICT = 200
2675  FOR I = 1 TO ICT: NEXT I
2680  RETURN
```

APPENDIX F

CODE FOR REACTOR START-UP

```
100 COLOR 1, 6
110 COLOR 1, 6
120 'ASPR AUTOMATIC CONTROL
140 DIM D%(10), V(10), XL%(10), XH%(10), FL(10)
141 OPEN "C:OL3.PRN" FOR OUTPUT AS #1
142 OPEN "C:OL4.PRN" FOR OUTPUT AS #2
150 BASADR% = &H300: 'BASE ADDRESS FOR DAS-8PGA
160 OUT &H330 + &HF, &H80: OUT &H330 + &HE, 32'CLEARS OUTPUTS
    ON THE DDA BOARD
162 PVAC = 45!
165 CLS
167 'INPUT OF CONTROLLER TUNING PARAMETERS
170 LOCATE 1, 20: INPUT " CONTROLLER GAIN "; PKC
173 LOCATE 5, 20: INPUT "INTEGRAL TIME CONSTANT"; TAUI
174 CV = .6611
175 CLS
176 K% = 0
177 N% = 0
180 LOCATE 1, 20: PRINT "ENTER PROCESS PARAMETERS";
190 LOCATE 2, 10: INPUT "ENTER SETPOINT PRESSURE , 3000--50
    MILLITORR"; P
191 SET = P
200 'pressure 0--5V
210 PS = 24.5 * P / (113755!)
220 PRS = INT(4095 * (PS))
230 PH% = INT(PRS / 256)
240 PL% = PRS - PH% * 256
250 OUT &H330 + 8, PL%
260 OUT &H330 + 9, PH%
270 'read pressure
280 OUT BASADR% + 2, 5
281 STIME11 = TIMER
```

```
282 FOR I = 1 TO 2000 STEP 20
284 FOR J = 1 TO 20: NEXT J
290 OUT BASADR% + 1, 0
300 XL%(5) = INP(BASADR%): XH%(5) = INP(BASADR% + 1)
310 D%(5) = 16 * XH%(5) + XL%(5) / 16
320 V(5) = (D%(5) * (10 / 4096) - 5) * 1000
330 LOCATE 3, 10: PRINT "PRESURE IS"; V(5) + 5!; "mT"
332 NEXT I
335 'INPUT OF GAS FLOW RATES
340 LOCATE 4, 10: INPUT "IS THE PRESSURE OK?[Y/N]"; P$
350 IF P$ = "Y" THEN GOTO 360 ELSE GOTO 282
352 IF K% = 0 THEN GOTO 360 ELSE GOTO 392
354 LOCATE 5, 10: INPUT "DO YOU WANT TO CHANGE FLOWRATE 1,
    [Y/N]"; FR1$
356 'IF FR1$ = "Y" THEN GOTO 390 ELSE GOTO 394
360 LOCATE 5, 10: INPUT "TURN ON #1GAS Ar [Y/N]"; GAS1$
370 IF GAS1$ = "Y" THEN A = 32 ELSE GOTO 400
380 OUT &H330 + &HD, A: 'A15
390  LOCATE 6, 10: INPUT "ENTER MASS FLOW RATE, #1GAS
    Ar, 40--0sccm"; MF1
392 IF K% = 0 THEN GOTO 400 ELSE GOTO 429
394 'LOCATE 7, 10: INPUT "DO YOU WANT TO CHANGE FLOWRATE 2,
    [Y/N]"; FR2$
396 'IF FR2$ = "Y" THEN GOTO 430 ELSE GOTO 434
400 LOCATE 7, 10: INPUT "TURN ON #2GAS CF4[Y/N]"; GAS2$
410 IF GAS2$ = "Y" THEN B = 4 ELSE GOTO 440
420 OUT &H330 + &HD, A + B: 'A16
429 MF2 = 70.3: IF K% > 0 THEN GOTO 432
430  LOCATE 8, 10: INPUT "ENTER MASS FLOW RATE,#2GAS
CF4,200--0sccm"; MF2
432 IF K% = 0 THEN GOTO 440 ELSE GOTO 509
434 'LOCATE 9, 10: INPUT "DO YOU WANT TO CHANGE FLOWRATE 4,
    [Y/N]"; FR4$
436 'IF FR4$ = "Y" THEN GOTO 510 ELSE GOTO 560
440 LOCATE 9, 10: INPUT "TURN ON #3GAS H2 [Y/N]"; GAS3$
```

```
450 IF GAS3$ = "Y" THEN C = 128 ELSE GOTO 480
460 OUT &H330 + &HD, A + B + C: 'A18
470 LOCATE 10, 10: INPUT "ENTER MASS FLOW RATE,#3GAS H2";
    MF3
480 LOCATE 11, 10: INPUT "TURN ON #4GAS O2 [Y/N]"; GAS4$
490 IF GAS4$ = "Y" THEN D = 64 ELSE GOTO 520
500 OUT &H330 + &HD, A + B + C + D: 'A17
509 MF4 = 0: IF K% > 0 THEN GOTO 512
510 LOCATE 12, 10: INPUT "ENTER MASS FLOW RATE,#4GAS
    O2,80--0sccm"; MF4
512 IF RF > 0 THEN GOTO 560 ELSE GOTO 520
520 LOCATE 13, 10: INPUT "ENTER RF POWER, 600--0 W"; RF
530 LOCATE 14, 10: INPUT "ENTER ETCHING TIME [MINUTES]";
    ITIME: STIME = ITIME * 60
540 LOCATE 15, 15: INPUT "ARE THESE VALUES CORRECT [Y/N]";
    SFB$
545 CSTART = TIMER
550 IF SFB$ = "Y" THEN GOTO 560 ELSE GOTO 170
700 POWER = 34.9013 + .771 * RF - .0017 * RF * RF
705 'SENDING SIGNALS TO THE BOARD
710 RFP = INT(4095 * POWER / 60000!)
720 RFH% = INT(RFP / 256)
730 RFL% = RFP - RFH% * 256
740 OUT &H330 + 10, RFH%:
750 OUT &H330 + 11, RFL%:
790 SET1 = 14.0267 + 10.848 * MF1
800 MFC1 = INT(4095 * SET1 / 500)
810 MFH1% = INT(MFC1 / 256)
820 MFL1% = MFC1 - MFH1% * 256
830 OUT &H330 + 0, MFL1%
840 OUT &H330 + 1, MFH1%
870 SET2 = 55.2 + 2.15 * MF2
880 MFC2 = INT(4095 * SET2 / 500)
890 MFH2% = INT(MFC2 / 256)
900 MFL2% = MFC2 - MFH2% * 256
```

```
910 OUT &H330 + 2, MFL2%
920 OUT &H330 + 3, MFH2%
950 MFC3 = INT(4095 * MF3 / 500)
960 MFH3% = INT(MFC3 / 256)
970 MFL3% = MFC3 - MFH3% * 256
980 OUT &H330 + 4, MFL3%
990 OUT &H330 + 5, MFH3%
1020 SET4 = 100 * (MF4 + 2.7328) / 17.1292
1030 MFC4 = INT(4095 * SET4 / 500)
1040 MFH4% = INT(MFC4 / 256)
1050 MFL4% = MFC4 - MFH4% * 256
1060 OUT &H330 + 6, MFL4%
1070 OUT &H330 + 7, MFH4%
1075 IF K% > 0 THEN GOTO 1252
1080 CLS
1090 'READING SIGNALS FROM THE BOARD
1100 FOR J = 1 TO 100
1110 FOR I = 0 TO 7
1120 OUT BASADR% + 2, I
1130 OUT BASADR% + 1, 0
1140 XL%(I) = INP(BASADR%): XH%(I) = INP(BASADR% + 1)
1150 D%(I) = 16 * XH%(I) + XL%(I) / 16
1160 V(I) = (D%(I) * (10 / 4096) - 5) * 100
1170 NEXT I
1180 LOCATE 3, 10: PRINT "#1 GAS-Ar FLOW RATE IS(sccm)";
     V(0) * 8.892 / 100 + .702
1181 FL(0) = V(0) * 8.892 / 100 + .702
1190 LOCATE 5, 10: PRINT "#2 GAS-CF4 FLOW RATE IS(sccm)"; .5
     * V(1) - 27.75
1191 FL(1) = .5 * V(1) - 27.75
1200 LOCATE 7, 10: PRINT "#3 GAS-H2 FLOW RATE IS"; V(2)
1210 LOCATE 9, 10: PRINT "#4 GAS-O2 FLOW RATE IS(sccm)";
     V(3) * 17.129 / 100 - 2.733
1211 FL(3) = V(3) * 17.129 / 100 - 2.733
```

```
1220 'LOCATE 11, 10: PRINT "PRESURE IS"; (V(5) + 4) * 10;
     "mT"
1225 FL(5) = (V(5) + 4) * 10
1230 LOCATE 13, 10: PRINT "RF POWER IS"; RF;
1234 GOSUB 2100
1240 NEXT J
1250 BEEP
1252 IF K% > 0 THEN GOTO 1254 ELSE GOTO 1260
1254 IF RF > 0 THEN GOTO 1430
1260 LOCATE 15, 10: INPUT "IS EVERYTHING OK, TURN ON RF?
     [Y/N]"; R$
1270 IF R$ = "Y" GOTO 1290 ELSE GOTO 1100
1280 'TURN ON RF
1290 OUT &H330 + &HE, 16
1300 START! = TIMER
1310 FOR I = 0 TO 100: NEXT I: 'TIME TELAY ?
1320 OUT &H330 + &HE, 64: 'SET RF ON TO LOW ?
1330 FOR I = 0 TO 5
1340 OUT BASADR% + 2, I
1350 OUT BASADR% + 1, 0
1370 XL%(I) = INP(BASADR%): XH%(I) = INP(BASADR% + 1)
1380 D%(I) = 16 * XH%(I) + XL%(I) / 16
1390 IF I = 4 THEN V(I) = (D%(I) * (10 / 4096)) * 10 / 3.5
     ELSE V(I) = (D%(I) * (10 / 4096) - 5) * 100
1400 V(I) = (D%(I) * (10 / 4096) - 5) * 100
1410 V(4) = (D%(I) * (10 / 4096)) * 10 / 3.5
1420 NEXT I
1440 LOCATE 3, 10: PRINT "#1 GAS-Ar FLOW RATE IS(sccm)";
     V(0) * 7.89242 / 100 + .702
1441 FL(0) = V(0) * 7.89242 / 100 + .702
1450 LOCATE 5, 10: PRINT "#2 GAS-CF4 FLOW RATE IS (sccm)";
    .5 * V(1) - 27.75
1451 FL(1) = .5 * V(1) - 27.75
1460 LOCATE 7, 10: PRINT "#3 GAS-H2 FLOW RATE IS"; V(2)
1470 LOCATE 9, 10: PRINT "#4 GAS-O2 FLOW RATE IS(sccm)";
```

```
    V(3) * 17.1292 / 100 - 2.7328
1471 FL(3) = V(3) * 17.1292 / 100 - 2.7328
1472 FL(5) = (V(5) + 4) * 10
1490 W = 3859.9339# - 498.5081 * V(4) + 20.2076 * V(4) ^ 2 -
    .2444 * V(4) ^ 3
1500 LOCATE 13, 10: PRINT "RF POWER IS"; W; "W"
1505 FINISH! = TIMER: RTIME = FINISH! - START!
1510 K% = K% + 1
1511 'ALLOWS USER TO CHANGE SETPOINTS
1512 IF RTIME > 30 AND RTIME < 30.3 THEN GOTO 352 ELSE GOTO
1513 IF RTIME > 30! AND RTIME < 60! THEN SET = 800!
1514 IF RTIME > 60! AND RTIME < 90! THEN SET = 500!
1515 IF RTIME > 90! AND RTIME < 150! THEN SET = 200!
1516 IF RTIME > 150! THEN SET = 500!
1517 GOSUB 2100
1520 IF RTIME < STIME THEN GOTO 1330 ELSE GOTO 1540
1550 OUT &H330 + &HE, 32
1560 LOCATE 17, 10: INPUT "TURN ON N2"; N$
1570 IF N$ = "Y" THEN GOTO 1580 ELSE GOTO 170
1590 OUT &H330 + &HD, 2: 'turn on N2
1600 LOCATE 19, 10: INPUT "Stop N2? [Y/N]"; N$
1610 IF N$ = "Y" GOTO 1620
1620 OUT &H330 + &HF, &H80
1630 OUT &H330 + &HE, 32
1640 CLS
1650 LOCATE 20, 10: PRINT "PROCESS FINISHED!"
1651 CLOSE #1
1652 CLOSE #2
1653 STOP
1660 END
```